Clemson University
TigerPrints

All Dissertations | Dissertations

12-2013

Sulfonated Perfluorocyclobutyl (PFCB) Aryl Ether Polymers: Synthesis, Reactivity, and Characterization for Polymer Electrolyte Applications

Jiyoung Park
Clemson University, jiyounp@g.clemson.edu

Follow this and additional works at: https://tigerprints.clemson.edu/all_dissertations

 Part of the Polymer Science Commons

Recommended Citation
Park, Jiyoung, "Sulfonated Perfluorocyclobutyl (PFCB) Aryl Ether Polymers: Synthesis, Reactivity, and Characterization for Polymer Electrolyte Applications" (2013). *All Dissertations*. 1237.
https://tigerprints.clemson.edu/all_dissertations/1237

This Dissertation is brought to you for free and open access by the Dissertations at TigerPrints. It has been accepted for inclusion in All Dissertations by an authorized administrator of TigerPrints. For more information, please contact kokeefe@clemson.edu.

Sulfonated Perfluorocyclobutyl (PFCB) Aryl Ether Polymers: Synthesis, Reactivity, and Characterization for Polymer Electrolyte Applications

---

A Thesis
Presented to
the Graduate School of
Clemson University

In Partial Fulfillment
of the Requirements for the Degree
Doctor of Philosophy
Chemistry

---

by
Jiyoung Park
December 2013

Accepted by:
Dr. Dennis W. Smith, Jr., Committee Chair
Dr. Stephen E. Creager, Co-Chair
Dr. Karl R. Dieter, Committee Member
Dr. Andrew G. Tennyson, Committee Member
Dr. Earl H. Wagener, Committee Member

ABSTRACT

Perfluorocyclobutyl (PFCB) aryl ether copolymers are excellent candidates for proton exchange membrane (PEM) component in PEM fuel cells. Sulfonated PFCB copolymer membranes exhibit not only high chemical/thermal/mechanical stability but also high proton conductivity. In this regard, PFCB aryl ether copolymers were synthesized via thermal step-growth [2 + 2] cyclopolymerization from aryl bis-(trifluorovinyl ether) (TFVE) monomers and oligomers. Experimental and computational studies confirmed that copolymerization of relatively electron-rich and electron-poor TFVE monomers gave selective-segmented copolymers in an one-pot polymerization. After sulfonation, the PFCB copolymers comprising hydrophilic and hydrophobic segments gave membranes with high proton conductivity. Cross-linked membranes of the sulfonated PFCB copolymers were also prepared via Friedel-Craft acylation to improve their mechanical properties and manage the high stress due to hydration/dehydration induced swelling. A phosphonic acid telechelic PFCB aryl ether ionomer was also synthesized and used as a grafting compound to inorganic fillers. The tailorable synthetic methodology, chemical/physical properties, effect of sulfonation level, block length and cross-linking of copolymers on water uptake, volume swelling, proton conductivity, and thermal properties and their potential application in PEM fuel cells is presented.

TABLE OF CONTENTS

LIST OF TABLES

List of Tables (Continued)

Table Page

LIST OF FIGURES

List of Figures (Continued)

Figure Page

List of Figures (Continued)

Figure Page

List of Figures (Continued)

List of Figures (Continued)

Figure Page

LIST OF SCHEMES

List of Schemes (Continued)

Scheme Page

CHAPTER ONE

INTRODUCTION

Perflurorcyclobutyl (PFCB) Aryl Ether Polymers

Cycloaddition reactions are a powerful tool to synthesize unique polymers.[1] Particularly, a step-growth [2 + 2] cyclo-dimerization of fluoro-olefins has been found out to be an effective protocol in preparation of semi-fluorinated, high-performance perfluorocyclobutyl (PFCB) containing polymers to yield high molecular weight polymers without using a catalyst or an initiator.[2, 3] The cyclodimerization of fluoro-olefins was first discovered from the research on pyrolysis of polytetrafluoroethylene (PTFE) as shown in Figure 1.1, by Lewis and Naylor at DuPont in 1947.[4]

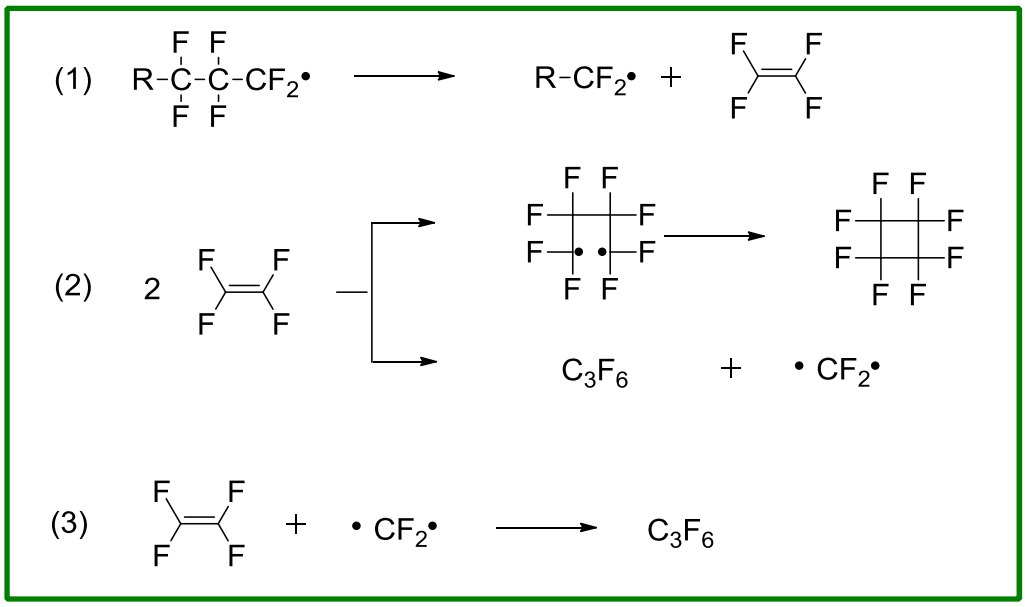

Figure 1.1 Proposed mechanism of PTFE degradation and secondary reactions.[4]

Following the report on the perfluorocyclobutane (PFCB) formation through the thermal dimerization of tetrafluoroethylene (TFE), the kinetics for forward (Ea = 25.4 kcal/mol) and reverse reactions (Ea = 74.1 kcal/mol) were reported in 1950s.[5, 6] This higher activation energy of reverse reaction than that of dimerization of TFE supports the thermal stability of the PFCB structure. Paul Bartlett and co-workers reported a half-life (the order of 10^{-10} sec) of diradical intermediate and head-to-head dimerization of TFE. An initial bond formation between the terminal carbons of TFE was confirmed by a reaction of 1,1-dichloro-2,2-difluoroethylene with the *cis-cis, cis-trans,* or *trans-trans* isomers of 2,4-hexadiene (Figure 1.2).[7] Recently, the existence of the diradical intermediate and the resulting *cis/trans* isomers of dimerized PFCB aryl ether were confirmed by electron paramagnetic resonance (EPR) and X-ray crystallography, respectively.[8, 9]

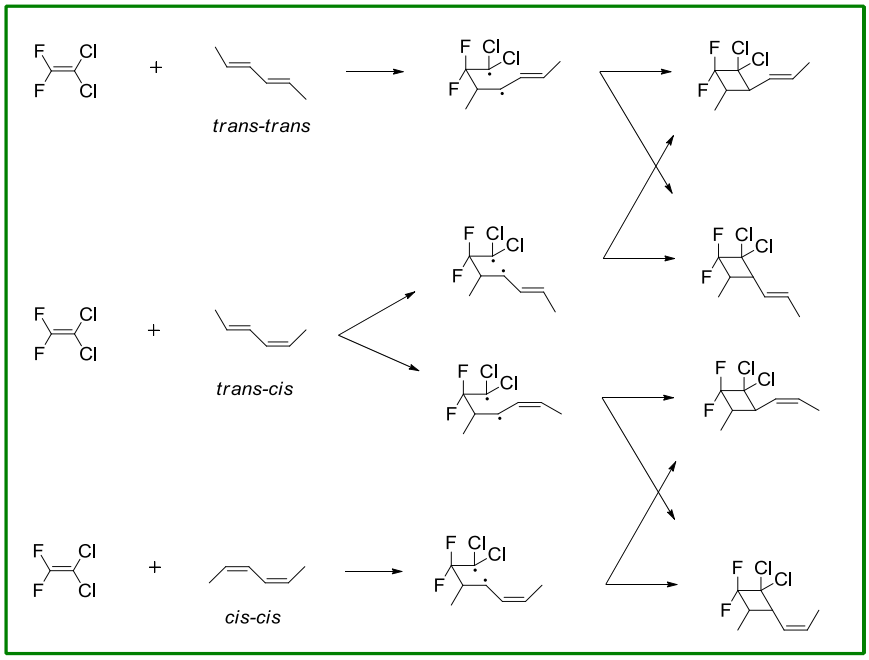

Figure 1.2 Isomer distributions with rotation of a difunctional intermediate.[7]

This unusual reactivity of TFE toward PFCB ring formation was explained by William A. Bernett with hybridization effects in the fluorocarbon with respect to the hydrocarbon ethylene.[10] He noted that the fluoro-olefin (sp^3) posses higher angular strain with respect to the hydrocarbon ethylene (sp^2). Therefore, the cyclo-dimerization of TFE occurs easily to form PFCB compound with relief of angular orbital strain (9 kcal/mol).[11] Figure 1.3 shows the energy states of fluorocarbon and hydrocarbon compounds.

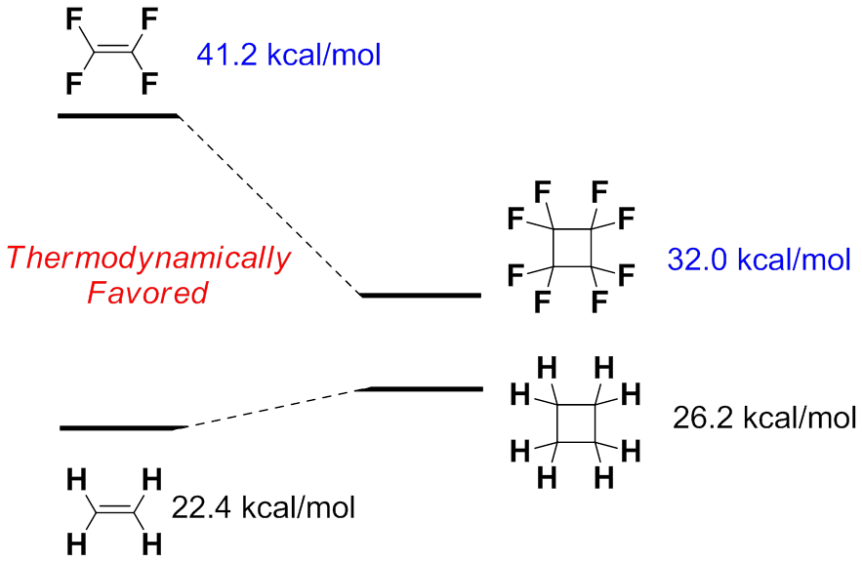

Figure 1.3 Energy diagram with bond strain energy of TFE and ethylene dimerization.[12]

The first high molecular weight PFCB-containing molecules synthesized *via* cycloaddition of fluoro-olefins were perfluoroalkyl ether oligomers reported by Beckerbauer at Dupont in 1968.[13] Afterwards perfluorocyclobutyl (PFCB) aryl ether polymers were introduced by David A. Babb and co-workers at Dow in the early 1990's.[14] To date, PFCB aryl ether polymer derivatives have been intensively

investigated for many applications because of their excellent solubility and processability as well as high chemical/thermal stability as a fluorinated polymer.[11, 15-27] Generally, semi-fluorinated PFCB aryl ether polymers can be simply prepared by (i) polycondensation of bisphenol and 1,2-bis(aryl ether) hexafluorocyclobutyl halide monomers and/or (ii) free-radical mediated [2 + 2] thermal cyclo-dimerization of aryl bis-(trifluorovinyl ether) (TFVE) monomers as shown in Scheme 1.1.

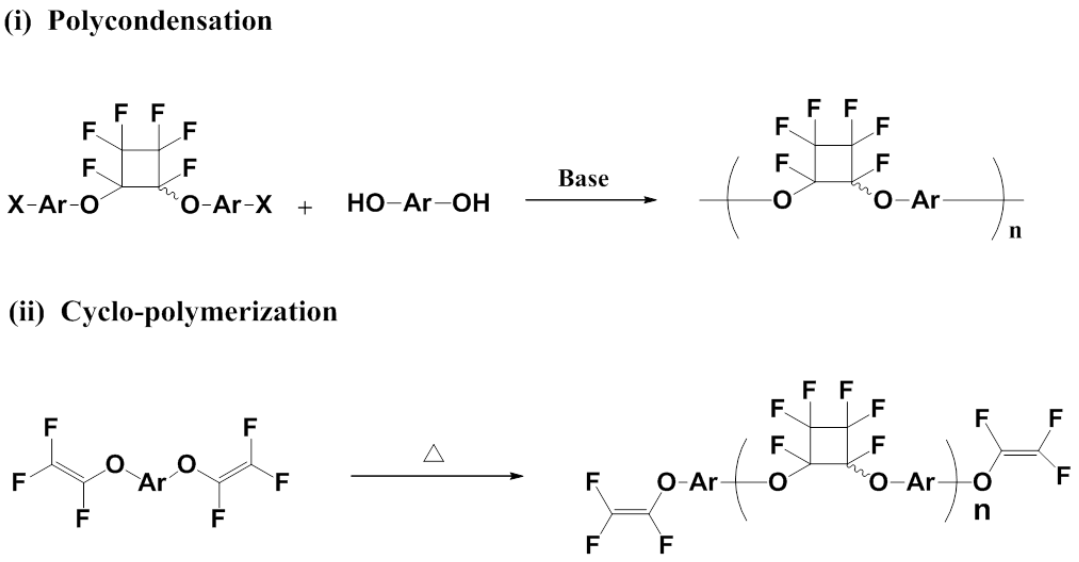

Scheme 1.1 (i) Polycondensation of bisphenol and 1,2-bis(aryl ether) hexafluorocyclo-butyl halide monomers and (ii) Free-radical mediated [2 + 2] thermal cyclo-dimerization of aryl bis-(trifluorovinyl ether) (TFVE) monomers to PFCB aryl ether polymers.

The polycondensation methodology has been recently attracted attention for other aryl fluorinated cyclic-compound such as perfluorocycloalkenyl (PFCA) aryl ether compounds.[28, 29] An advantage of thermal cyclo-polymerization is that it proceeds either

in high-boiling-point solvents or as a melt without initiator or catalyst. In addition, the resulting telechelic polymers with intact TFVE end groups can be applied for further transformation.[4] For example, aryloxylation of substituted phenols with aryl TFVE small molecules and oligomers was reported as a facile tailorable methodology for incorporating functional groups on the polymer chain ends.[30-33]

In summary, PFCB aryl ether polymers are well-established versatile polymers that allow for the design of new high-performance polymers having unique functionalities in the polymer backbone and also at the chain ends.[2, 11, 30, 31] The unique properties of PFCB ether unit (e.g., high thermal/chemical stability, excellent solubility/processability, and low dielectric constant) have been applied in a wide range of applications including high-performance coatings[17], electro-optics[17, 19], photonics[34], force-responsive materials[26], and proton-exchange membrane fuel cells (PEMFCs)[25, 35-37]. The PFCB aryl ether technology and selected physical properties of PFCB aryl ether polymers are summarized in Scheme 1.2 and Table 1.1. A review by Scott T. Iacono and co-workers has illustrated the preparation and general utility of PFCB aryl ether polymers.[38]

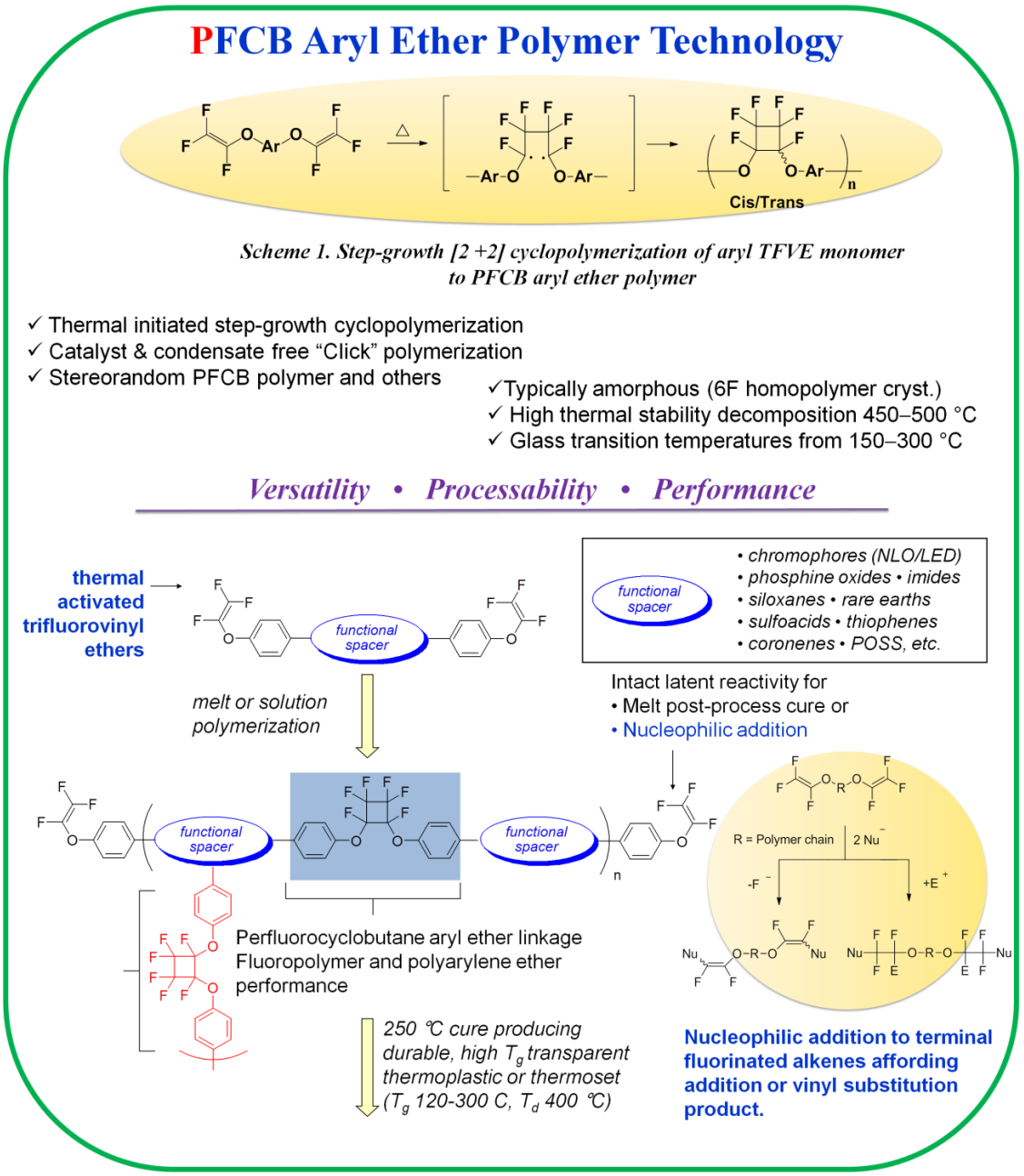

Scheme 1.2 PFCB aryl ether polymer technology.[38]

Table 1.1 Selected physical properties of PFCB aryl ether polymers.[38]

Property	Range
Mechanical	
Glass transition (DSC or DMA)	110–350 ºC
Thermal decomposition (TGA in N_2 & air)	>450 ºC
Tensile strength	50.3–66.0 MPa
Tensile modulus	1,770–2,270 MPa
Flexural strength	74.0–92.4 MPa
Percent elongation (break)	4.1–12.5%
Interfacial shear	123–163 MPa
Hardness	175–653 MPa
Processing	
Cure temperature/time (ºC)	150–220/0.1–3.0 h
Molecular weight (GPC)	1,200–30,000 Mw
Solution viscosity (RMS)	0.02–100 Pa s
Crystallinity (WAXD)	0–35%
Solid content	50–90%
Patterning technique	μ-molding, RIE, O_2 plasma
Spin coat thickness (μm, single)	1–30
Percent water absorption (wt%) (24 h)	0.021
Optical	
Loss (1,550 nm)	<0.25 dB/cm
Birefringence	<0.003
Refractive index (1,550 nm)	1.442–1.505
dn/dt (1,550 nm)	-0.7 to -1.5 ($X10^{-4}$)
Insulation	
Dielectric constant (10 kHz)	2.4–2.45
Dissipation factor (10 kHz)	0.0003–0.0004

[*J. Polym. Sci., Part A: Polym. Chem.* **2007,** *45*, 5705-5721] Reprinted by permission of John Wiley & Sons, Inc. under the license number 3284890693746. Copyright © 2007 by John Wiley Sons, Inc.)

Development of Fluoropolymers

Fluoropolymers exhibit excellent high performance characteristics that are not satisfied by other hydrocarbon based polymers. These include high chemical/heat resistance, low surface energy, piezoelectricity, selective permeability, and excellent electric insulation. Taking advantage of their special properties, fluoropolymers are used in many industries such as electrical and electronic, architectural and domestic, automotive, aerospace, and medical devices.[39]

These unique properties are imparted by a small fluorine atom. The strong bonding energy (472 kJ/mol) of the C-F bond compared to the C-H bond (413 kJ/mol) contributes to higher thermal stability. The small dipole moment of fluorine compounds contributes to their low surface energy, low refractive index, and low friction coefficient. A strong electron attracting ability of fluorine also leads to greater lipophilicity and excellent ability to block metabolic pathways.

The most common commercial fluoropolymers are synthesized from tetrafluoroethylene (TFE), chlorotrifluoroethylene (CTFE), and vinylidene fluoride (VDF) monomers via homopolymerization or copolymerization with initiator and are used in many applications such as non-stick coatings for cookware, insulating materials for electronics, chemical processing equipment liners, and surgical patches. Examples commercial synthetic fluoropolymers and their applications are listed in Figure 1.4 and Table 1.2.[39]

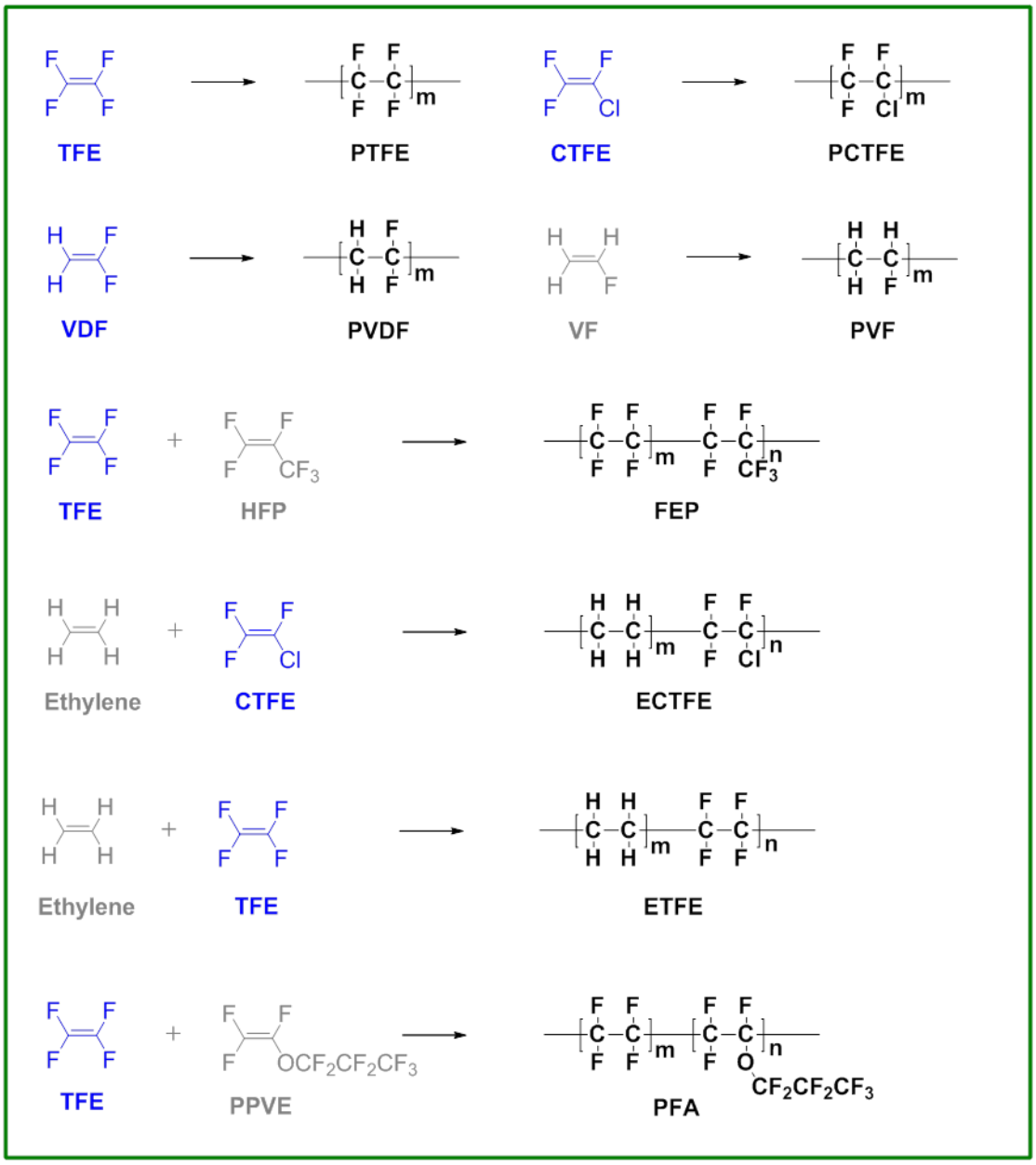

Figure 1.4 Examples of commercial fluoropolymers and their synthetic scheme. Key: tetrafluoroethylene(**TFE**), polytetrafluoroethylene(**PTFE**)[40], chlorotrifluoroethylene (**CTF**E), polychlorotrifluoroethylene (**PCTFE**)[41], vinylidene fluoride (**VDF**), polyvinylidene-fluoride (**PVDF**), vinylfluoride (**VF**), polyvinylfluoride (**PVF**),**:** hexafluoropropylene (**HFP**), fluorinated ethylene propylene (**FEP**), copolymer of Ethylene and CTFE (**ECTFE**)[42], copolymer of ethylene and TFE (**ETFE**)[43], perfluoropropylvinylether (**PPVE**)[44, 45], perfluoro-alkyoxy resin (**PFA**)[30, 31].

Table 1.2 Examples of commercial fluoropolymers and their applications.[39]

Fluoropolymer	Commercial Products	Melting Temp. (°C)	Applications
PTFE	• Teflon (DuPont) • Polyflon (Daikin) • Dyneon PTFE (Dyneon) • Fluon (Ashai Glass)	317–337	Wire Cable Chemical processing
PCTFE	• Kel-F (3M) • Neoflon PCTFE (Daikin) • Aclar (Honeywell) • Voltalef (Arkema)	210-215	Sealing Barrier film Packaging
FEP	• Teflon FEP (DuPont) • Neoflon FEP (Daikin) • Dyneon FEP (Dyneon)	260-282	Cable insulation
ECTFE	• Halar (Solvay)	235–245	Flame resistant Insulation
ETFE	• Tefzel (DuPont) • Fluon (Asahi Glass) • Halon ETFE (Solvay) • Neoflon ETFE (Daikin) • Dyneon ETFE (Dyneon)	254–279	Wire Cable insulation
PVF	• Tedlar (Dupont)	190-200	Film Coating Lamination
PVDF	• Kynar (Arkema) • Solef (Solvay) • Neoflon PVDF (Daikin)	155–192	Wire, Cable Coating Electronic
PFA	• Teflon PFA (DuPont) • Aflon PFA (Asahi Glass) • Dyneon PFA (Dyneon) • Neoflon PFA (Daikin) • Hyflon PFA (Solvay)	302–310	Flame resistant Insulation

However, many fluoropolymers (e.g., PTFE, PCTFE, FEP, ECTFE, and ETFE) have poor solubility/processability with high melt flow temperature due to their high crystallinity. Therefore, semi-crystalline and amorphous fluoropolymers have been developed to improve the processability, for example Dyneon THV from 3M, Cytop from Asahi Glass[44], Teflon AF from DuPont[45, 46], and Hyflon-AD from Solvay[47] as shown in Figure 1. 5.

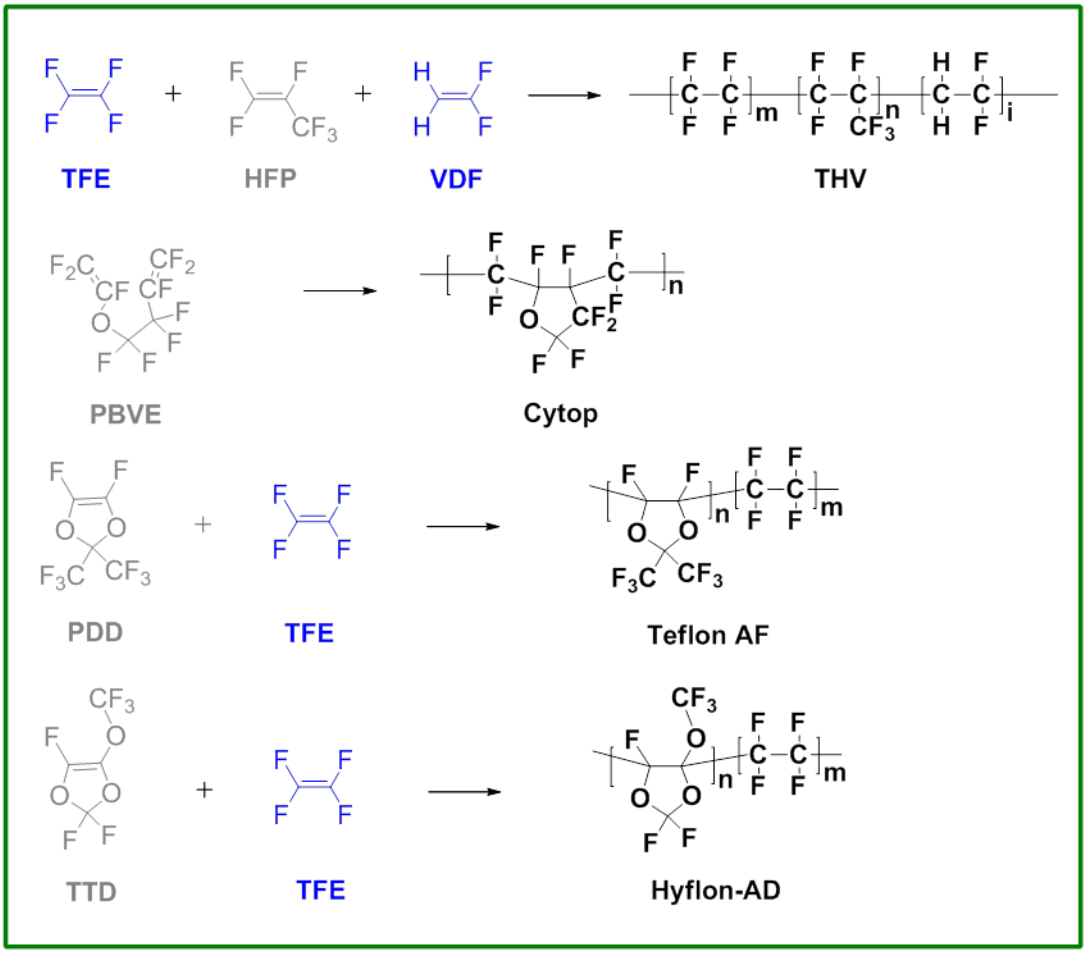

Figure 1.5 Examples of commercial semi-crystalline and amorphous fluoropolymers. Key: Copolymer of TFE, HFP, and VDF (**THV**), Perfluoro-3-butenyl-vinyl ether (**PBVE**), Perfluoro-2,2-dimethyl-1,3-dioxole (**PDD**), 2,2,4-trifluoro-5-trifluoro-methoxy-1,3-dioxole (**TTD**).

References

1. Goodall, G. W.; Hayes, W. Advances in Cycloaddition Polymerizations. *Chem. Soc. Rev.* **2006,** *35*, 280-312.

2. Babb, D. A.; Ezzell, B. R.; Clement, K. S.; Richey, W. F.; Kennedy, A. P. Perfluorocyclobutane Aromatic Ether Polymers. *J. Polym. Sci., Part A: Polym. Chem.* **1993,** *31*, 3465-3477.

3. Babb, D. A. Polymers from the Thermal ($2\pi + 2\pi$) Cyclodimerization of Fluorinated Olefins. In *Fluoropolymers 1: Synthesis*, Hougham, G.; Cassidy, P. E.; Johns, K.; Davidson, T., Eds. Plenum Press: New York, 1999; pp 25–50.

4. Lewis, E. E.; Naylor, M. A. Pyrolysis of Polytetrafluoroethylene. *J. Am. Chem. Soc.* **1947,** *69*, 1968-1970.

5. Lacher, J. R.; Tompkin, G. W.; Park, J. D. The Kinetics of the Vapor Phase Dimerization of Tetrafluoroethylene and Trifluorochloroethylene. *J. Am. Chem. Soc.* **1952,** *74*, 1693-1696.

6. Atkinson, B.; Trenwith, A. B. The Thermal Decomposition of Tetrafluorethylene. *J. Am. Chem. Soc.* **1953**, 2082-2087.

7. Montgomery, L. K.; Schueller, K.; Bartlett, P. D. Cycloaddition. II. Evidence of a Biradical Intermediate in the Thermal Addition of 1,1-Dichloro-2,2-difluoroethylene to the Geometrical Isomers of 2,4-Hexadiene. *J. Am. Chem. Soc.* **1964,** *86*, 622-628.

8. Mifsud, N.; Mellon, V.; Jin, J.; Topping, C. M.; Echegoyen, L.; Smith, D. W. First Identification of Biradicals during Thermal [2π + 2π] Cyclopolymerization of Trifluorovinyl Aromatic Ethers. *Polym. Int.* **2007,** *56*, 1142-1146.

9. Clark Ligon Jr, S.; Krawiec, M.; Kitaygorodskiy, A.; Smith Jr, D. W. First Separation and Characterization of *cis* and *trans* 1,2-bisaryloxy Perfluorocyclobutanes. *J. Fluorine Chem.* **2003,** *123*, 139-146.

10. Bernett, W. A. Hybridization Effects in Fluorocarbons. *J. Org. Chem.* **1969,** *34*, 1772-1776.

11. Smith, D. W.; Babb, D. A. Perfluorocyclobutane Aromatic Polyethers. Synthesis and Characterization of New Siloxane-Containing Fluoropolymers. *Macromolecules* **1996,** *29*, 852-860.

12. Iacono, S. T. Semifluorinated Polymers via Cycloaddition and Nucleophilic Addition Reactions of Aromatic Trifluorovinyl Ethers. Ph.D Thesis, Clemson University, 2008.

13. Beckerbauer, R., Fluorocarbon Ethers. U.S. Patent 3,397,191, Aug 13, 1968.

14. Babb, D. A.; Clement, K. S.; Richey, W. F.; Ezzell, B. R., Perfluorocyclobutane Ring-containing Polymers. U.S. Patent 5,037,917, Aug 6, 1991.

15. Jiang, X. Z.; Liu, S.; Liu, M. S.; Herguth, P.; Jen, A. K. Y.; Fong, H.; Sarikaya, M. Perfluorocyclobutane-Based Arylamine Hole-Transporting Materials for Organic and Polymer Light-Emitting Diodes. *Adv. Funct. Mater.* **2002,** *12*, 745-751.

16. Smith, D. W.; Chen, S.; Kumar, S. M.; Ballato, J.; Topping, C.; Shah, H. V.; Foulger, S. H. Perfluorocyclobutyl Copolymers for Microphotonics. *Adv. Mater.* **2002,** *14*, 1585-1589.

17. Jin, J.; Smith, D. W.; Topping, C. M.; Suresh, S.; Chen, S.; Foulger, S. H.; Rice, N.; Nebo, J.; Mojazza, B. H. Synthesis and Characterization of Phenylphosphine Oxide Containing Perfluorocyclobutyl Aromatic Ether Polymers for Potential Space Applications. *Macromolecules* **2003,** *36*, 9000-9004.

18. Ballato, J.; Foulger, S. H.; Smith, J. D. W. Optical Properties of Perfluorocyclobutyl Polymers. II. Theoretical and Experimental Attenuation. *J. Opt. Soc. Am. B* **2004,** *21*, 958-967.

19. Spraul, B. K.; Suresh, S.; Glaser, S.; Perahia, D.; Ballato, J.; Smith, D. W. Perfluorocyclobutyl-Linked Hexa-peri-hexabenzocoronene Networks. *J. Am. Chem. Soc.* **2004,** *126*, 12772-12773.

20. Ford, L. A.; DesMarteau, D. D.; Smith Jr, D. W. Perfluorocyclobutyl (PFCB) Aromatic Polyethers: Synthesis and Characterization of New Sulfonimide Containing Monomers and Fluoropolymers. *J. Fluorine Chem.* **2005,** *126*, 651-658.

21. Perpall, M. W.; Smith, D. W.; DesMarteau, D. D.; Creager, S. E. Alternative Trifluorovinyl Ether Derived Fluoropolymer Membranes and Functionalized Carbon Composite Electrodes for Fuel Cells. *J. Macromol. Sci., Polym. Rev.* **2006,** *46*, 297-313.

22. Iacono, S. T.; Budy, S. M.; Mabry, J. M.; Smith, D. W. Synthesis, Characterization, and Surface Morphology of Pendant Polyhedral Oligomeric

Silsesquioxane Perfluorocyclobutyl Aryl Ether Copolymers. *Macromolecules* **2007,** *40*, 9517-9522.

23. Neilson, A. R.; Budy, S. M.; Ballato, J. M.; Smith, D. W. Mixed Chromophore Perfluorocyclobutyl (PFCB) Copolymers for Tailored Light Emission. *Macromolecules* **2007,** *40*, 9378-9383.

24. Mujkic, M.; Iacono, S. T.; Neilson, A. R.; Smith, D. W. Recent Optical Applications of Perfluorocyclobutyl Aryl Ether Polymers. *Macromol. Symp.* **2009,** *283–284*, 326-335.

25. Qian, G.; Smith, D. W., Jr.; Benicewicz, B. C. Synthesis and Characterization of High Molecular Weight Perfluorocyclobutylcontaining Polybenzimidazoles (PFCB–PBI) for High Temperature Polymer Electrolyte Membrane Fuel Cells. *Polymer* **2009,** *50*, 3911–3916.

26. Klukovich, H. M.; Kean, Z. S.; Iacono, S. T.; Craig, S. L. Mechanically Induced Scission and Subsequent Thermal Remending of Perfluorocyclobutane Polymers. *J. Am. Chem. Soc.* **2011,** *133*, 17882-17888.

27. Lee, K.-S.; Jeong, M.-H.; Kim, Y.-J.; Lee, S.-B.; Lee, J.-S. Fluorinated Aromatic Polyether Ionomers Containing Perfluorocyclobutyl as Cross-Link Groups for Fuel Cell Applications. *Chem. Mater.* **2012,** *24*, 1443-1453.

28. Cracowski, J.-M.; Sharma, B.; Brown, D. K.; Christensen, K.; Lund, B. R.; Smith, D. W. Perfluorocyclopentenyl (PFCP) Aryl Ether Polymers via Polycondensation of Octafluorocyclopentene with Bisphenols. *Macromolecules* **2011,** *45*, 766-771.

29. Sharma, B.; VanDerveer, D. G.; Liff, S. M.; Smith Jr, D. W. Bis-perfluorocycloalkenyl (PFCA) Aryl Ether Monomers towards a Versatile Class of Semi-fluorinated Aryl Ether Polymers. *Tetrahedron Lett.* **2013,** *54*, 3609-3612.

30. Moody, J. D.; VanDerveer, D.; Smith Jr, D. W.; Iacono, S. T. Synthesis of Internal Fluorinated Alkenes via Facile Aryloxylation of Substituted Phenols with Aryl Trifluorovinyl Ethers. *Org. Biomol. Chem.* **2011,** *9*, 4842-4849.

31. Park, J.; Oh, J.-M.; Creager, S. E.; Smith Jr, D. W. Grafting of Chain-End-Functionalized Perfluorocyclobutyl (PFCB) Aryl Ether Ionomers onto Mesoporous Carbon Supports. *Chem. Commun.* **2012,** *48*, 8225-8227.

32. Buquoi, J. Q.; Smith, D. W.; Iacono, S. T. Kinetic Study of Semifluorinated Arylene Vinylene Ether Polymers. *J. Polym. Sci., Part A: Polym. Chem.* **2011,** *49*, 4441-4447.

33. Keck, S.; Knoerzer, T. A.; Smith, D. W.; Iacono, S. T. Preparation of Partially Fluorinated Aryl/alkyl Vinylene Ether Polymers. *Polym. Int.* **2013,** *62*, 1485-1491.

34. Smith, D. W.; Chen, S.; Kumar, S. M.; Ballato, J.; Topping, C.; Shah, H. V.; Foulger, S. H. Perfluorocyclobutyl Copolymers for Microphotonics. *Adv. Mater.* **2002,** *14*, 1585-1589.

35. Iacono, S. T.; Ewald, D.; Sankhe, A.; Rettenbacher, A.; Smith, D. W., Jr. Sulfonated Fluorovinylene Aromatic Ether Polymers for Proton Exchange Membranes. *High Perform. Polym.* **2007,** *19*, 581–591.

36. Mackinnon, S. M.; Fuller, T. J.; Coms, F., Sulfonated Perfluorocyclobutane Block Copolymers and Proton Conductive Polymer Membranes. U.S. Patent 7,897,692, Mar 1, 2011.

37. Wagener, E.; Smith Jr, D. W.; Topping, C.; Jayasinghe, R.; Jin, J.; Singh, A.; Mackinnon;, S. M.; Timothy J, F.; Craig S, G., In *Workshop on Advances in Polymer Electrolyte Membrane Fuel Cell Systems, Am. Chem. Soc., Div. Polym. Chem.*: Pacific Grove CA, 2009.

38. Iacono, S. T.; Budy, S. M.; Jin, J.; Smith, D. W. Science and Technology of Perfluorocyclobutyl Aryl Ether Polymers. *J. Polym. Sci., Part A: Polym. Chem.* **2007,** *45*, 5705-5721.

39. Teng, H. Overview of the Development of the Fluoropolymer Industry. *Appl. Sci.* **2012,** *2*, 496-512.

40. Plunkett, R. J., Tetrafluoroethylene Polymers. U.S. Patent 2,230,654, Feb 4, 1941.

41. Dittman, A. L.; Wrightson, J. M., Manufacture of Halocarbons. U.S. Patent 2,636,908, April 2, 1953.

42. Ford, T. A., Copolymers of Vinylidene Fluoride with Ethylene and Halogenated Ethylenes. U.S. Patent 2,468,054 Apr 26, 1949.

43. Dana P, C.; Chadds Ford, P.; Kerbow, D. L.; Vienna, W. V.; Leek, T. J.; Orange, T.; Olson, A.; Parkersburg, W. V., Heat Stable Tetrafluoroethylene-perfluoro(alkyl vinyl ether) Copolymers. U.S. Patent 4,599,386, Jul 8, 1986.

44. Nakamura, M.; Kaneko, I.; Oharu, K.; Kojima, G.; Matsuo, M.; Samejima, S.; Kamba, M., Novel Fluorine-containing Cyclic Polymer. U.S. Patent 4,897,457, Jan 30, 1990.

45. Resnick, P. R., Fluorinated Dioxoles. U.S. Patent 3,865,845, Feb 11, 1975.

46. Resnick, P. R., Polymers of Fluorinated Dioxoles. U.S. Patent 3,978,030, Aug 31, 1976.

47. Navarrini, W.; Tortelli, V.; Colaianna, P.; Abusleme, J. A., Perfluorodioxoles, the Preparation Process thereof, and Homopolymers and Copolymers obtained therefrom. European Patent 0,633,257, Apr 9, 1997.

CHAPTER TWO

PERFLUOROCYCLOBUTYL ARYL ETHER SEGMENTED COPOLYMERS

Introduction

PFCB containing polymers are used in a wide range of applications such as force responsive materials[1], high performance coatings[2, 3], electro-optics[2, 4-6], photonics[7-9], and fuel cells[3, 10-18]. Although the most well-established materials are highly processable and tailorable PFCB aryl ether homopolymers[19-23], which are usually synthesized via step-growth [2 + 2] cyclo-polymerization, PFCB copolymers have also been described intensively in literatures[7, 24]. In most cases the PFCB copolymers are known to be random in nature[7] for which the monomer sequences are unknown and difficult to control due to the statistical nature of step-growth mechanisms.[25] Precise control on monomer distribution in copolymers not only provides opportunities for understanding unique properties of resulting copolymers[26-28] but also offers a means of controlling polymer morphology, for example via post-modification and/or self-assembly of sequenced-controlled functional copolymers[29-34]. A need exists for well-defined PFCB copolymers, which provide wide variability of polymer structures, and for which the chemical nature of the copolymers may be understood and controlled so as to allow for rational design of materials via chemical reactions at the polymer backbones. For example, selective functionalization of such sequence-controlled copolymers could create a material having well defined pathways for ion transport in energy devices such as fuel cells and photovoltaic cells.

Recently, Tetramer Technologies, L.L.C. and General Motors have reported PFCB aryl ether block copolymers having sulfonic acid groups for proton exchange membrane fuel cells (PEMFCs).[13-16] A marked improvement of proton conductivity and mechanical properities was observed in the selectively-sulfonated hydrophilic-hdrophobic block copolymer membranes, relative to the homopolymer membranes. However, explicit evidence of the blocky structures in their copolymers was not provided in their report. Furthermore, multi-step polymerizations were required to synthesize the PFCB block copolymers, for example at least one pre-made oligomer was needed. We herein describe a facile synthetic route for segmented PFCB aryl ether copolymers, which are synthesized directly from two aryl TFVE monomers having different reactivities, as well as evidence of the blocky copolymer structures using ^{19}F NMR spectroscopic data. Along with selective copolymerization, the effect of their microstructures on sulfonation selectivity is also discussed in this chapter. To the best of our knowledge, this report contains the first realization of selective [2 + 2] cyclo-copolymerization of TFVE monomers toward segmented PFCB copolymer and its monomer sequence distribution in the copolymer chains.

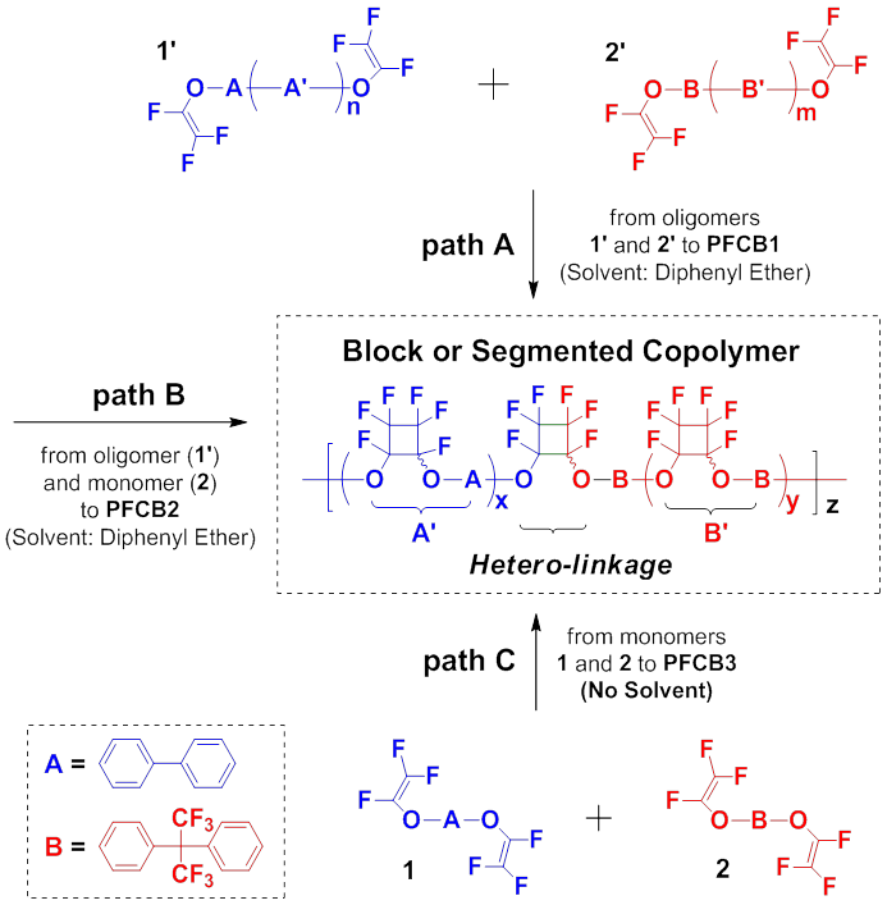

Scheme 2.1 Thermal [2 + 2] cycloaddition reactions of TFVEs toward blocky copolymers.

Synthesis of PFCB Aryl Ether Copolymers

Scheme 2.1 illustrates a PFCB aryl ether copolymer architecture consisting of two different segments (e.g., A' and B') with hetero- linkages. To investigate the effect of copolymer compositions and/or structures on their chemical/thermal properties, we prepared two copolymers through path A and B, which afforded a block copolymer.[13] This synthesis of the PFCB aryl ether segmented copolymer is straightforward and can be

performed on a large scale with high efficiency and technical simplicity. The [2 + 2] cycloaddition of TFVE moities is thermally induced easily under argon atmosphere without a catalyst or initiator due to the stabilization contributed by an ether linkage and the smaller angular strain of PFCB rings (32.0 kcal/mol) than that of fluoro-olefins (41.2 kcal/mol).[35-37] This synthetic methodology does not demand a multi-step process such as protection-deprotection cycles to obtain segmented copolymers. Furthermore, it turned out that preparation of oligomers are not necessary for segmented copolymers. Our version of a [2 + 2] step-growth cyclocopolymerization was carried out via selective cycloaddition reactions of two aryl TFVE monomers: a monomer (1) bearing biphenyl group, the monomer (2) incorporating the isofluoropropyl electron withdrawing group between two phenyl rings as shown in Scheme 2.1, path C. The PFCB aryl ether copolymers were designated as PFCB1, PFCB2, and PFCB3, which were synthesized using a combination of (i) two oligomers (1' and 2'), (ii) oligomer and monomer (1' and 2), and (iii) two monomers (1 and 2), respectively (Scheme 1 and Table 1).

As described in Scheme 2.2, different chain length of BP (n=0, 22) and 6F (m= 0, 30) reactants were used to investigate the effect of block length and compositions on physiochemical properties of polymers. The polymerization to achieve the high molecular weight was successfully conducted by controlling the polymerization time and temperature ranged from 140-210 °C. The thermally initiated [2 + 2] cyclopolymerization proceeded easily under argon atmosphere and afforded fibrous polymers.

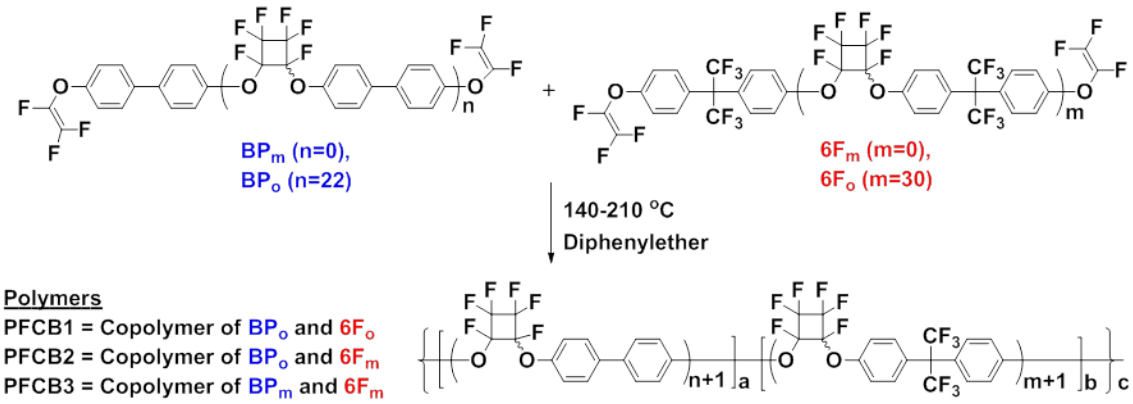

Scheme 2.2 Preparation of PFCB Aryl Ether Copolymers.

Table 2.1 Compositional ratios of PFCB aryl ether copolymers.

Polymer	**Weight Feed Ratio** of Starting Reagents	**Molar Ratio** of repeating units (**BP : 6F**) [a]	
		Theoretical Ratio (feeding amount)	**Experimental Ratio** (^{19}F NMR)
PFCB1 (BP_o-*co*-$6F_o$)	1:1 (BP_o: $6F_o$)	35:65	55:45
PFCB2 (BP_o-*co*-$6F_m$)	1:1 (BP_o : $6F_m$)	59:41	53:47
PFCB3 (BP_m-*co*-$6F_m$)	1:1 (BP_m : $6F_m$)	50:50	50:50

[a] Theoretical and experimental molar ratio of BP and 6F repeating units estimated by initial feeding amount of starting reagents and ^{19}F NMR spectroscopic data of resulting copolymer, respectively.

One of the advantages of this synthetic route is to be able to quantify the degree of polymerization by monitoring the decrease and increase in intensity of the fluorooelfin end groups and PFCB moities by ^{19}F NMR spectroscopy. The molecular structure of copolymers and the conversion of TFVE groups to the PFCB ether moieties were confirmed by ^{1}H and ^{19}F NMR spectroscopy (Figure 2.1). As seen from the ^{19}F NMR of PFCB2, the characteristic AMX pattern as three sets of doublets of doublets (i.e., –119.2 ppm (*trans to O*), –126.1 ppm (*cis to O*) and –133.8 ppm (*geminal to O*)) of fluorovinyl end groups on the BP oligomer and 6F monomer completely disappeared. This indicates high conversion of TFVE end groups to perfluorocyclobutyl ether moieties via cyclopolymerization. The relative integrals of these singlet and multiplet peaks for isofluoropropyl-F_6 and cyclobutyl-F_6 were used to calculate the ratios of the BP and 6F compositions. Table 2.1 summarizes the experimental compositional ratios of each repeat unit of the polymers, which were determined by ^{19}F NMR measurements, in comparison with the theoretical compositions of BP and 6F repeat units. The experimental compositions for PFCB2 and PFCB3 agreed well with the theoretical values. On the other hand, the experimental composition ratio of BP and 6F unit for PFCB1 was not in good agreement with its theoretical one. Lower 6F composition ratio than theoretical value of PFCB1 is thought to have been caused by low reactivity of long chain 6F oligomer.

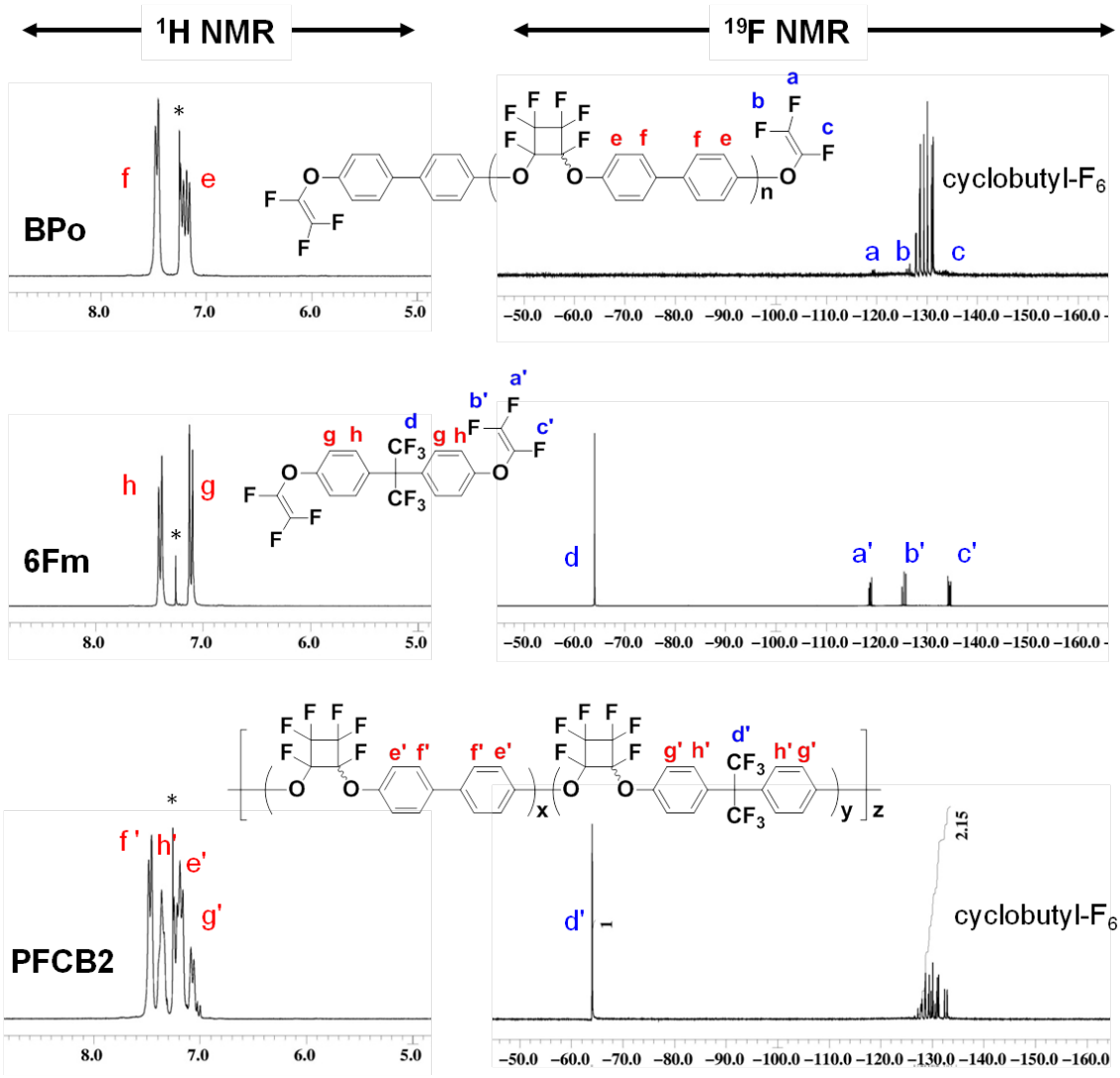

Figure 2.1 ^{1}H NMR (in $CDCl_3$*, left) and ^{19}F NMR (in $CDCl_3$*, right) spectra of BP oligomer (BPo), 6F monomer (6Fm), and PFCB2 (BPo-*co*-6Fm) copolymer.

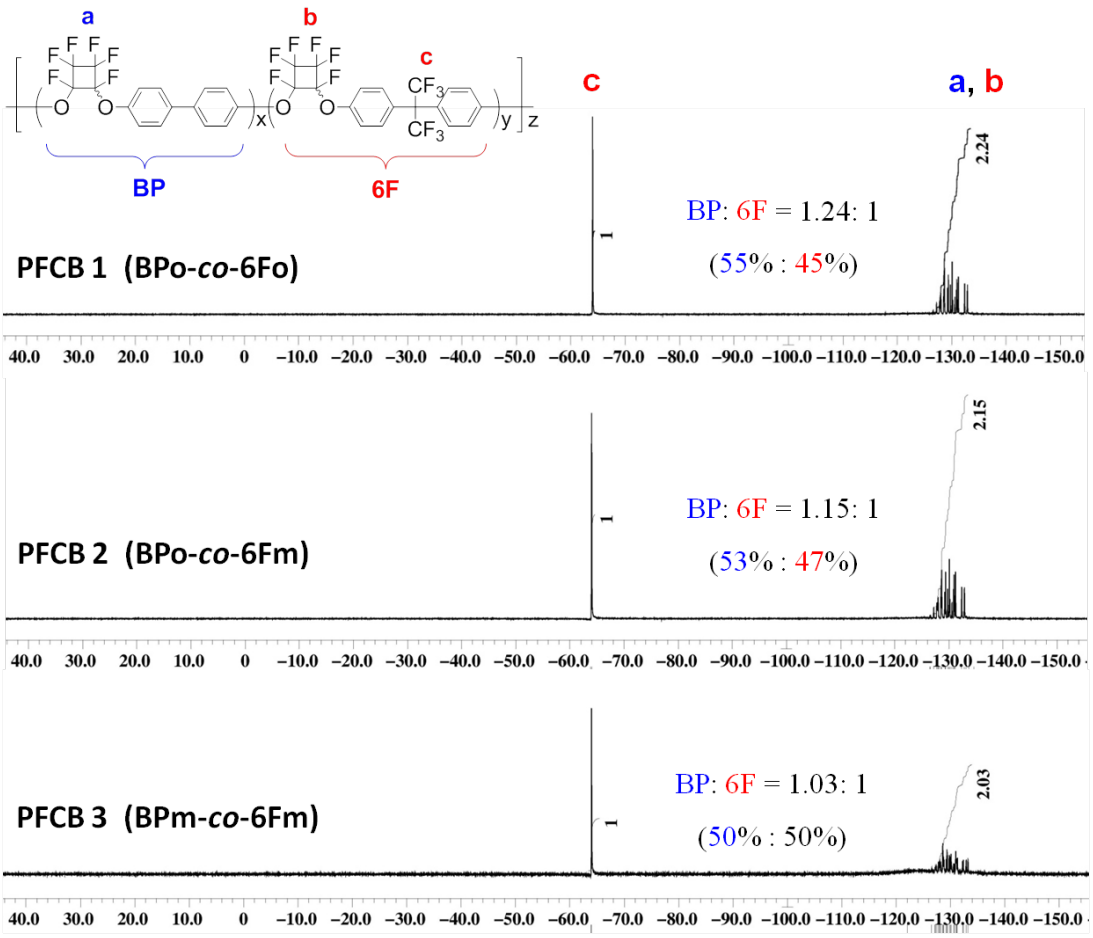

Figure 2.2 ^{19}F NMR (in $CDCl_3$) spectra of (a) PFCB1 (BPo-*co*-6Fo), (b) PFCB2 (BPo-*co*-6Fm), and (c) PFCB3 (BPm-*co*-6Fm) copolymers with their compositional ratios of the BP and 6F enchainment.

The compositional analysis can also be achieved by ^{1}H NMR. However, a quantitative analysis on the monomer distribution cannot be made in this work because protons in the hetero-linkage of BP and 6F have almost the same values as those of homo-linkage of BP and 6F. On the other hand, the ^{19}F NMR spectra provide probes for the monomer distribution in the polymer backbone. The monomer sequences of copolymers were found to be sensitive to the chemical shift for fluorines of the resulting PFCB isomers as shown in Figure 2.3. Remarkably, the fluorines of each isomer are uniquely and clearly distinguished by ^{19}F NMR spectroscopy. Since PFCB moities produced *via* co-dimerization was distinguished from the homo-dimerized PFCB rings in the ^{19}F NMR spectra, the cis/trans diastereomeric ratio of PFCB ether moities[38, 39] and the compositional ratios of the BP and 6F repeat unit in the PFCB copolymer chains can also be simply estimated by ^{19}F NMR spectroscopy (Figure 2.3).

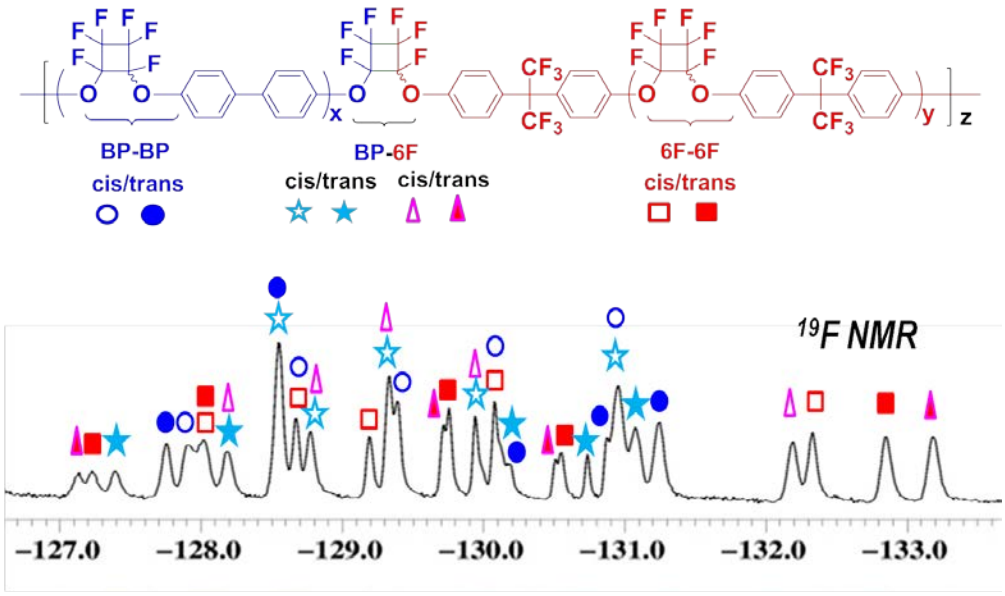

Figure 2.3 ^{19}F NMR (in $CDCl_3$*, right) spectra of **PFCB3** (BPm-*co*-6Fm) copolymer.

The PFCB ring bears six different chemical environments in the mixture with six possible isomers (2 stereo-isomers for each 3-regio-isomers); *cis* and *trans* in BP homo-linkage, *cis* and *trans* in 6F homo-linkage, and *cis* and *trans* BP-6F hetero-linkage. Scheme 2.3 illustrates homo- and hetero-linkage types of BP and 6F repeat units. All of the three linkages were identified as *cis/trans* (50:50) isomers and the fractional values of heterolinkage and homolinkages in the copolymer were estimated from the intensities of their peaks (Figure 2.4). This clear ^{19}F NMR spectroscopic data is a great tool to understand monomer distribution in the PFCB copolymer structures. The understanding monomer distribution of PFCB aryl ether copolymers are worthy of notice to develop a more advanced class of high-performance PFCB containing macromolecules such as a sequence-controlled macromolecules. The percent of hetero-linkage and homo-linkages calculated from the intensities of their signals in the specific range of ^{19}F NMR from –127 to –134 ppm are listed in Table 2.2.

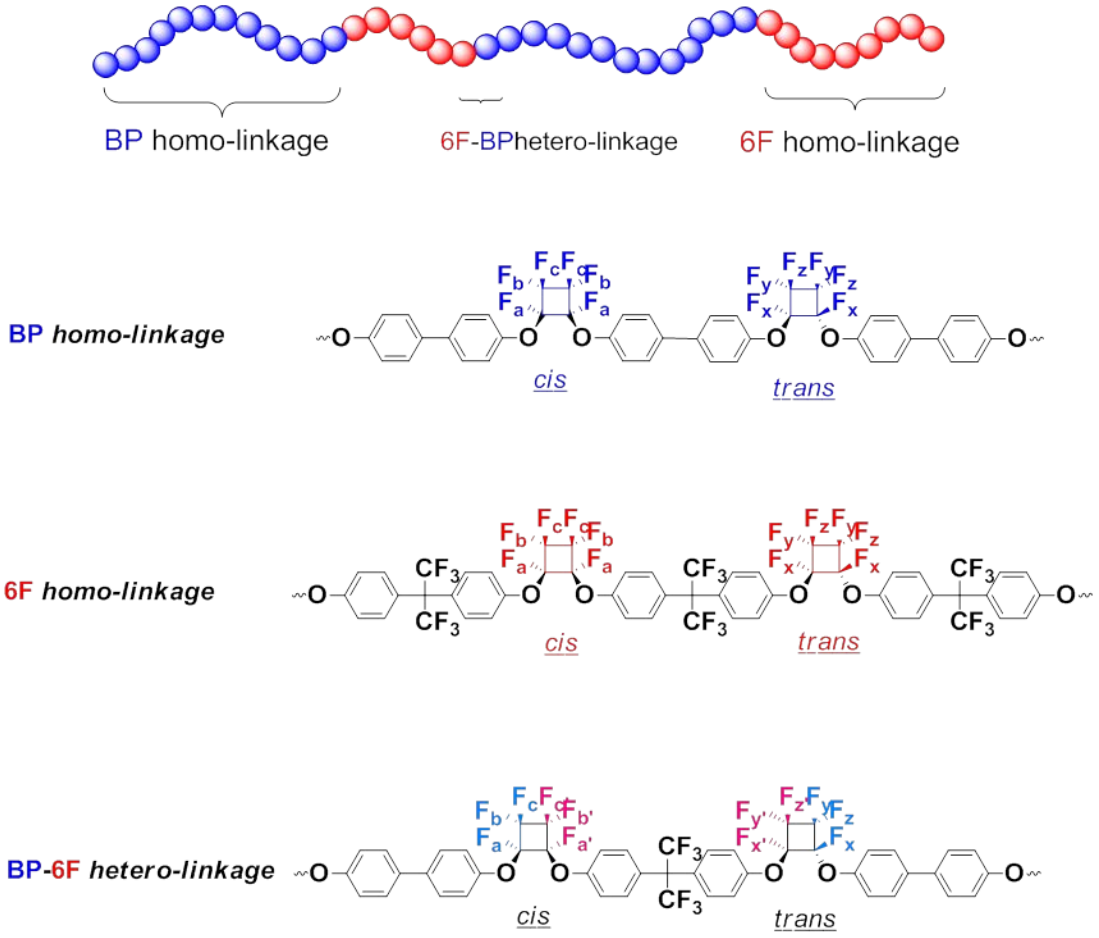

Scheme 2.3 Illustration of diastereomeric PFCB ethers.

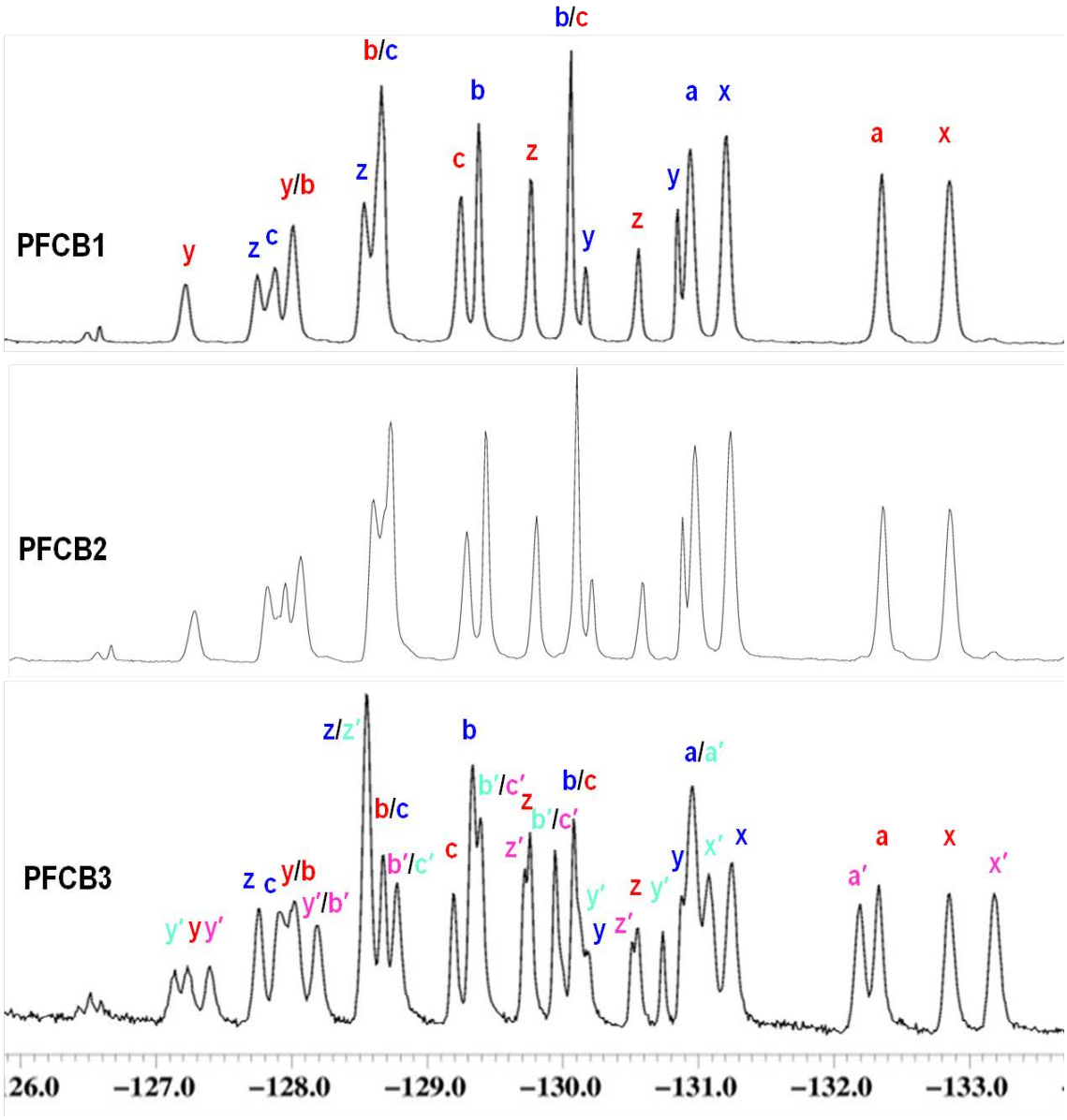

Figure 2.4 ^{19}F NMR (in $CDCl_3$*, right) spectra from –127 to –134 ppm of (a) PFCB1 (BPo-*co*-6Fo), (b) PFCB2 (BPo-*co*-6Fm), and (c) PFCB3 (BPm-*co*-6Fm) copolymers.

Table 2.2 Monomer distribution in PFCB aryl ether copolymers.

Polymer	Molar ratio of BP : 6F [a]	Sequence distribution(%) [b]		
		BP-BP	6F-6F	BP-6F
PFCB1 (BP_o-*co*-$6F_o$)	55:45	55	45	NA
PFCB2 (BP_o-*co*-$6F_m$)	53:47	53	44	3
PFCB3 (BP_m-*co*-$6F_m$)	50:50	35	33	32

[a] Molar ratio of BP and 6F repeating units estimated from the ^{19}F NMR spectrum of the resulting copolymer. [b] Monomer sequence distribution determined by ^{19}F NMR; BP-BP, 6F-6F, and and BP-6F refers to BP homo-linkage, 6F homo-linkage, and BP-6F hetero-linkage, respectively.

Theoretically, two pre-made PFCB oligomers produce blocky copolymers (Scheme 2.1, Path A). As expected, the PFCB1 (BPo-*co*-6Fo) was a block copolymer which is composed of negligible BP-6F heterolinkage with 49% of the BP homolinkage and 51% of the 6F homolinkage (Figure 2.4). In addition, the block copolymer (PFCB2) was also prepared through a selective-copolymerization of BP oligomers and 6F monomers in one-pot single copolymerization. In general, a selective copolymerization tends to occur when the comonomer ratio is very low. In addition, when it comes to a

steric aspect, cyclo-addition reaction of monomers takes place more quickly than oligomers because the long oligomer chains need proper spatial orientation to be able to undergo polymerization.[36] The relatively rapid homo-polymerization of 6F monomers results in the block- or segmented copolymer formation as illustrated in Scheme 2.4. The block copolymer (PFCB2) formation was confirmed by ^{19}F NMR showing only small portion of the BP-6F heterolinkage (3%). We note that these quantitative studies using ^{19}F NMR spectroscopic data provides the first explicit evidence of its blocky copolymer structure.

At an equal molar ratio of monomers, the selectivity toward dimerization is known to be dramatically reduced along with increasing statistical nature with a high comonomer concentration at the early polymerization stages. Therefore, the polymerization of two TFVE monomers has been thought to give random copolymers up to date. However, it turned out that the copolymerization of BP monomers and 6F monomers afforded a segmented copolymer (**PFCB3**), which is composed of a 1:1:1 ratio of BP-BP to 6F-6F homolinkage to BP-6F heterolinkage as shown in Figure 2.4. Scheme 2.5 illustrates the rationalization of copolymer types (e.g., block, segmented, random, and alternative copolymer) along with linkage ratios. This experimental data provides a first realization of segmented copolymer formation from TFVE monomers *via* selective copolymerization in a single polymerization.

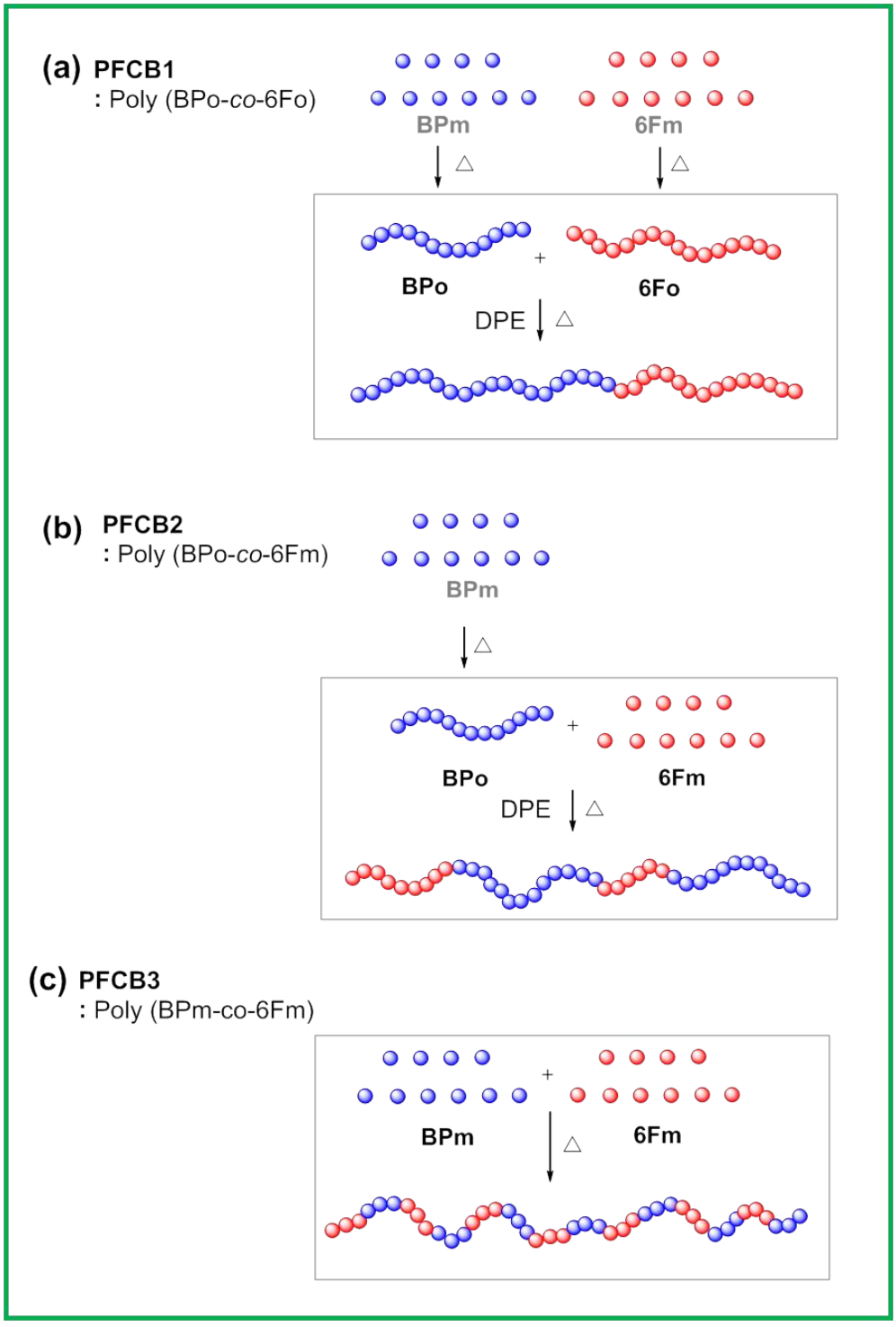

Scheme 2.4 Illustration of copolymer formations: (a) PFCB1, (b) PFCB2, and (c) PFCB3 segmented-copolymer.

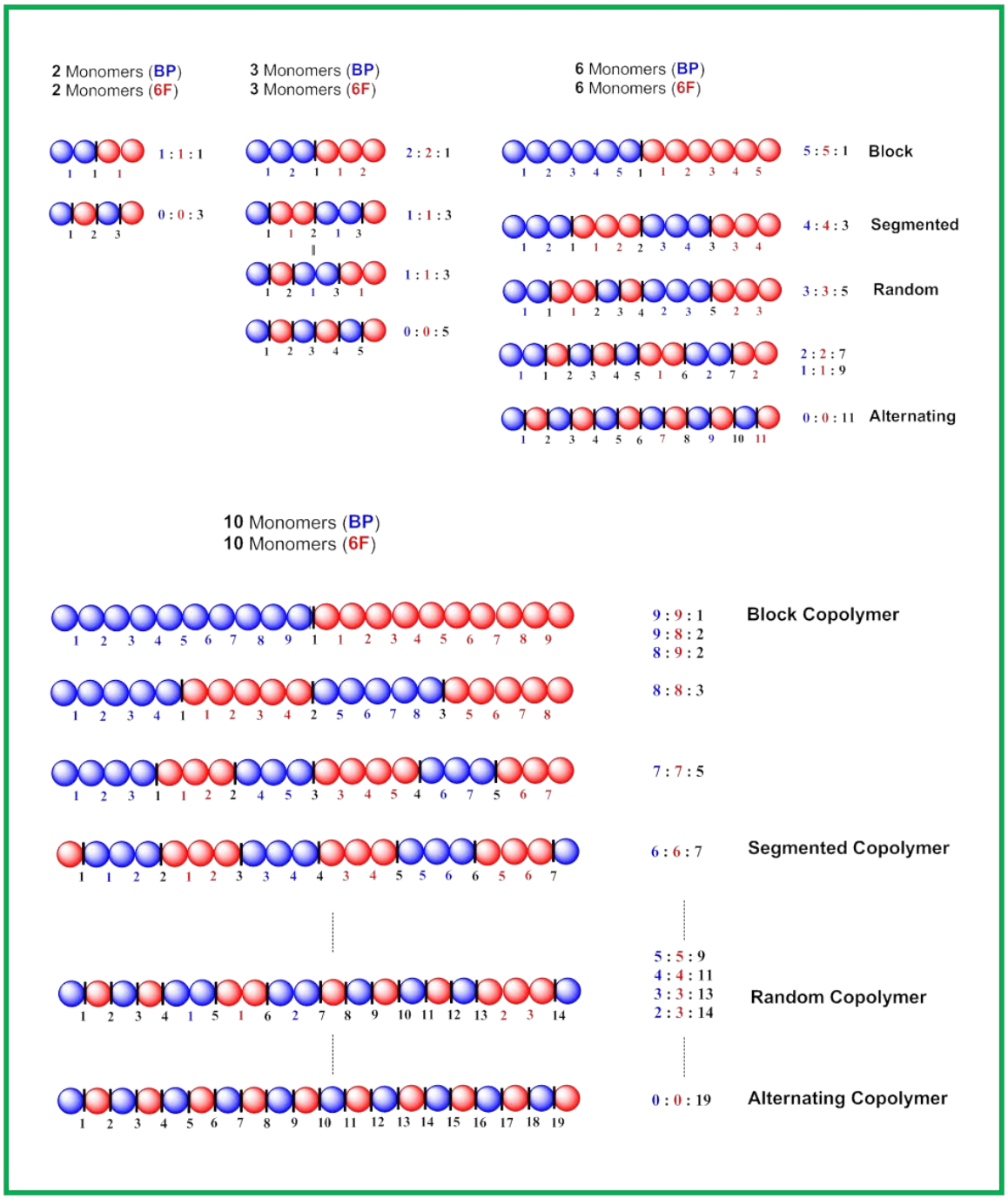

Scheme 2.5 Rationalization of copolymer types along with ratios of BP homo-linkage, 6F homo-linkage, and BP-6F hetero-linkage: Block, Segmented, Random, and Alternating Copolymer.

These selective copolymerization results of PFCB2 and PFCB3 are consistent with previous kinetic studies for the [2 + 2] cycloaddition of fluorovinyl ethers with electronic and steric aspect.[36, 40] Spraul and co-workers reported the second-order rate constants for cyclodimerization of aryl TFVE with various substitutions using a Hammett plot of log*K* vs. p*Ka*.[40] This study probed the electronic effects of substitutions on the aromatic trifluorovinyl ether cyclodimerization and demonstrated the trifluorovinyl ether monomers with electron withdrawing groups on the phenyl rings were less reactive toward cyclodimerization than those with electron donating groups. The calculated reaction constant (ρ) values are – 0.46 at 120 °C and – 0.59 at 130 °C, which implies that TFVE monomers hold a large charge separation in their transition state (TS). Therefore, 6F monomer containing electron withdrawing group between the phenyl rings destabilize the TS and leads higher energy barrier between reactants and diradical intermdiate resulting in less reactivity toward cyclodimerization than that of BP monomer. Previously, Wlassics[36] has reported the kinetic experiments for the cycloaddition of fluoroolefins and the effect of the substitution directly on the fluoroolefins and fluorovinyl ethher cyclodimerization. Wlassics[25] has also reported the effect of the chain length on the kinetics of cyclodimerization. Homo-dimerization of oligomers takes place more slowly than co-dimerization or homo-dimerization of monomers in a steric aspect.

In order to explain the reactivity and selectivity of cycloaddition reaction of the fluoroolefines (e.g., **1** and **2**), the barrier heights for these cycloaddition reactions were computationally studied using several DFT methods with collaborator Tugba G. Kucukkal and Prof. Steven J. Stuart.[41, 42] All calculations were performed with no

solvent taking advantage of the fact that the experimental study of path A did not involve a solvent. Transition state structures were located at the B3LYP/6-31G(d)[43-47] level of theory. In the present study (Scheme 2.6), the trans and/or cis configurations of transition states are considered as the barrier heights associated with the C-C bond formation for cis and trans conformations are found to be sufficiently close, for example the activation energies for the cis and trans configurations of S1 are 27.8 kcal mol^{-1} and 28.0 kcal mol^{-1}, respectively. The two reactions present low activation barriers: 28.0 kcal mol^{-1} for TS-S11 and 28.1 kcal mol^{-1} for TS-S12. On the other hand, the TS-S22 (43.4 kcal mol^{-1}) is higher in energy than those associated with the BP. Also, energies of the B3LYP/6-31G(d)-optimized transition state geometries were further calculated at the B3LYP/6-31+G(d)[43-48], B3LYP/6-311++G(d,p)[43-48], mPW1PW91/6-31G+(d,p) [45-49], wB97X/cc-pVTZ[50-53], and M062X/6-31+G(d,p)[45-49, 54] levels of theory. The same trend in the activation energies was consistently observed with all the methods, i.e. the activation energy of SS2 was found to be ~10-17 kcal mol^{-1} larger than that of S11. In the light of these results, faster homodimerization of BP is expected, while slow homodimerization is expected with the 6F. This agrees with the experimentally observed selectivity. The Ea value for S11, S12, and S22 with different DFT methods is given in the Table 2.3.

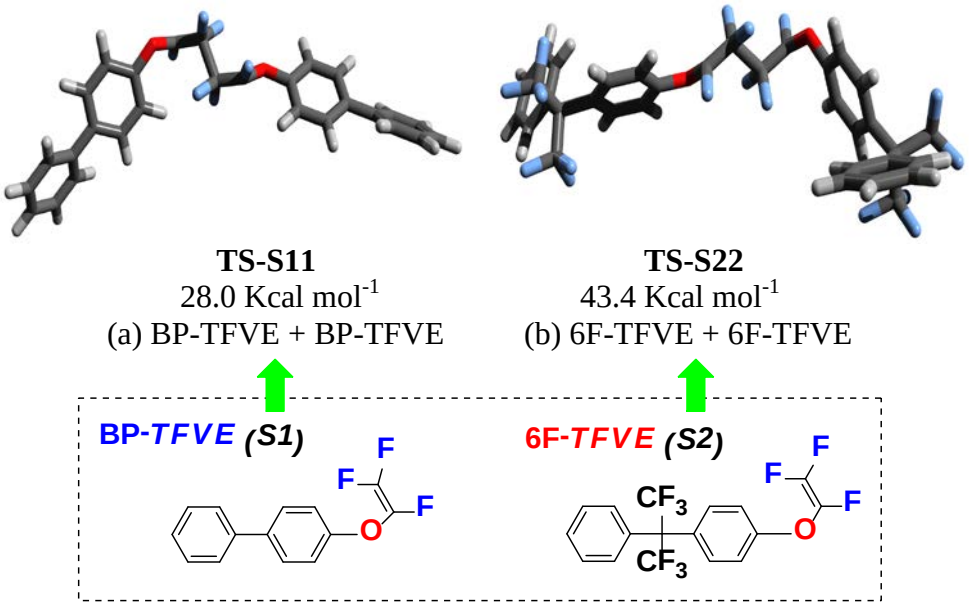

Scheme 2.6 Optimized TS structures of dimers.

Table 2.3 Computational Data: Ea for S11, S12, and S22 with different DFT methods.

	E_a(kcal/mol)				
	B3LYP/ 6-31+G(d)	**B3LYP/ 6-311++G(d,p)**	**mPW1PW91/ 6-31G+(d,p)**	**ωB97X/ cc-VTZ**	**M062X/ 6-31+G(d,p)**
S11 (S1 + S1)	28.0	29.9	27.3	39.9	28.0
S12 (S1 + S2)	28.1	30.0	27.5	40.1	28.5
S22 (S2 + S2)	43.4	40.2	43.5	57.3	46.0

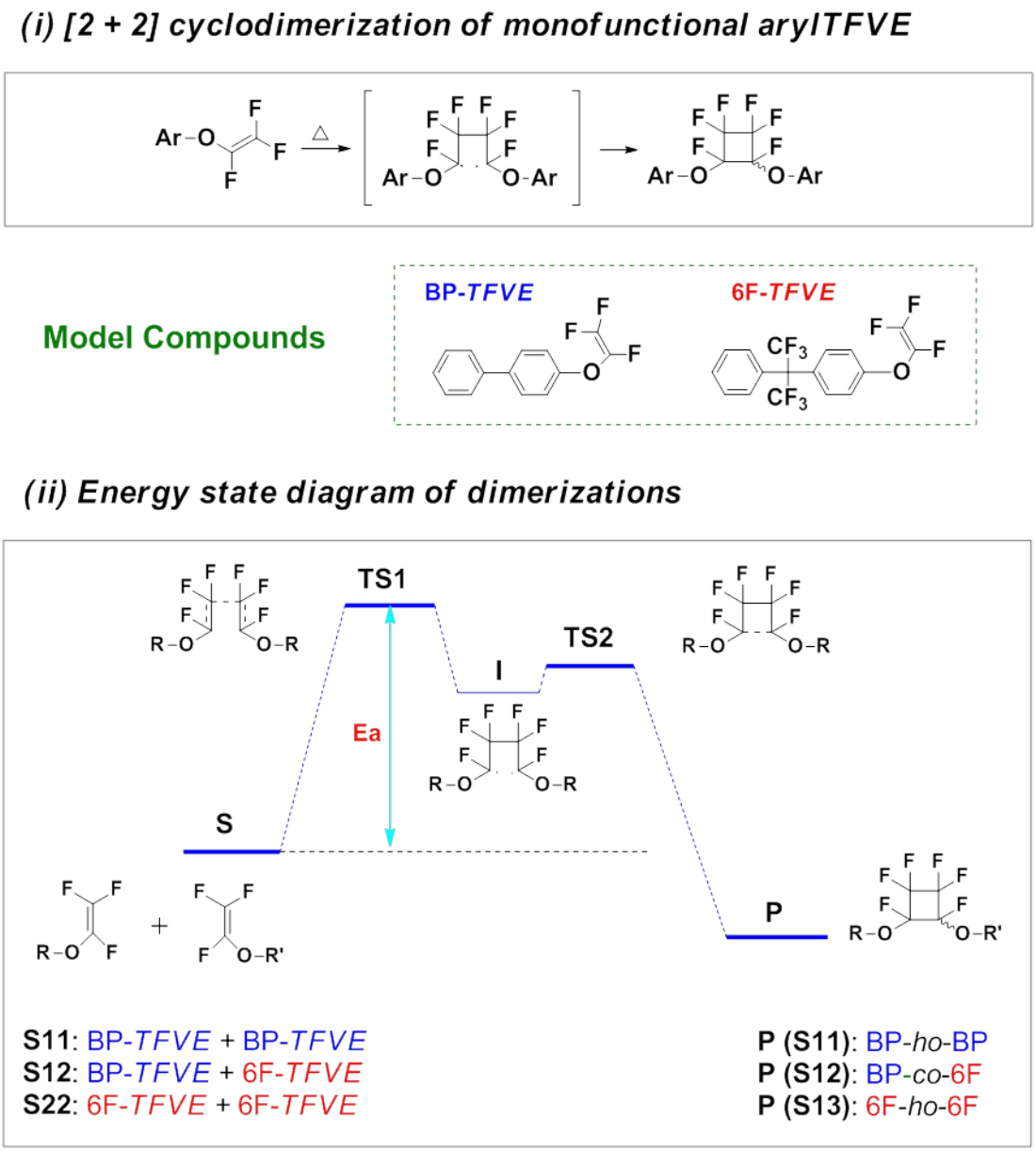

Scheme 2.7. Energy state diagrams for homo-dimerizations and co-dimerizations of aryl TFVE small molecules.

Consequently, the reactivity that is influeced by electronic and steric factors can be listed in the following order: BP_m > $6F_m$ > BP_o > $6F_o$. Therefore, the cyclopolymerization reaction kinetics in the preparation of PFCB aryl ehter copolymers can be described as follows; **path A** - PFCB1: BP_o-*ho*-BP_o > BP_o-*co*-$6F_o$ > 6Fo-*ho*-6Fo, **path B** - PFCB2: $6F_m$-*ho*-$6F_m$ >> $6F_m$-*co*-BP_o > BP_o-*ho*-BP_o, **path C** - PFCB3: BP_m-*ho*-BP_m ≥ BP_m-*co*-$6F_m$ > $6F_m$-*ho*-$6F_m$, where -*ho*- and -*co*- is referred to as *homodimerization* and *codimerization*, respectively. The monomer distribution of copolymers affected by different reactivity of reactants is illustrated in Scheme 2.4. Although the segment length of PFCB3 is relatively short as compared with PFCB1 and PFCB2, this finding provides the possibility to control a segment length by adjusting reactivity differences of monomers and/or via sequential monomer addition. [55, 56]

Properties of PFCB Aryl Ether Copolymers

The molecular weight of the copolymers was estimated by size-exclusion chromatography and listed in Table 2.4. The number-average molecular weight of copolymers, PFCB1, PFCB2, and PFCB3, was found to be 27, 32, and 38 kDa, respectively. The low M_w of PFCB1 is due to the high crystallinity[39] and low solubility of long-chain 6F oligomer along with its low reactivity, whereas copolymerization with 6F monomer, PFCB2 and PFCB3, showed higher M_w (32 and 38 kDa, respectively). Molecular weight distribution (*Mw/Mn*) ranged from 2.1 to 2.4 which are close to ideal value for step-growth polymerization reaction. We note that high M_w of PFCB3 was obtained under solvent-free reaction condition.

Thermal gravimetric analyses showed that all blocky copolymers display a good thermal stability (Table 2.4 and Figure 2.5). Figure 2.6 presents a DSC thermogram of PFCB block- and segmented copolymers. The glass transition temperature (T_g) of PFCB1 was observed at 114 °C. In addition, the DSC trace exhibited a broad exothermic peak around 165 °C assigned to crystallization temperature (T_c), followed by a second endothermic peak around 190 °C attributed to the crystalline melting temperature (T_m) of polymers. These peaks (T_c and T_m) are indicative of crystallinity of PFCB1 due to the long 6F segments derived from a pre-made oligomer. On the other hand, PFCB2 and PFCB3 exhibited amorphous nature showing only a single T_g peak at 119 and 127 °C, respectively. The semi-crystalline (PFCB1) and amorphous (PFCB2 and PFCB3) copolymers exhibit high solubility in common polar organic solvents, such as CH_2Cl_2, $CHCl_3$, and THF.

Table 2.4 Selected properties of PFCB aryl ether copolymers.

Polymer	**GPC** [a]			**T_g** [b] **/°C**	**T_d** [c] **/°C**
	M_n / g mol^{-1}	**M_w / g mol^{-1}**	**PDI**		
PFCB1 (BP_o-*co*-$6F_o$)	27000	59000	2.14	114	470
PFCB2 (BP_o-*co*-$6F_m$)	32000	66000	2.06	115	471
PFCB3 (BP_m-*co*-$6F_m$)	38000	91000	2.39	127	464

[a] GPC in $CHCl_3$ using polystyrene as standard. [b] DSC (10 °C/min) in nitrogen determined by second heating cycle, [c] 5% weight loss based on TGA (10 °C/min) of polymers in nitrogen.

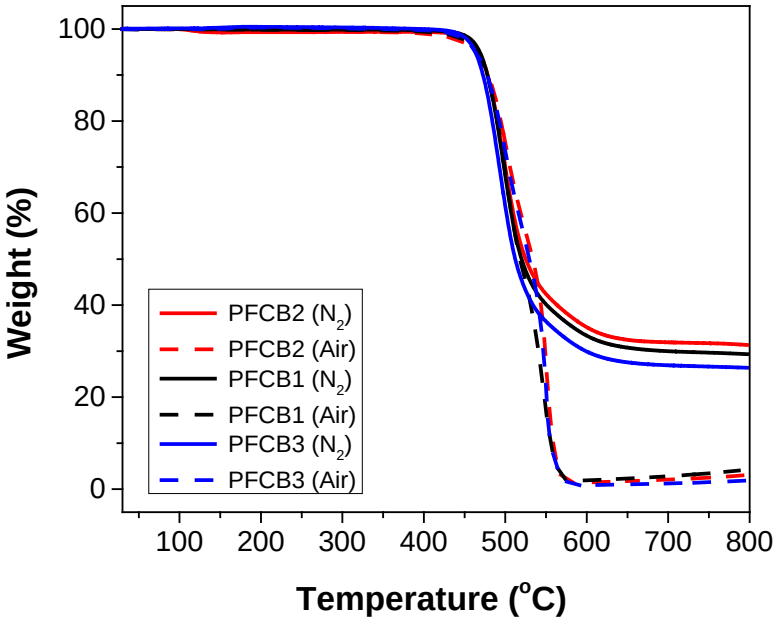

Figure 2.5 TGA curves of PFCB copolymers.

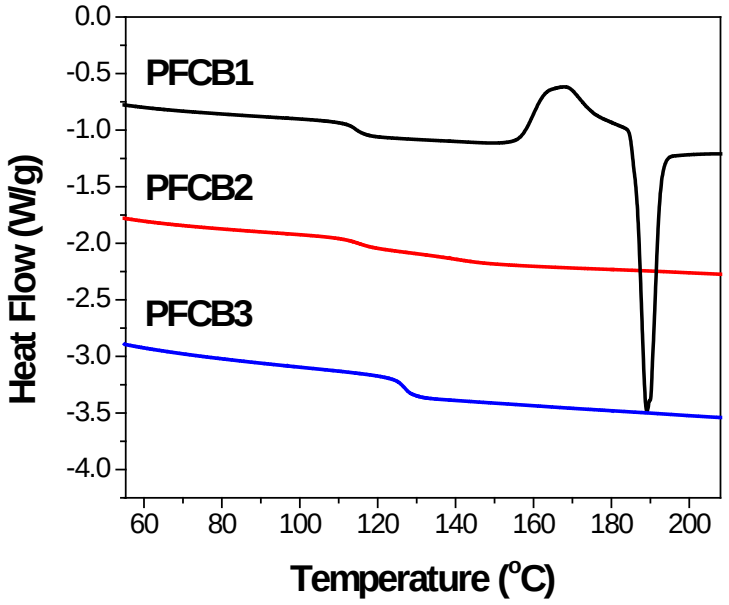

Figure 2.6 DSC of PFCB copolymers.

Applications of PFCB Aryl Ether Copolymers

These highly processable and thermal stable PFCB aryl ether polymers are good candidates for further transformation. For example, electrophilic aromatic substitution reaction of phenyl rings provides a facile tailorable methodology for incorporating functionalizable moieties on the polymer chains.[57] Taking this advantage, PFCB polyelectrolytes were prepared by aryl group sulfonation throughout the polymers to investigate the potential utility of ionomers for PEMFCs. The PFCB aryl ether copolymers (PFCB2 and PFCB3) were sulfonated using chlorosulfonic acid. The PFCB2 segmented copolymer showed outstanding sulfonation selectivity as illustrated in Scheme 2.8. On the other hand, PFCB3 did not exhibit high selective-sulfonation because of the high portion of heterolinkages. Our observation on the post-sulfonation gives a important role of understanding and controlling monomer distributions in the copolymer structrues. The effect of microstructure and segment chain length on the polyelectrolyte properties will be discussed in the Chapter 3.

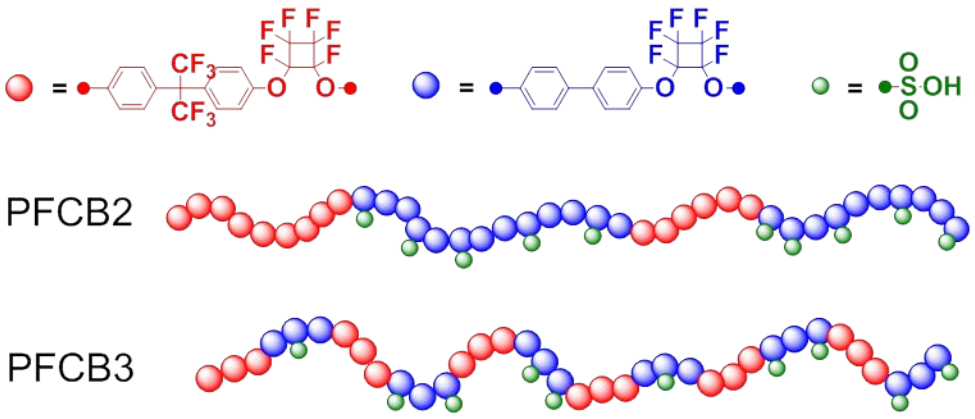

Scheme 2.8 Sulfonation Selectivity on PFCB2 and PFCB3.

Conclusions

In summary, high molecular weight PFCB aryl ether segmented copolymer was obtained in a solvent/catalyst/initiator free polymerization. The direct segmented-copolymer formation from a oligomer/monomer or monomer/monomer couples in a single copolymerization was confirmed using ^{19}F NMR spectroscopy. This is the first report to prove a selective copolymerization of fluoroolefines having different reactivity and to state the monomer distributions in PFCB aryl ether copolymers. These findings would extend the relame of PFCB chemistry with its kinetic study of copolymerization toward designing and/or developing novel PFCB copolymers having tuned microstrucutures by using reactivity differences of monomers and/or by controlling monomer feeding ratios.

Experimental Details

Materials

Commercially available monomers, 4,4'-bis(4-trifluorovinyloxy)biphenyl (BP) and 2,2'-bis(4-trifluorovinyloxy) biphenyl-1,1,1,3,3,3-hexafluoropropane (6F) and their oligomers (BPo and 6Fo) were kindly donated by Tetramer Technologies, L.L.C. 6F monomer was purified by column with hexane before use. Diphenyl ether was obtained from Aldrich and used as received.

Instrumentations

^{1}H and ^{19}F NMR spectra were recorded on a JEOL Eclipse + 300 with 15s relaxation times (T_1). Gel permeation chromatography (GPC) data were collected in $CHCl_3$ from a Waters 2690 Alliance System with photodiode array detection. Molecular weights were obtained using polystyrene as a standard. Elemental microanalysis data for carbon, hydrogen, and fluorine were obtained from Atlantic Microlab, Inc. (Norcross, GA). Thermal gravimetric analysis (TGA) was performed on a Mettler-Toledo 851 instrument in nitrogen and air at a heating rate of 10 °C/min up to 800 °C. Differential scanning calorimetry (DSC) analysis was performed on a TA Q1000 instrument in nitrogen at a heating rate of 10 °C/min up to 200 °C. The glass transition temperature (T_g) of PFCB copolymers was obtained from a second heating cycle using TA Universal Analysis 2000 software suite.

Preparation of Polymers

Synthesis of PFCB1 (Copolymerization of BPo with 6Fo.) Synthesis of copolymer PFCB1 was conducted as follows: 5g of BP oligomer (BP_o) and 5g of 6F oligomer ($6F_o$, Mn= 15,000 g/mol), 10 mL of diphenylether were added to three-neck 250 mL flask, equipped with a condenser, argon inlet and a mechanical stirrer. The reaction mixture was slightly heated at 60 °C and the melted system was sparged with argon gas for 30 min. The thermal step-growth cyclopolymerization was conducted at 140 °C for 24 h, 160 °C for 72 h, 180 °C for 24 h, and 210 °C for 14 h under argon blanket. The resulting viscous crude polymer was cool down and dissolved in tetrahydrofuran (THF). The solution was precipitated in a large excess of methanol. The resulting fibrous copolymer was purified in a soxhlet extractor with methanol for 24 h to remove diphenylether and unreacted monomers. The copolymer was dried at 60 °C in vacuum for 24 h. Yield: 60%, ^{1}H NMR (300 MHz, $CDCl_3$) δ 7.47 (d, J = 9 Hz, $H_{f'}$), 7.40–7.30 (m, $H_{g'}$), 7.30–7.20 (m, overlapped by $H_{e'}$ and $CDCl_3$), 7.07 (d, J = 6 Hz, $H_{h'}$); ^{19}F NMR (283 MHz, $CDCl_3$) δ –64 (s, $F_{d'}$), –126 – (–133) (m, the overlap of cyclobutyl–F_6 on BP and 6F segments). Elemental Analysis: Found: C, 51.47; H, 1.89; F, 38.57.

Synthesis of PFCB2 (Copolymerization of BPo with 6Fm.) A block copolymer PFCB2 of BP oligoemr (BPo, Mn= 8,000 g/mol, 10g), 6F monomer (6Fm, 10g), was prepared using the same synthesis and purification routine of polymer PFCB2. Yield: 80-85%, ^{1}H NMR (300 MHz, $CDCl_3$) δ 7.47 (d, J = 9 Hz, $H_{f'}$), 7.40–7.30 (m, $H_{g'}$), 7.30–7.20 (m, overlapped by $H_{e'}$ and $CDCl_3$), 7.07 (d, J = 6 Hz, $H_{h'}$); ^{19}F NMR (283 MHz, $CDCl_3$) δ

–64 (s, $F_{d'}$), –126 – (–133) (m, the overlap of cyclobutyl–F_6 on BP and 6F segments). Elemental Analysis: Found: C, 50.59; H, 1.94; F, 40.08.

Synthesis of PFCB3 (Copolymerization of BPm with 6Fm.) A copolymer of BPm and 6Fm was also synthesized without solvent, diphenylether, at 140 °C for 24 h, 160 °C for 48 h, 180 °C for 24 h with argon inlet. The resulting viscous copolymer was cool down and dissolved in THF. The solution was precipitated in a methanol and the resulting fibrous copolymer was purified in a soxhlet extractor with methanol for 24 h. The copolymer was dried at 60 °C in vacuum for 24 h. Yield: 85%, ^{1}H NMR (300 MHz, $CDCl_3$) δ 7.47 (d, J = 9 Hz, $H_{f'}$), 7.40–7.30 (m, $H_{g'}$), 7.30–7.20 (m, overlapped by $H_{e'}$ and $CDCl_3$), 7.07 (d, J = 6 Hz, $H_{h'}$); ^{19}F NMR (283 MHz, $CDCl_3$) δ –64 (s, $F_{d'}$), –126 – (–133) (m, the overlap of cyclobutyl–F_6 on BP and 6F segments). Elemental Analysis: Found: C, 50.27; H, 1.83; F, 40.23.

Computational Details

All calculations were performed using the Gaussian 09 software by Tugba Kucukkal and Prof. Steven J. Stuart.[58] The transition state structures were located at the B3LYP/6-31G(d) level of theory at singlet state (singlet transition states were found to have lower energy than the triplet). Presence of only one imaginary frequency was confirmed by frequency calculations and the vibrational frequencies were visualized using the Avogadro software[59] to ensure that the imaginary frequency motion corresponds to the Carbon-Carbon (C2-C2) bond formation. Finally, the single point

energy calculations were performed on the B3LYP/6-31G(d) optimized transition state structures at five different levels of theory: B3LYP/6-31+G(d), B3LYP/6-311++G(d,p), mPW1PW91/6-31+G(d,p), wB97X/cc-pVTZ and M062X/6-31+G(d,p). The reactant, intermediate, and product structures were optimized using the aforementioned five methods.

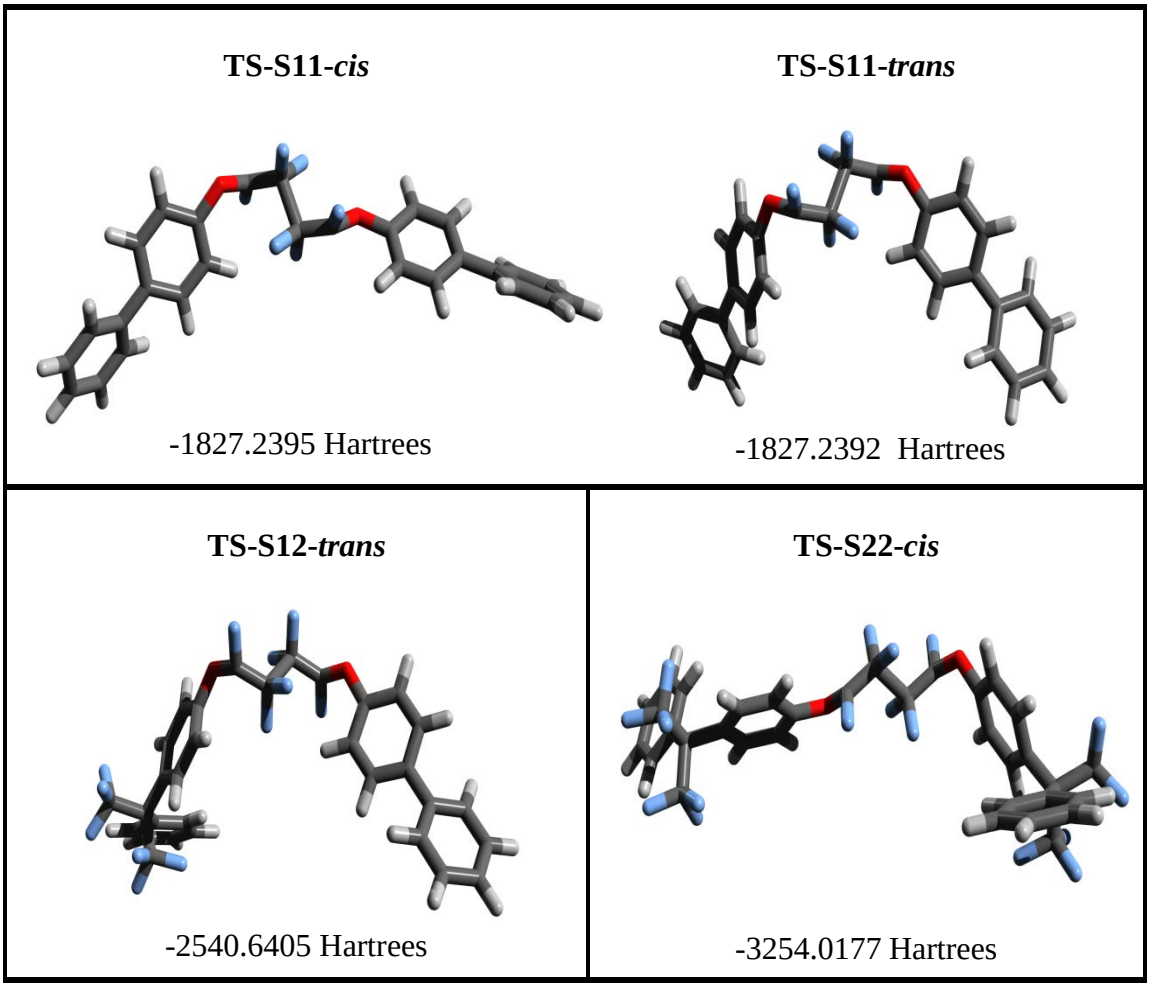

Figure 2.7 Optimized transition state structures for S11, S12 and S22.

Table 2.5 Computational Data: Geometries of TS-S11, TS-S12 and TS-S22.

	Bond Length (Å)		**Angle (°)**	
	C1-C2 (C3-C4)	**C2-C3**	**C1-C2-C3 (C2-C3-C4)**	**C1-C2-C3-C4**
TS-S11-*cis*	1.42 (1.41)	1.78	111.6 (113.1)	-179.5
TS-S11-*trans*	1.42 (1.41)	1.78	113.0 (111.8)	-178.7
TS-S12-*trans*	1.42 (1.41)	1.79	113.0 (111.3)	-179.2
TS-S22-*cis*	1.41 (1.42)	1.79	112.0 (111.6)	-177.8

Table 2.6 Computational Data: Energies (Hartrees) of reactants, products, and transition states at the B3LYP/6-31+G(d) level of theory.

	Reactant	**TS**	**Product**
S11	-1827.2836	-1827.2395 (*cis*) -1827.2392 (*trans*)	-1827.3423 (*cis*) -1827.3437 (*trans*)
S12	-2540.6851	-2540.6405 (*trans*)	-2540.7439 (*cis*) -2540.7451 (*trans*)
S22	-3254.0866	-3254.0177 (*cis*)	-3254.1451 (*cis*) -3254.1464 (*trans*)

References

1. Klukovich, H. M.; Kean, Z. S.; Iacono, S. T.; Craig, S. L. Mechanically Induced Scission and Subsequent Thermal Remending of Perfluorocyclobutane Polymers. *J. Am. Chem. Soc.* **2011,** *133*, 17882-17888.

2. Jin, J.; Smith, D. W.; Topping, C. M.; Suresh, S.; Chen, S.; Foulger, S. H.; Rice, N.; Nebo, J.; Mojazza, B. H. Synthesis and Characterization of Phenylphosphine Oxide Containing Perfluorocyclobutyl Aromatic Ether Polymers for Potential Space Applications. *Macromolecules* **2003,** *36*, 9000-9004.

3. Iacono, S. T.; Budy, S. M.; Mabry, J. M.; Smith, D. W. Synthesis, Characterization, and Surface Morphology of Pendant Polyhedral Oligomeric Silsesquioxane Perfluorocyclobutyl Aryl Ether Copolymers. *Macromolecules* **2007,** *40*, 9517-9522.

4. Spraul, B. K.; Suresh, S.; Glaser, S.; Perahia, D.; Ballato, J.; Smith Jr, D. W. Perfluorocyclobutyl-Linked Hexa-peri-hexabenzocoronene Networks. *J. Am. Chem. Soc.* **2004,** *126*, 12772-12773.

5. Ballato, J.; Foulger, S. H.; Smith, J. D. W. Optical Properties of Perfluorocyclobutyl Polymers. II. Theoretical and Experimental Attenuation. *J. Opt. Soc. Am. B* **2004,** *21*, 958-967.

6. Mujkic, M.; Iacono, S. T.; Neilson, A. R.; Smith, D. W. Recent Optical Applications of Perfluorocyclobutyl Aryl Ether Polymers. *Macromol. Symp.* **2009,** *283–284*, 326-335.

7. Smith, D. W.; Chen, S.; Kumar, S. M.; Ballato, J.; Topping, C.; Shah, H. V.; Foulger, S. H. Perfluorocyclobutyl Copolymers for Microphotonics. *Adv. Mater.* **2002,** *14*, 1585-1589.

8. Jiang, X. Z.; Liu, S.; Liu, M. S.; Herguth, P.; Jen, A. K. Y.; Fong, H.; Sarikaya, M. Perfluorocyclobutane-Based Arylamine Hole-Transporting Materials for Organic and Polymer Light-Emitting Diodes. *Adv. Funct. Mater.* **2002,** *12*, 745-751.

9. Neilson, A. R.; Budy, S. M.; Ballato, J. M.; Smith, D. W. Mixed Chromophore Perfluorocyclobutyl (PFCB) Copolymers for Tailored Light Emission. *Macromolecules* **2007,** *40*, 9378-9383.

10. Ford, L. A.; DesMarteau, D. D.; Smith Jr, D. W. Perfluorocyclobutyl (PFCB) Aromatic Polyethers: Synthesis and Characterization of New Sulfonimide Containing Monomers and Fluoropolymers. *J. Fluorine Chem.* **2005,** *126*, 651-658.

11. Perpall, M. W.; Smith, D. W.; DesMarteau, D. D.; Creager, S. E. Alternative Trifluorovinyl Ether Derived Fluoropolymer Membranes and Functionalized Carbon Composite Electrodes for Fuel Cells. *J. Macromol. Sci., Polym. Rev.* **2006,** *46*, 297-313.

12. Qian, G.; Smith, D. W., Jr.; Benicewicz, B. C. Synthesis and Characterization of High Molecular Weight Perfluorocyclobutyl Containing Polybenzimidazoles (PFCB–PBI) for High Temperature Polymer Electrolyte Membrane Fuel Cells. *Polymer* **2009,** *50*, 3911-3916.

13. Wagener, E.; Smith Jr, D. W.; Topping, C.; Jayasinghe, R.; Jin, J.; Singh, A.; Mackinnon, S. M.; Timothy J, F.; Craig S, G., In *Workshop on Advances in Polymer*

Electrolyte Membrane Fuel Cell Systems, Am. Chem. Soc., Div. Polym. Chem.: Pacific Grove CA, 2009.

14. Mackinnon, S. M.; Fuller, T. J.; Coms, F., Sulfonated Perfluorocyclobutane Block Copolymers and Proton Conductive Polymer Membranes. U.S. Patent 7,897,692, 2011.

15. Fuller, T. J.; MacKinnon, S. M.; Schoeneweiss, M. R., Polyelectrolyte Membranes derived from Soluble Perfluorocyclobutane Polymers with Sulfonyl Chloride Groups, U.S. Patent 7,989,512 Aug 02, 2011.

16. Fuller, T. J.; MacKinnon, S. M.; SchoeneWeiss, M. R., Polyelectrolyte Membranes made of Poly(Perfluorocyclobutanes) with Pendant Perfluorosulfonic Acid Groups and Blends with Poly(Vinylidene Fluoride) U.S. Patent 8,053,530, Nov 08, 2011.

17. Lee, K.-S.; Jeong, M.-H.; Kim, Y.-J.; Lee, S.-B.; Lee, J.-S. Fluorinated Aromatic Polyether Ionomers Containing Perfluorocyclobutyl as Cross-Link Groups for Fuel Cell Applications. *Chem. Mater.* **2012,** *24*, 1443-1453.

18. Kalaw, G. J. D.; Wahome, J. A. N.; Zhu, Y.; Balkus Jr, K. J.; Musselman, I. H.; Yang, D.-J.; Ferraris, J. P. Perfluorocyclobutyl (PFCB)-based Polymer Blends for Proton Exchange Membrane Fuel Cells (PEMFCs). *J. Membr. Sci.* **2013,** *431*, 86-95.

19. Babb, D. A.; Boone, H. W.; Smith, D. W.; Rudolf, P. W. Perfluorocyclobutane Aromatic Ether Polymers. III. Synthesis and Thermal Stability of a Thermoset Polymer containing Triphenylphosphine Oxide. *J. Appl. Polym. Sci.* **1998,** *69*, 2005-2012.

20. Babb, D. A.; Ezzell, B. R.; Clement, K. S.; Richey, W. F.; Kennedy, A. P. Perfluorocyclobutane Aromatic Ether Polymers. *J. Polym. Sci., Part A: Polym. Chem.* **1993,** *31*, 3465-3477.

21. Smith, D. W.; Babb, D. A. Perfluorocyclobutane Aromatic Polyethers. Synthesis and Characterization of New Siloxane-Containing Fluoropolymers†. *Macromolecules* **1996,** *29*, 852-860.

22. Cheatham, C. M.; Lee, S.-N.; Laane, J.; Babb, D. A.; Smith, D. W. Kinetics of Trifluorovinyl Ether Cyclopolymerization via Raman Spectroscopy. *Polym. Int.* **1998,** *46*, 320-324.

23. Mifsud, N.; Mellon, V.; Jin, J.; Topping, C. M.; Echegoyen, L.; Smith, D. W. First Identification of Biradicals during Thermal [2π + 2π] Cyclopolymerization of Trifluorovinyl Aromatic Ethers. *Polym. Int.* **2007,** *56*, 1142-1146.

24. Zhu, K.; Iacono, S. T.; Budy, S. M.; Jin, J.; Smith, D. W. Facile One-Pot Synthesis and Thermal Cyclopolymerization of Aryl Bistrifluorovinyl Ether Monomers Bearing Reactive Pendant Groups. *J. Polym. Sci., Part A: Polym. Chem.* **2010,** *48*, 1887-1893.

25. Lutz, J.-F. Sequence-Controlled Polymerizations: the Next Holy Grail in Polymer Science? *Polym. Chem.* **2010,** *1*, 55-62.

26. Zamfir, M.; Lutz, J.-F. Ultra-Precise Insertion of Functional Monomers in Chain-Growth Polymerizations. *Nat. Commun.* **2012,** *3*, 1-8.

27. Stayshich, R. M.; Meyer, T. Y. New Insights into Poly(lactic-co-glycolic acid) Microstructure: Using Repeating Sequence Copolymers To Decipher Complex NMR and Thermal Behavior. *J. Am. Chem. Soc.* **2010,** *132*, 10920-10934.

28. Lutz, J.-F.; Ouchi, M.; Liu, D. R.; Sawamoto, M. Sequence-Controlled Polymers. *Science* **2013,** *341*.

29. Jiang, X.; Zhang, M.; Li, S.; Shao, W.; Zhao, Y. Facile Synthesis and Versatile Topological Transformation of Mono-Cleavable Symmetric Starlike Terpolymers. *Chem. Commun.* **2012,** *48*, 9906-9908.

30. Jiang, X.; Shao, W.; Jiang, K.; Zhang, M.; Liu, H.; Ye, C.; Zhao, Y. Synthesis and Versatile Postpolymerization Modification of Couplable A(BC)mD Heterografted Comblike Block Quaterpolymers. *Polym. Chem.* **2013,** *4*, 3272-3281.

31. Yu, T.-B.; Bai, J. Z.; Guan, Z. Cycloaddition-Promoted Self-Assembly of a Polymer into Well-Defined β Sheets and Hierarchical Nanofibrils. *Angew. Chem., Int. Ed.* **2009,** *48*, 1097-1101.

32. Matyjaszewski, K. Architecturally Complex Polymers with Controlled Heterogeneity. *Science* **2011,** *333*, 1104-1105.

33. Matsuda, M.; Satoh, K.; Kamigaito, M. Periodically Functionalized and Grafted Copolymers via 1:2-Sequence-Regulated Radical Copolymerization of Naturally Occurring Functional Limonene and Maleimide Derivatives. *Macromolecules* **2013,** *46*, 5473-5482.

34. Badi, N.; Chan-Seng, D.; Lutz, J.-F. Microstructure Control: An Underestimated Parameter in Recent Polymer Design. *Macromol. Chem. Phys.* **2013,** *214*, 135-142.

35. Bernett, W. A. Hybridization Effects in Fluorocarbons. *J. Org. Chem.* **1969,** *34*, 1772–1776.

36. Wlassics, I. 2π + 2π Cycloaddition Kinetics of Some Fluoro Olefins and Fluoro Vinyl Ethers. *J. Fluorine Chem.* **2004,** *125*, 1519-1528.

37. Conrad, M. P. C.; Shoichet, M. S. Synthesis and Thermal Stability of Hybrid Fluorosilicone Polymers. *Polymer* **2007,** *48*, 5233-5240.

38. Clark Ligon Jr, S.; Krawiec, M.; Kitaygorodskiy, A.; Smith Jr, D. W. First Separation and Characterization of cis and trans 1,2-bisaryloxy Perfluorocyclobutanes. *J. Fluorine Chem.* **2003,** *123*, 139-146.

39. Smith Jr, D. W.; Jin, J.; Shah, H. V.; Xie, Y.; DesMarteau, D. D. Anomalous Crystallinity in a Semi-Fluorinated Perfluorocyclobutyl (PFCB) Polymer Containing the Hexafluoro-i-propylidene (6F) Linkage. *Polymer* **2004,** *45*, 5755-5760.

40. Spraul, B. K.; Suresh, S.; Jin, J.; Smith, D. W., Jr. Synthesis and Electronic Factors in Thermal Cyclodimerization of Functionalized Aromatic Trifluorovinyl Ethers. *J Am Chem Soc* **2006,** *128*, 7055–7064.

41. Hohenberg, P.; Kohn, W. Inhomogeneous Electron Gas. *Phys. Rev.* **1964,** *136*, B864–B871.

42. Kohn, W.; Sham, L. J. Self-Consistent Equations Including Exchange and Correlation Effects. *Phys. Rev.* **1965,** *140*, A1133-A1138.

43. Becke, A. D. Density Functional Thermochemistry. III. The Role of Exact Exchange. *J. Chem. Phys.* **1993,** *98*, 5648-5652.

44. Lee, C.; Yang, W.; Parr, R. G. Development of the Colle-Salvetti correlation-energy formula into a functional of the electron density. *Phys. Rev. B* **1988,** *37*, 785-789.

45. Ditchfield, R.; Hehre, W. J.; Pople, J. A. Self-Consistent Molecular-Orbital Methods. IX. An Extended Gaussian-Type Basis for Molecular-Orbital Studies of Organic Molecules. *J. Chem. Phys.* **1971,** *54*, 724-728.

46. Hehre, W. J.; Ditchfield, R.; Pople, J. A. Self-Consistent Molecular Orbital Methods. XII. Further Extensions of Gaussian---Type Basis Sets for Use in Molecular Orbital Studies of Organic Molecules. *J. Chem. Phys.* **1972,** *56*, 2257-2261.

47. Frisch, M. J.; Pople, J. A.; Binkley, J. S. Self-Consistent Molecular Orbital Methods 25. Supplementary Functions for Gaussian Basis Sets. *J. Chem. Phys.* **1984,** *80*, 3265-3569.

48. Clark, T.; Chandrasekhar, J.; Spitznagel, G. W.; Schleyer, P. V. *J. Comput. Chem.* **1983,** *4*, 294-301.

49. Adamo, C.; Barone, V. Exchange Functionals with Improved Long-Range Behavior and Adiabatic Connection Methods without Adjustable Parameters: The mPW and mPW1PW Models. *J. Chem. Phys.* **1998,** *108*, 664-675.

50. Chai, J.-D.; Head-Gordon, M. Systematic Optimization of Long-Range Corrected Hybrid Density Functionals. *J. Chem. Phys.* **2008,** *128*, 0841061-08410615.

51. Dunning, J. T. H. Gaussian Basis Sets for use in Correlated Molecular Calculations. I. The Atoms Boron through Neon and Hydrogen. *J. Chem. Phys.* **1989,** *90*, 1007-1023.

52. Kendall, R. A.; Dunning, J. T. H.; Harrison, R. J. Electron Affinities of the First-Row Atoms Revisited. Systematic Basis Sets and Wave Functions. *J. Chem. Phys.* **1992,** *96*, 6796-6806.

53. Wilson, A. K.; van Mourik, T.; Dunning Jr, T. H. Gaussian Basis Sets for use in Correlated Molecular Calculations. VI. Sextuple Zeta Correlation Consistent Basis Sets for Boron through Neon. *J. Mol. Struct.* **1996,** *388*, 339-349.

54. Zhao, Y.; Truhlar, D. The M06 Suite of Density Functionals for Main Group Thermochemistry, Thermochemical Kinetics, Noncovalent Interactions, Excited States, and Transition Elements: Two New Functionals and Systematic Testing of Four M06-Class Functionals and 12 Other Functionals. *Theor Chem Account* **2008,** *120*, 215-241.

55. Edson, J. B.; Wang, Z.; Kramer, E. J.; Coates, G. W. Fluorinated Bis(phenoxyketimine)titanium Complexes for the Living, Isoselective Polymerization of Propylene: Multiblock Isotactic Polypropylene Copolymers via Sequential Monomer Addition. *J. Am. Chem. Soc.* **2008,** *130*, 4968-4977.

56. Chan-Seng, D.; Zamfir, M.; Lutz, J.-F. Polymer-Chain Encoding: Synthesis of Highly Complex Monomer Sequence Patterns by Using Automated Protocols. *Angew. Chem., Int. Ed.* **2012,** *51*, 12254-12257.

57. Park, J.; Oh, J.-M.; Creager, S. E.; Smith Jr, D. W. Grafting of Chain-End-Functionalized Perfluorocyclobutyl (PFCB) Aryl Ether Ionomers onto Mesoporous Carbon Supports. *Chem. Commun.* **2012,** *48,* 8225-8227.

CHAPTER THREE

PROTON EXCHANGE MEMBRANES BASED ON PERFLUOROCYCLOBUTYL ARYL ETHER COPOLYMERS

Introduction

Proton exchange membranes (PEMs) have been extensively studied over several decades as an essential component of fuel cells.[1-5] Recently, PEMs have also attracted interest as polyelectrolyte in the thermochemical cycles (e.g., hybrid sulfur (HyS) cycle[7], which is a two-step water-splitting process consisting of electrochemical and thermochemical steps) for hydrogen production in large scale.[6, 8-11] These PEMs which mediate the electrochemical reaction (Scheme 3.1) between anode and cathode by conducting protons offer high efficiency for both energy conversion and hydrogen production with small foot print.

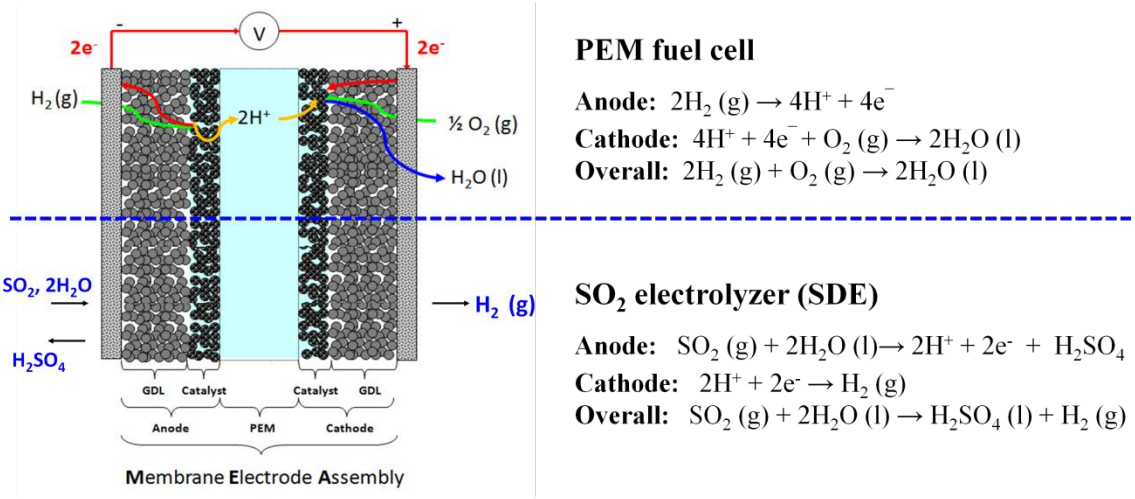

Scheme 3. 1 PEM fuel cell and PEMFC concept in hybrid sulfur (HyS) cycle.[1, 9, 12]

The most common polyelectrolytes used in fuel cells and thermochemical cycles are perfluorosulfonic acid polymers[11, 13], such as Nafion™ (Scheme 3.2), because of their high proton conductivity, low electronic conductivity, mechanical integrity, and high oxidative/thermal/chemical stability.[13] However, they have limitations for practical applications due to their high production cost, high permeability to reactant gases and limited operation temperature with loss of hydration at high temperature (> 80 °C) and deteriorated properties above their glass transition temperature (T_g = ca. 115 °C).[14, 15]

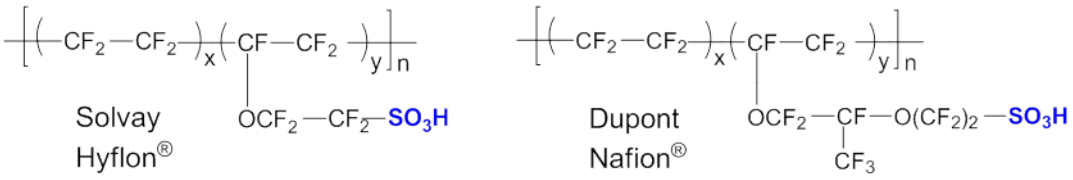

Scheme 3.2 Perfluorosulfonic polymers.[6]

Therefore, a significant effort has been made to develop alternative high performance PEMs to current state-of-the-art, Nafion™.[16-18] The major approach has been the acid functionalized aromatic polymers modified by introduction of sulfonic acid groups onto high-performance thermoplastic polymers (Scheme 3.3), such as poly(arylene ether ether ketone)s, polystyrene, poly(phenylene sulfide) and poly(arylene ether sulfone)s, because of their excellent thermal stability and substantiality to electrophilic sulfonation reaction as well as economic cost.[19-24] However, these hydrocarbon-based PEMs have shown relatively lower oxidative/hydrolytic stability

mainly caused by hydrolysis of ether and sulfide linkage.[25-29] To overcome these oxidative/hydrolytic degradation issues, hydrocarbon-based polymers without ether or sulfide linkage have been studied for PEMs. For example, several sulfonated derivatives of poly(phenylene)[30], polyimide[31-33], and polybenzothiazoles[34] have shown high hydrolytic and oxidative stability without sacrificing other desired properties.

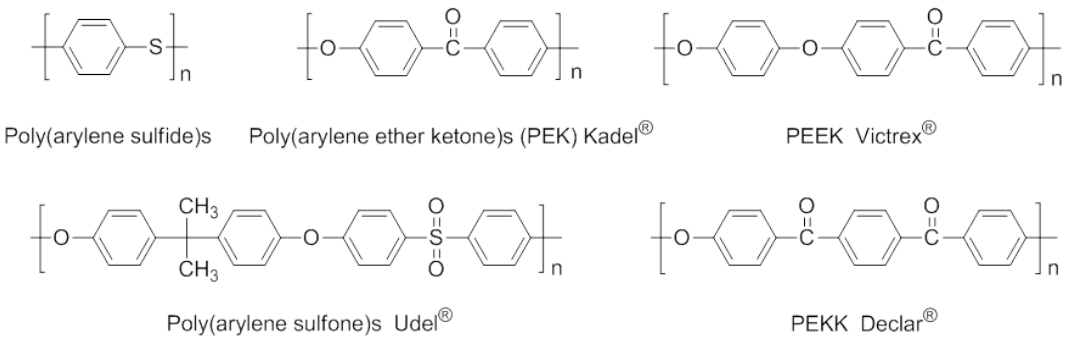

Scheme 3.3 Hydrocarbon based polymers.

Partially fluorinated aromatic polymers have also been considered as good candidate materials to improve oxidative and hydrolytic stability.[35-40] Particularly, perfluorocyclobutyl (PFCB) aryl ether polymers, a class of high-performance thermoplastic materials, have received attention as potential PEM materials because of their ease of synthesis and low dielectric constant of PFCB moiety as well as the electrochemical stability.[41, 42] The excellent resistant to hydroxyl/peroxyl free radicals and high proton conductivity of the polymer electrolytes containing PFCB aryl ether units have been reported.[41] The PFCB units also provide excellent thermal

and chemical stabilities and high hydrophobicity of the polymer backbone, while the presence of the stereorandom PFCB ether groups contribute to solubility and processability as an amorphorous polymer.[43] Simple chemical modification of these highly processable PFCB aryl ether polymers through post-sulfonation can be easily employed to produce proton-conductive polymers. For example, sulfonated PFCB (sPFCB) aryl ether homopolymer prepared by polycondensation and followed post-sulfonation was reported by Scott and co-workers.[34] The sPFCB homopolymer afforded highly thermal stable, transparent and flexible membranes. However, they showed somewhat low proton conductivity of 0.011 Scm^{-1} at 80 °C and 100 % RH despite a high sulfontaion level (IEC = 1.7 mequiv/g). This finding could be explained by the insufficient connectivity of the channels for proton transport in the sulfonated PFCB homopolymer membranes. This indicated that not only the sulfonation level of polymer but also the polymer architecture is an important factor for PEM materials because the well-connected hydrophilic domains in the polymer morphology structure behave as proton transport channel.

One promising approach to enhance properties in terms of PEM performance is to improve the nanophase separation between hydrophilic and hydrophobic domains. The well-connected hydrophilic and hydrophobic channels in the polymer morphology structure contribute to better proton transportation and dimensional stability, respectively.[39, 40, 44-46] Herein, we report preparation and properties of hydrophilic-hydrophobic PFCB aryl ether segmented copolymer membranes. The sulfonated PFCB aryl ether copolymers were prepared by facile post-selective-

sulfonation of PFCB copolymers. The membrane properties, such as water uptake, volume swelling, and proton conductivity with respect to sulfonation level will be discussed in this Chapter.

Synthesis of PFCB Aryl Ether Copolymer Electrolytes

Previously, a series of thermally stable PFCB blocky copolymers (PFCB1, PFCB2, and PFCB3) was prepared directly from oligomer/monomer or monomer/monomer couples in a single copolymerization (Chapter 2). These segmented copolymers were used to study the effect of their microstructures on sulfonation selectivity and their potential utility as an electrolyte for PEM fuel cells. Table 3.1 summarizes the molecular weight and the experimental composition ratios of the polymers which were used for sulfonation study.

Table 3.1 Molecular weight and thermal properties of copolymers.

Polymer	**Weight Feed Ratio** of Starting Reagents	**Experimental Compositional Ratio (BP:6F)**[a]	M_n[b]	**PDI**	T_g (°C)[c]
PFCB1	1:1 (BP_o : $6F_o$)	55:45	27000	2.14	114
PFCB2	1:1 (BP_o : $6F_m$)	53:47	32000	2.06	119
PFCB2-2	*2:1 (BP_o : $6F_m$)*	*76:24*	*38000*	*2.21*	*137*
PFCB3	1:1 (BP_m : $6F_m$)	50:50	38000	2.39	127

[a] Molar ratio of BP and 6F determined by ^{19}F NMR, [b] GPC in $CHCl_3$ using polystyrene as standard, [c] DSC (10 °C/min in nitrogen) determined by second heating cycle.

A high molecular weight PFCB2-2 copolymer was also prepared through a selective-copolymerization of BP oligomers (76%) and 6F monomers (24%) in one-pot single copolymerization to investigate the effect of compositions. Its experimental compositional ratio estimated from the intensities of isofluoropropyl-F_6 singlet and cyclobutyl-F_6 peaks agreed well with the theoretical values (Figure 3.1). The block copolymer PFCB2-2 formation was confirmed by ^{19}F NMR showing only small portion (8%) of the BP-6F hetero-linkage and 92% of segmented sequence of BP and 6F as shown in Figure 3.2. The number-average-molecular-weight and T_g of PFCB2-2 copolymer were found to be 38 kDa and 137 °C, respectively.

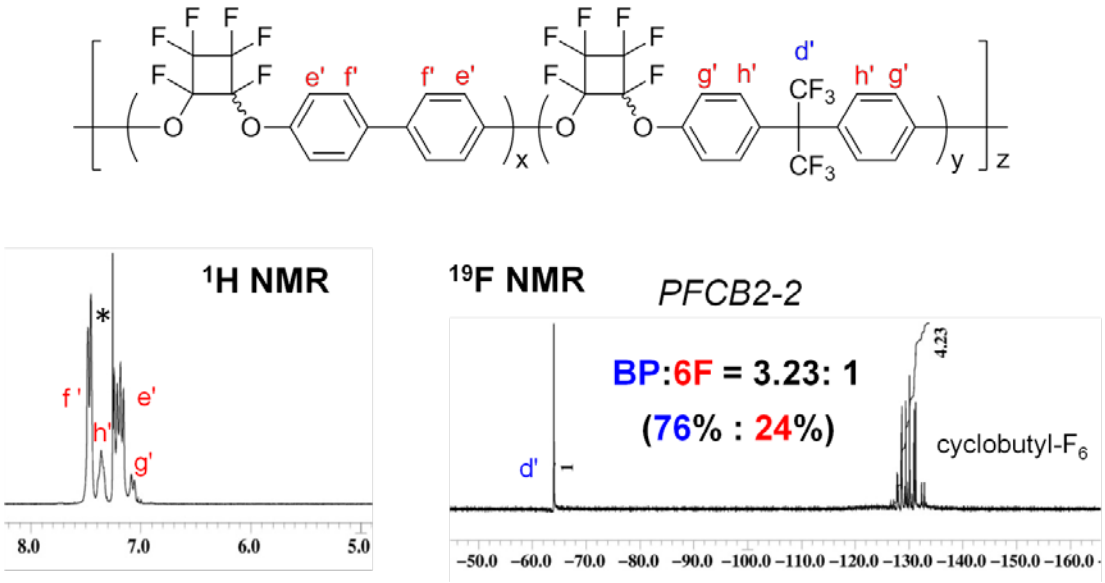

Figure 3.1 ^{19}F NMR (in $CDCl_3$) spectrum of PFCB2-2 (BPo-*co*-6Fm) and its compositional ratio of the BP and 6F repeat unit in the copolymer chain (Theoretical compositional ratio = 74: 24).

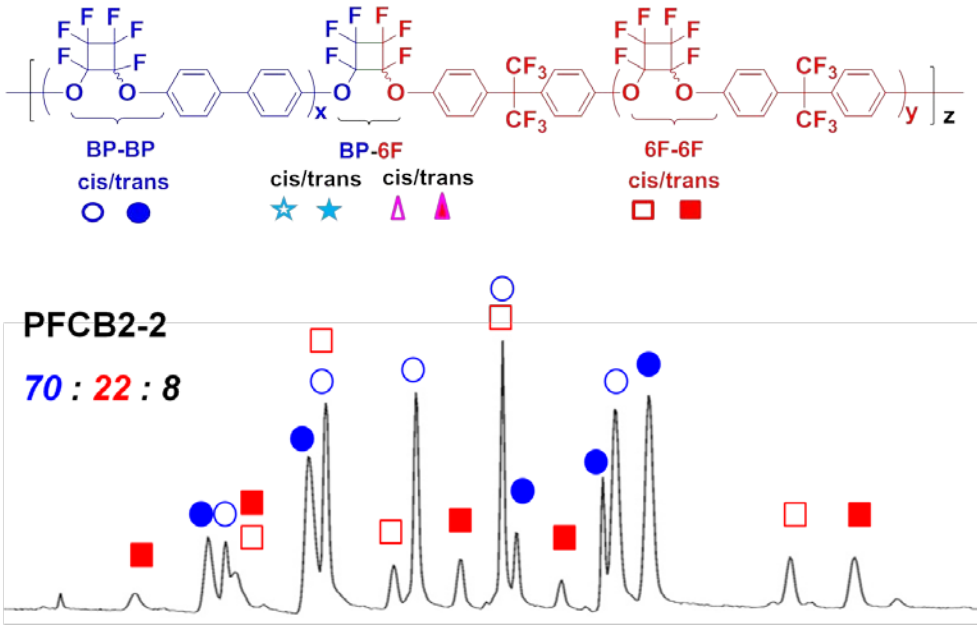

Figure 3.2 ^{19}F NMR (in $CDCl_3$*, right) spectrum from -127 to -134 ppm of PFCB2-2 (BPo-*co*-6Fm).

The PFCB copolymers were sulfonated via post-sulfonation using chlorosulfonic acid. Scheme 3.4 illustrates hydrophilic-hydrophobic PFCB aryl ether segmented-copolymers synthesized via selective copolymerization (Scheme 3.4 1a) and selective-sulfonation (Scheme 3.4 1b). Since CF_3 groups present in the 6F segment withdraw electrons from two benzene rings, the 6F segment is electronically deactivated toward electrophilic aromatic substitution reactions. Therefore, the sulfonation is expected to be occurred only on the benzene rings of the BP segment and allows the formation of hydrophilic domains in the PFCB copolymer as illustrated in Scheme 3.5.

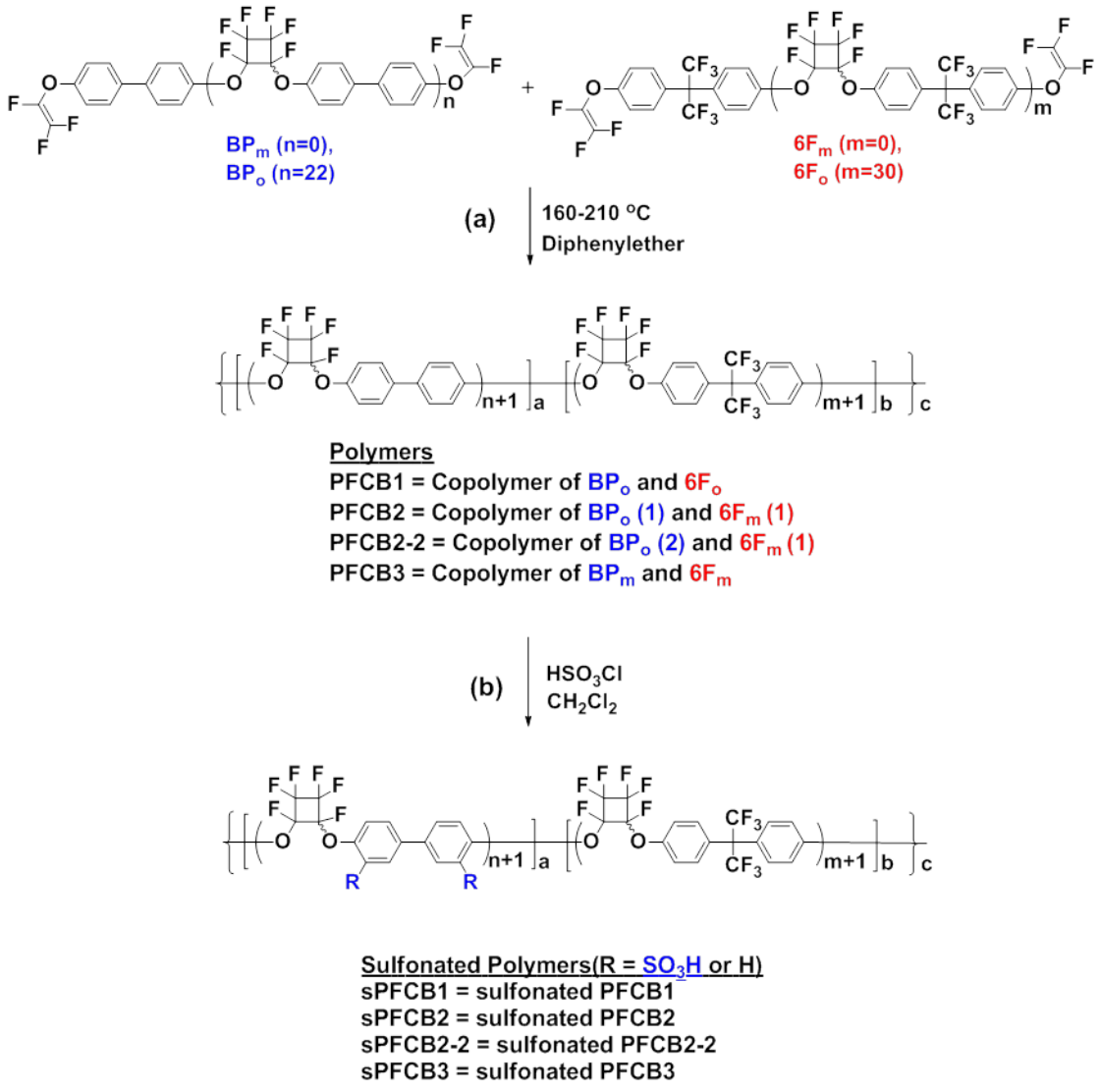

Scheme 3.4 (a) PFCB1, PFCB2, PFCB2-2, and PFCB3 copolymers for sulfonation study (b) Sulfonation of PFCB aryl ether copolymers with chlorosulfonic acid.

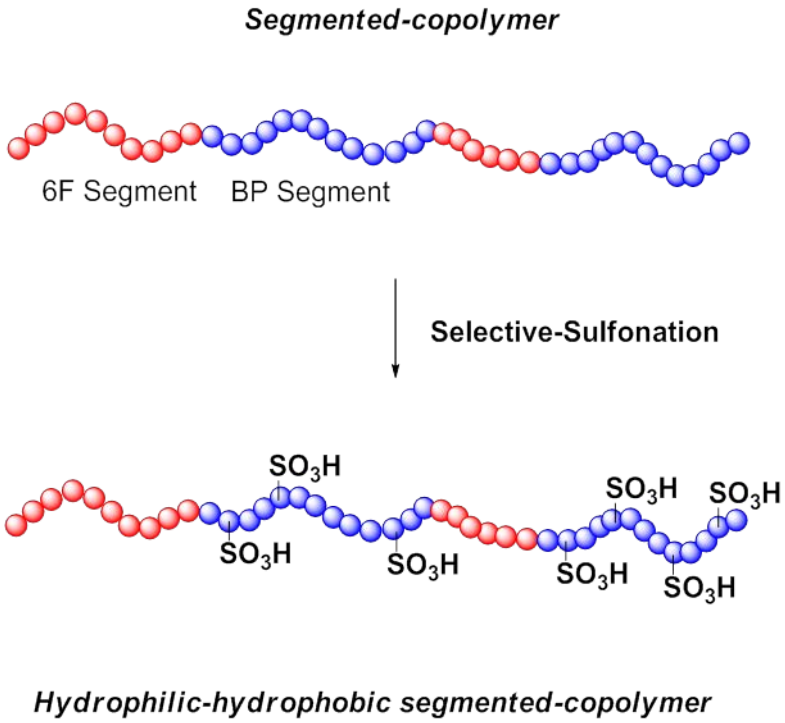

Scheme 3.5 Selective sulfonation of PFCB aryl ether segmented copolymers.

As expected, PFCB block copolymers showed outstanding sulfonation selectivity under a mild sulfonation condition. The ^{1}H NMR confirmed the presence of hydrophilic-hydrophobic segments in these copolymers. The ^{1}H NMR spectra of unsulfonated and sulfonated polymers are overlaid in Figure 3.3 and show obvious changes in signal position and intensities. The proton (H_e) adjacent to the sulfonic acid group was clearly separated at high frequency from the other aromatic protons due to deshielding from the sulfonic acid groups. The integration of the protons (H_e) adjacent to neighboring sulfonic acid moieties and known reference protons (H_{a-d}) of copolymers allowed the degree of

sulfonation of the sulfonated PFCB copolymers to be determined. The ^{1}H NMR results revealed that more sulfonic acid groups were incorporated into the polymer backbone as increasing feeding amount of chlorosulfonic acid in the post-sulfonation step. The results also showed that the peak intensities of H_a, which is ortho to PFCB ether on BP segment, gradually decreased with increasing sulfonation level. These NMR results exhibited that the post-sulfonation has occurred selectively at the ortho position of the phenyl rings on the BP segment in PFCB block copolymers. On the other hand, PFCB3 segmented copolymer did not exhibit highly selective-sulfonation because of the high portion of heterolinkages. The sulfonation was observed in all phenyl rings in BP segment and BP-6F heterolinkage except at the meta position of 6F unit. Our observation on the post-sulfonation gave a important role of understanding and controlling monomer distributions in the copolymer structures.

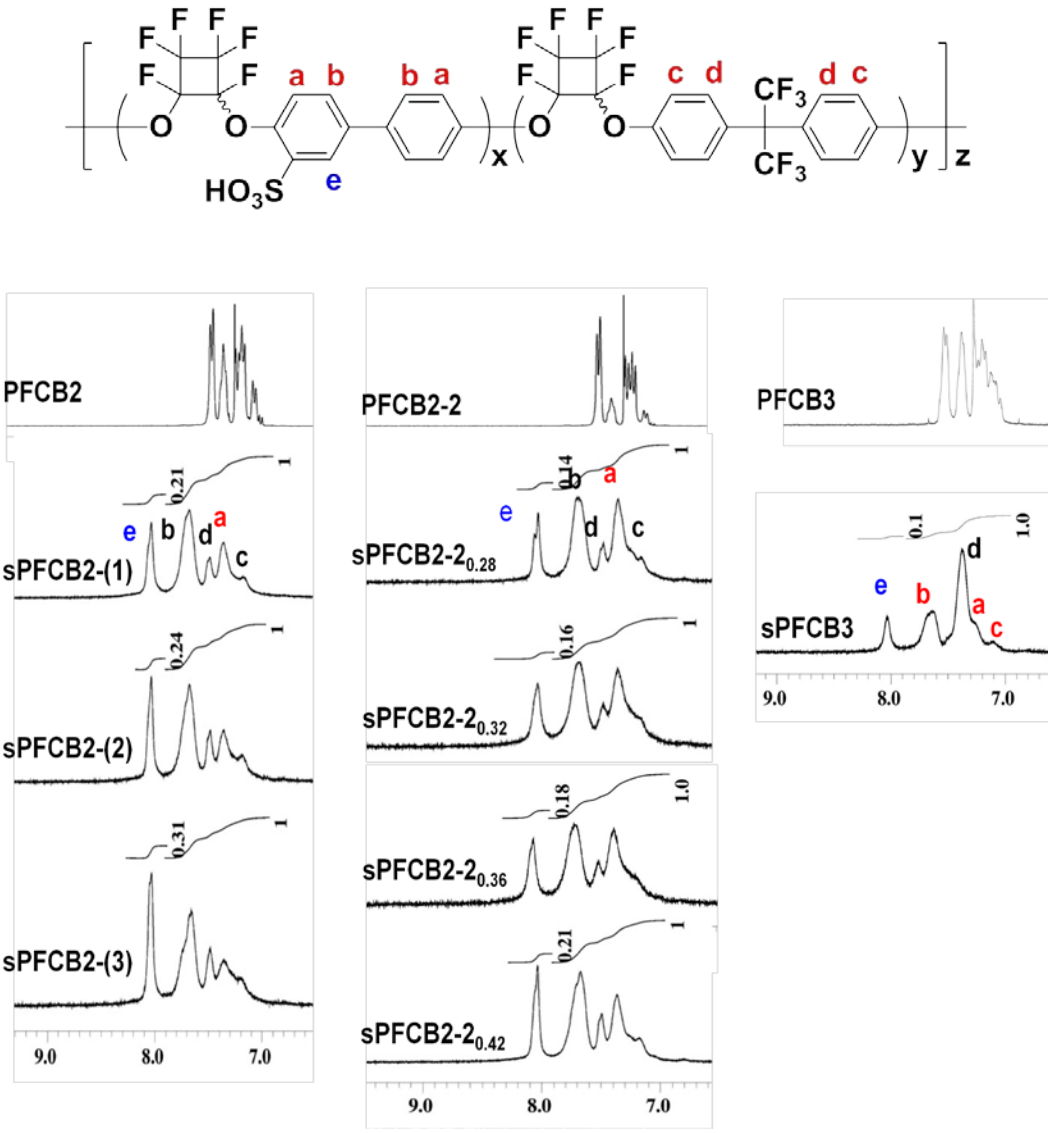

Figure 3.3 ^{1}H NMR (in $CDCl_3$ and DMSO-*d6*) spectra of sulfonated PFCB block copolymers in comparison with those of the un-sulfonated counterparts.

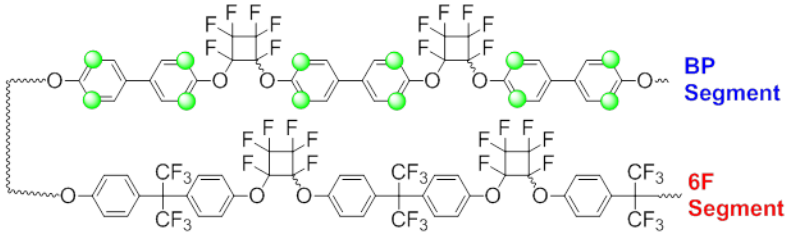

PFCB2 and PFCB2-2: "Selective" Sulfonation on BP Segments

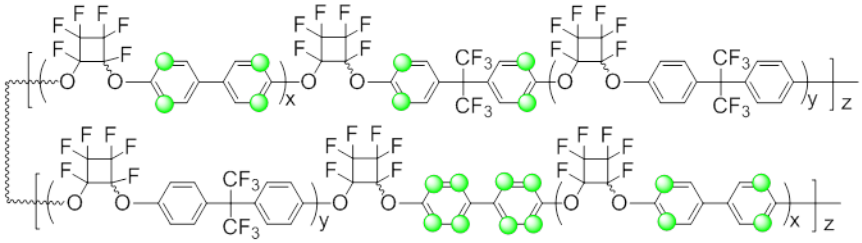

PFCB3: Sulfonation on Heterolinkage and BP Segments

Scheme 3.6 Sulfonation selectivity of PFCB aryl ether copolymers.

The high molecular weight is an important factor for PEM materials since the polymer chain entanglements are in part responsible for producing physically robust membranes. Therefore, PFCB2-2 (38 kDa) and PFCB3 (38 kDa) were mainly used for membrane characterization in this chapter. The degree of sulfonation (*Ds*) for these sulfonated PFCB2-2 and PFCB3 copolymers was determined by using the ^{1}H NMR results. The estimated *Ds* values are listed in Table 3.2. As a complementary study, elemental microanalysis (EA) was also performed to confirm the attachment of sulfonic acid group and the sulfur content of a series of sulfonated copolymers are listed in Table 3.2.

Table 3.2 Summary of sulfonation level and sulfur contents.

sPFCB copolymers	**Exp. (BP : 6F)** [a]	**Feed Ratio (g) CSA: Polymer**	**DS** [b]	**S content (wt%)** [c]
sPFCB2-2$_{0.28}$	76:24	1.0:1	0.28	5.54
sPFCB2-2$_{0.32}$		1.5:1	0.32	6.00
sPFCB2-2$_{0.36}$		2.0:1	0.36	6.47
sPFCB2-2$_{0.42}$		2.5:1	0.42	6.54
sPFCB3	50:50	2.5:1	0.26	5.60

[a] Experimental molar ratio of BP and 6F determined by ^{19}F NMR, [b] Degree of sulfonation determined by ^{1}H NMR, [c] Sulfur content determined by elemental analysis (EA).

The attachment of sulfonic acid group and the sulfur content of a series of sulfonated copolymers were further confirmed by elemental microanalysis. The elemental analysis for sulfur, carbon, hydrogen and fluorine were performed and IEC_{EA} was calculated from the sulfur content using the following equation;

$$IEC_{EA} = 1000S/M_w$$

where *S* is the sulfur content determined by elemental microanalysis, M_w corresponds to the sulfur atomic weight (32 g/mol), and 1000 is the multiplying factor to obtain an IEC value in mmol/g. The degree of sulfonation (*Ds*) determined from the NMR was also used to estimate ion-exchange capacity (IEC) of each polymer sample. The calculated IEC values (IEC_{NMR} and IEC_{EA}) that were determined by two different methods are listed and compared in Table 3.3. As expected, the IEC values determined from both EA and NMR increased with the degree of sulfonation, and the IEC values from NMR are in good agreement with those determined by EA.

Table 3.3 Summary of sulfonation level and corresponding ion-exchange capacity values for sulfonated PFCB copolymers.

$_S$PFCB copolymers	**DS** [a]	**Ion Exchange Capacity (mmol/g)**		
		IEC_{NMR} [b]	**IEC_{EA}** [c]	**$IEC_{Tit.}$** [d]
sPFCB2-2$_{0.28}$	0.28	1.50	1.73	1.54
sPFCB2-2$_{0.32}$	0.32	1.72	1.88	1.85
sPFCB2-2$_{0.36}$	0.36	1.93	2.02	1.92
sPFCB2-2$_{0.42}$	0.42	2.25	2.04	2.05
sPFCB3	0.26	1.26	1.75	1.63

[a] Degree of sulfonation determined by ^{1}H NMR, [b] IEC_{NMR} calculated using DS [a], [c] IEC_{EA} calculated using sulfur content from sulfur content determined by EA, [d] All IEC values reported in this work are the average of three titrations.

A neutralization titration was also carried out in a parallel analysis to verify the IEC values determined by NMR and EA. The dry samples (approximately 20 mg) were soaked in 20 mL of 3.0 M NaCl solution for 24 h to exchange the H^+ of the polymer to the Na^+ form completely. The released amount of H^+ was then titrated to an end point of pH 7 with 0.01 M NaOH using phenolphthalein as an indicator (Scheme 3.7). The IEC of the polymer was calculated by

$$\text{IEC (mmol/g)} = (\Delta V_{NaOH} \times C_{NaOH}) / Ws$$

where ΔV_{NaOH} is the volume of NaOH required to reaches the end point, C_{NaOH} is the concentration of the base, and *W*s is the weight of the sulfonated polymer. All IEC values reported in this work are the average of three titrations. The IEC values estimated using three different methods were reasonably consistent with one another (Table 3.3).

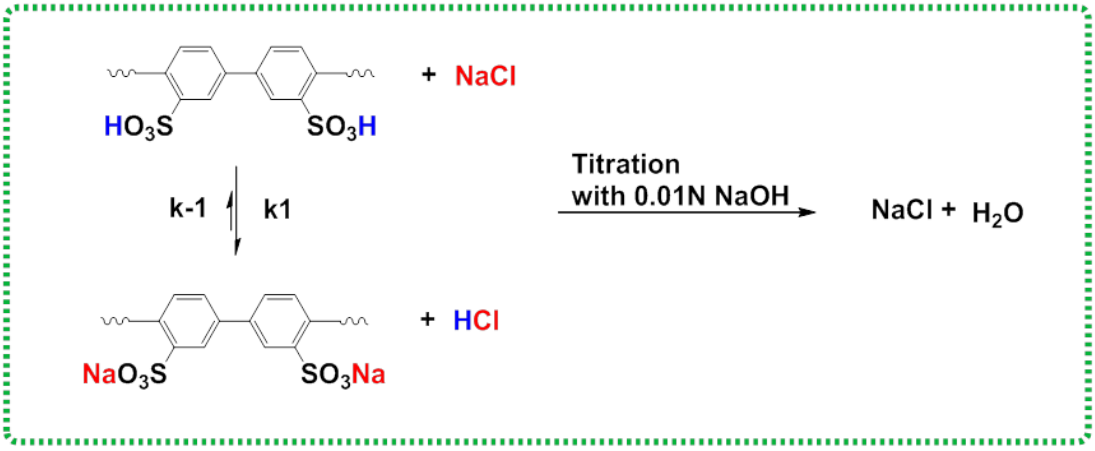

Scheme 3.7 Neutralization titration of sulfonated polymers.

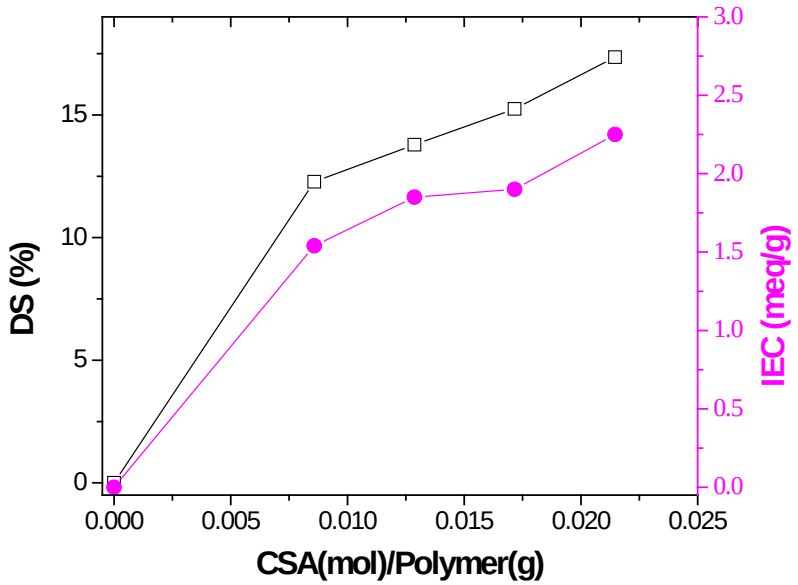

Figure 3.4 Plot of DS and IEC versus the equivalents of chlorosulfonic acid.

Thermal Peoperties of sPFCB Aryl Ether Copolymer Electrolytes

The thermal stability of the polymers was investigated by thermal gravimetric analysis (TGA) under nitrogen. All of the sulfonated PFCB polymers showed a three-step weight loss pattern consisting of dehydration, desulfonation and degradation of polymer backbone as shown in Figure 3.5. The first weight loss of ~3% from 50 to 150 °C is ascribed to the removal of physically adsorbed water. The second weight loss from 240 to 400 °C attributed to a desulfonation process increased from 15% to 17% as increasing the sulfonation level. The third weight loss around 400 °C is due to the degradation of the PFCB polymer backbone which contributed to the high thermal

stability of membranes. These amount of sulfonic group as a function of IEC determined by TGA and high decomposition temperature of last stage support that the introduction of sulfonic acid group was successfully controlled without chain scission.

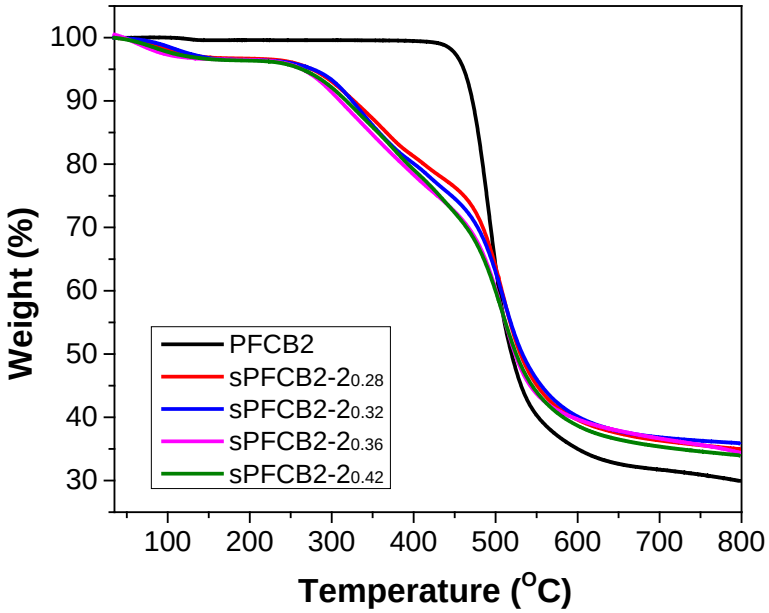

Figure 3.5 TGA curves of PFCB 2 and sPFCB2-2 copolymers.

Table 3.4 Thermal stability of sPFCB2-2 copolymers.

S-Polymers	wt. loss (%)[a]		
	1st stage (dehydration)	**2nd stage** (desulfonation)	**3rd stage** (degradation of polymer backbone)
sPFCB2-2$_{0.28}$	3.3	15.6	45.9
sPFCB2-2$_{0.32}$	3.4	16.4	43.8
sPFCB2-2$_{0.36}$	4.00	18.7	43.5
sPFCB2-2$_{0.42}$	3.6	18.4	43.4

[a] wt. loss (%) determined by TGA (10 °C/min) in nitrogen

Proton-exchange membrane materials require a higher glass transitional temperature (T_g) than the operating temperature of a PEM fuel cell to maintain their mechanical properties even under hydrated condition. It is also well known that water can act as a plasticizer and lower T_g of polymers. Therefore, high-T_g polymers are desirable to be used in high-temperature PEM fuel cell applications. The glass transitional temperature of PFCB polymers was estimated using a DSC. However, the glass transition peaks of sPFCB2-2$_{0.28}$, sPFCB2-2$_{0.32}$, sPFCB2-2$_{0.36}$, and sPFCB2-2$_{0.42}$ were not resolved clearly enough to determine a glass transition temperature (T_g).

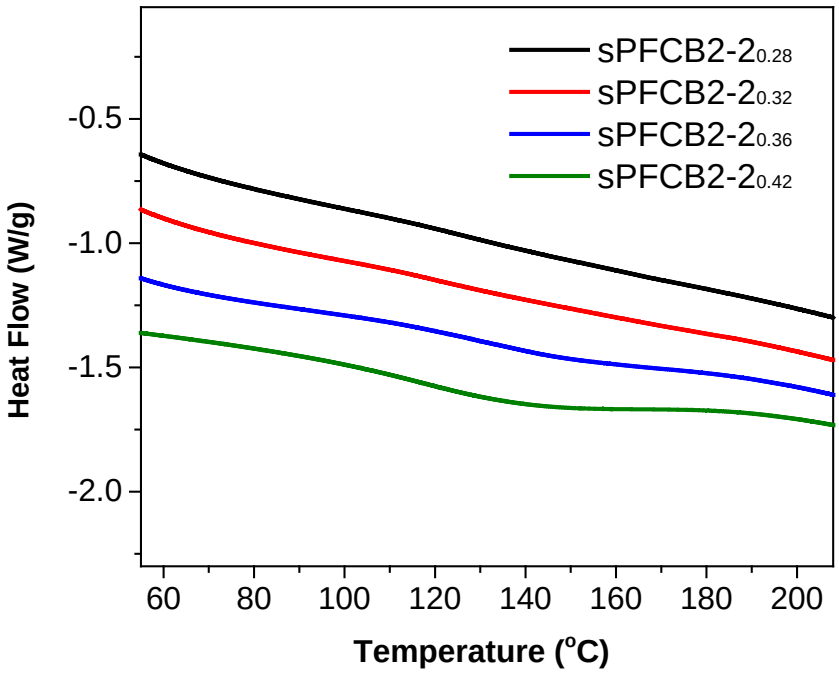

Figure 3.6 DSC of sulfonated PFCB aryl ether copolymers (10 °C/min in nitrogen).

To accurately identify the T_gs of sulfonated sample, the Dynamic Mechanical Analysis (DMA) of sPFCB films (sample size: 15 × 10, thickness: 0.25-0.35 mm) was performed in air at the heating rate of 10 °C/min. From this dynamic mechanical analysis, the storage modulus (E'), loss modulus (E''), and damping factor (Tan delta) were collected as a function of temperature (Figure 3.7 ~ Figure 3.9). T_gs were taken from the E' onset, E'' peak, and the maximum of tan delta peaks.

Figure 3.7 shows the tan delta-temperature curves for a sulfonated segmented copolymer (sPFCB3$_{0.26}$) sample and sulfonated block copolymer (sPFCB2-2$_{0.28,}$ sPFCB2-2$_{0.32,}$ and sPFCB2-2$_{0.42}$) samples. The T_gs identified form the tan delta peaks are listed in

Table 3.5 as comparison with T_g of unsulfonated PFCB polymers which was estimated by DSC. In general, T_gs of sulfonated samples are greater than their nonsulfonated analogues because the sulfonic acid groups can interact via hydrogen bonding and result in higher steric congestion of a polymer backbone. As expected, the DMA curves of sPFCB3$_{0.26}$ film showed high T_gs for the sulfonated films in the range of 130-220 °C. On the other hand, sPFCB block copolymer samples exhibited two α-relaxation peaks that correspond to the T_g of polymer. One tan delta peak was observed at 125-150 °C and the other one at 192-196 °C. The first tan delta peak around 140 °C is close to the T_g of the unsulfonated polymer, suggesting a phase separation of unsulfonated polymer chains from the sulfonated polymer domain. Two tan delta peaks are attributable to the nonpolar domain and the ionic cluster domain, respectively. We note that there is no influence of sulfonation level for the samples.

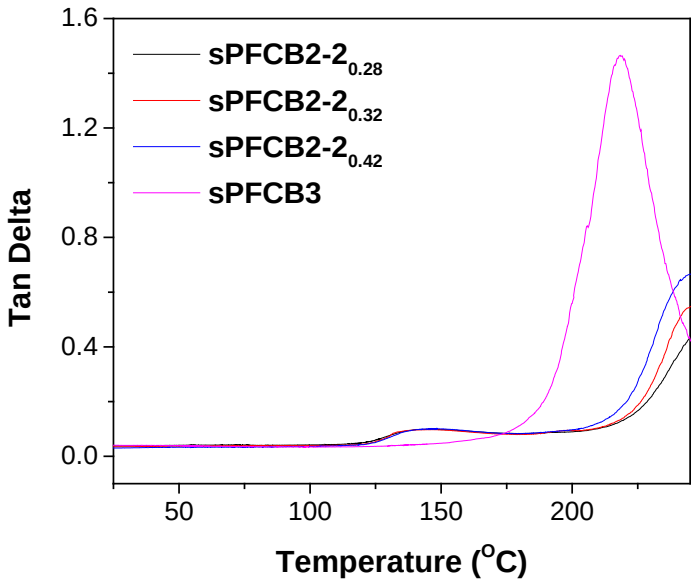

Figure 3.7 Tan Delta peaks of sPFCB2-2 copolymers (DMA, 10 °C/min in nitrogen).

Table 3.5 Glass transition temperature of sPFCB films determined by Tan Delta peak.

Sample		**Sample**	**Tan Delta peak** [b]	
Polymer	T_g (°C) [a]	**Films**	T_{g1}	T_{g2}
		M-sPFCB2-$2_{0.28}$	141	193
PFCB2-2	137	M-sPFCB2-$2_{0.32}$	141	196
		M-sPFCB2-$2_{0.42}$	141	195
PFCB3	127	M-sPFCB$3_{0.26}$	220	none

[a] T_g of unsulfonated polymer determined by DSC (10 °C/min) in nitrogen, [b] T_g by Tan Delta peak (Tan Delta Peak occurs at the highest temperature between the glassy and rubbery states of a polymer**).**

Two phase morphology of sulfonated block copolymers was further confirmed by E' onset and E" peak. Figure 3.8 and 3.9 show the storage modulus and loss modulus versus temperature curves of sulfonated samples. For sulfonated block copolymers, a two-step decrease in E' was observed as the temperature increases. However, the membrane sample derived from a segmented copolymer, sPFCB3, exhibited only one glass transition at T_g = ~200 °C which indicates that there is no distinctive separation between hydrophilic and hydrophobic phase domains.

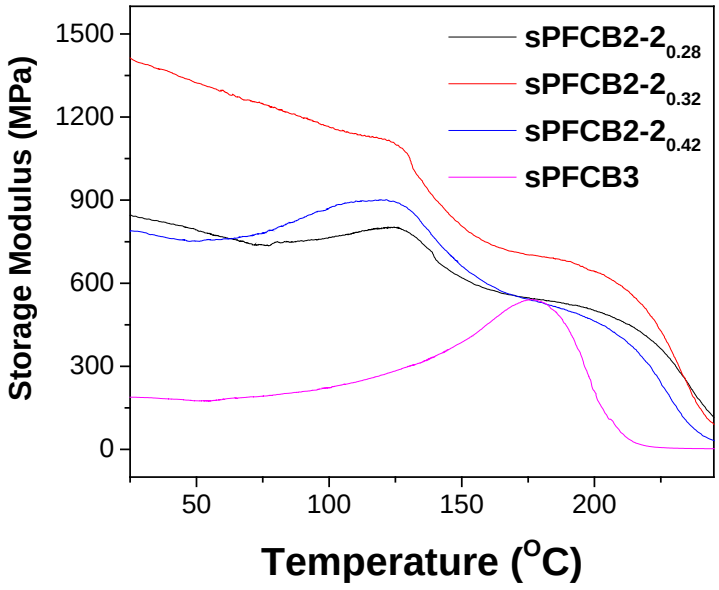

Figure 3.8 Storage modulus of sPFCB2-2 copolymers films.

Loss modulus E" is known to be a measure of the energy dissipated which is related to the viscous response of the polymer. As shown in Figure 3.9, one transition was observed at T_{g1} of 136-139 °C and the other transition at T_{g2} of 192-196 °C, which are attributable to the nonpolar domain and the ionic cluster domain respectively. During DMA test, the color change (from colorless to brown) of samples was observed at around 220 °C. This implies that the third peak around 225 °C was due to desulfonation.

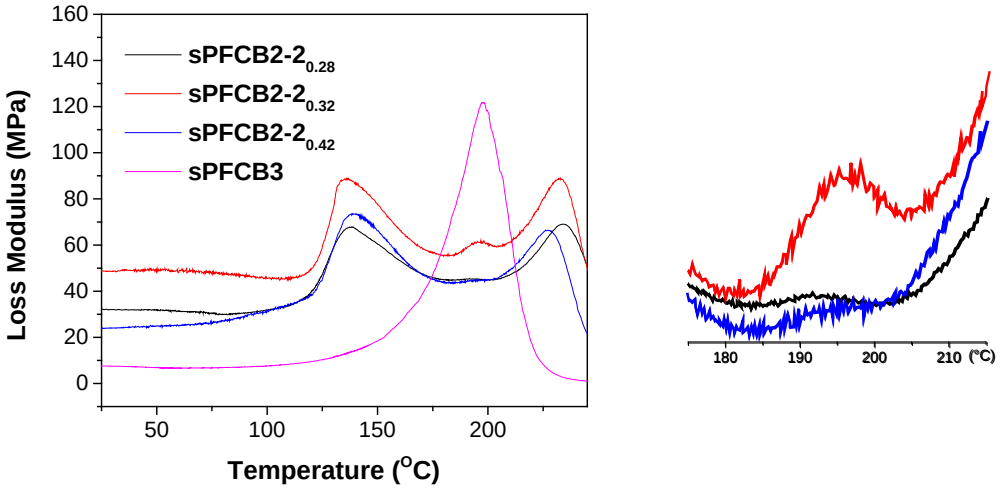

Figure 3.9 Loss modulus of sPFCB2-2 copolymer films.

Table 3.6 Glass transition temperature of SPFCB films taken from E' onset and E'' peak.

Polymer	T_g (°C) [a]	Films	E' onset [b] (Storage Modulus)		E'' peak [c] (Loss Modulus)	
			T_{g1}	T_{g2}	T_{g1}	T_{g2}
PFCB2-2	137	**M-sPFCB2-2$_{0.28}$**	130	214	138	192
		M-sPFCB2-2$_{0.32}$	128	212	136	196
		M-sPFCB2-2$_{0.42}$	129	206	139	193
PFCB3	127	**M-sPFCB2-2$_{0.26}$**	183	none	200	none

[a]T_g of unsulfonated polymer determined by DSC (10 °C/min) in nitrogen, [b]T_g by E' onset, [c]T_g by E'' peak.

Preparation of PFCB Aryl Ether Polyelectrolyte Membranes

The resulting polymers are solution processible in polar organic solvents to give transparent and flexible membranes. All of the sulfonated polymers were readily soluble in DMAc and formed transparent, flexible, and tough membranes after solution casting as shown in Figure 3.10. The membranes showed lower IEC values than original sulfonated polymers due to the conversion to the salt form during membrane casting process. The ^{1}H NMR confirmed the presence of salt form in the polymer backbones (Figure 3.11). The proton adjacent to the salt sulfonic group was separated at higher frequency from the peak of the proton neighboring to the sulfonic acid group. To remove salt in membranes, therefore, all sPFCB membranes were acidified using 1M HCl solution and the resulting pure acid form was confirmed by ^{1}H NMR (Figure 3.11).

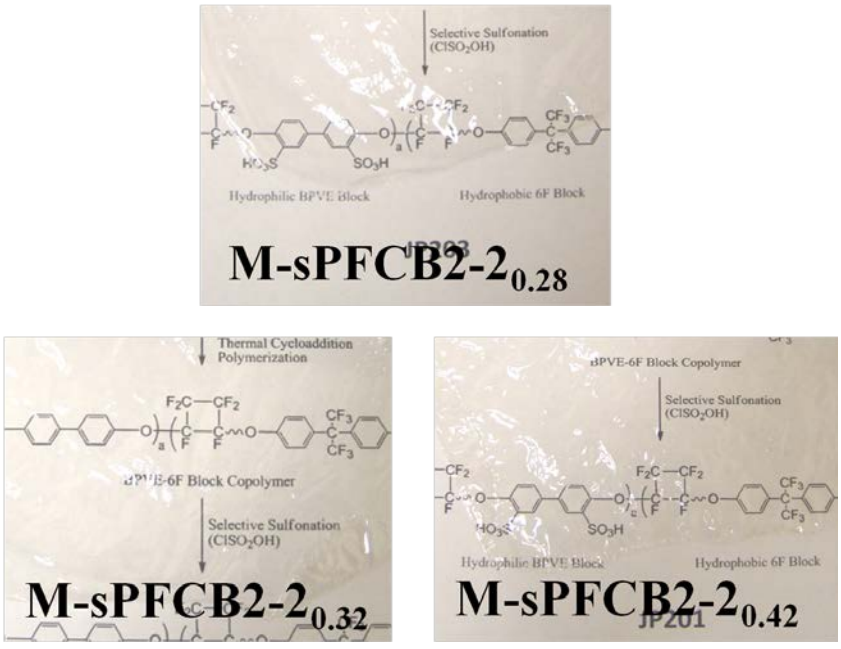

Figure 3.10 Photos of sulfonated PFCB aryl ether copolymer membranes (membrane size: approx. 6 inch^{2}).

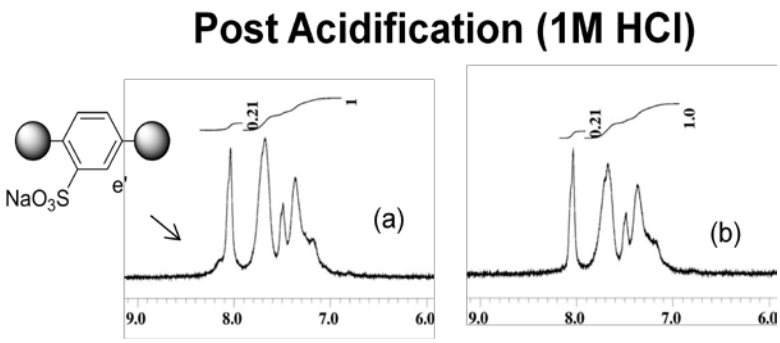

Figure 3.11 ^{1}H NMR of (a) crude and (b) post-acidified membrane (MsPFCB2-$2_{0.42}$).

Properties of PFCB Aryl Ether Polyelectrolyte Membranes

Morphology of sPFCB membranes

Membrane morphology of sPFCB samples was investigated by using tapping-mode atomic-force microscopy to obtain phase imaging data. Previously, P.T. James and coworkers have studied the effect of a tip-sample interaction on AFM phase-volume images.[47] The water-rich regions trigger damp the cantilever oscillation due to their attractive electrostatic force, then, once in contact with great water affinity, dissipate more energy. That is, the adhesive force between a tip and sample cause phase shift in the energy dissipation and the differences in the energy dissipation cause phase contrast, dark and light areas, corresponding to the hydrophilic and hydrophobic domains, respectively.

Figure 3.12 shows the phase images of the M-sPFCB12-$2_{0.28}$, M-sPFCB2-$2_{0.42}$, and M-sPFCB$3_{0.26}$ samples. The phase images presented that all of the $_{S}$PFCB membranes possess well-separated hydrophilic and hydrophobic domains. The M-

sPFCB2-$2_{0.28}$ sample presents well-connected hydrophilic channels (dark areas) made up of small hydrophilic clusters (~5 nm). However, the M-sPFCB2-$2_{0.42}$ sample exhibits larger hydrophilic clusters. This increase in the cluster size is reasonable because the higher sulfonation degree favors the formation of larger ionic clusters. These phase images showing the distinct nanophase-separated structures agrees well with the two clear T_g*s* observed from the DMA results. The AFM phase imaging also revealed that the compositional ratio of the copolymers affects the membrane morphology. For a segmented PFCB3 polymer membrane, M-sPFCB$3_{0.26}$, hydrophobic domains dominate over hydrophilic compared with M-sPFCB2-$2_{0.28}$ which has the similar sulfonation degree because of its higher content of fluorine in the PFCB 3 copolymer chains (Note the difference in the domain sizes shown in Figure 3.12.

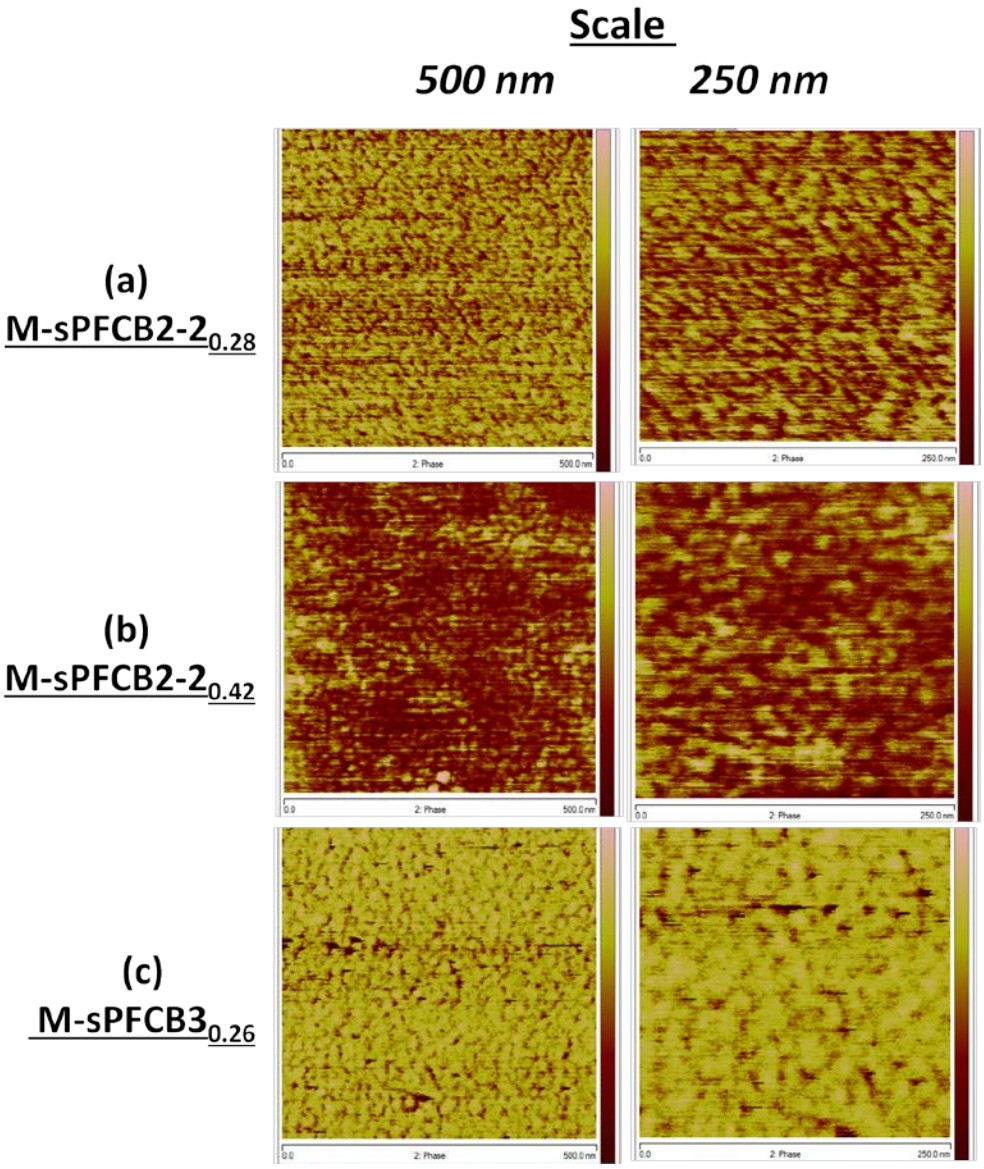

Figure 3.12 AFM phase images of sPFCB copolymer membranes.

Proton Conductivity of sPFCB membranes

The conductivity of sPFCB samples increased as increasing sulfonation level as expected. The highest conductivity were found to be 0.09 at 100% RH with highly sulfonated membrane. Interestingly, segmented copolymer (M-sPFCB3$_{0.26}$) showed higher conductivity than these two blockcopolymer membranes (M-sPFCB1$_{0.28}$ and M-sPFCB1$_{0.32}$) despite lower sulfonation level. This result could mean that the morphology of the segmented copolymer is efficient to transport protons. Although the polymer backbone is rigid, the SPFCB block copolymer can form co-continuous hydrophilic channels to absorb water because of a large free volume derived from stereo-isomer of PFCB ether moities.

Table 3.7 Proton conductivity of membranes at 100% RH.

Membrane	IEC (meq/g)	Thickness (μm)	Conductivity (S/cm)
M-sPFCB2-2$_{0.28}$	1.73	20	0.032
M-sPFCB2-2$_{0.32}$	1.88	23	0.046
M-sPFCB2-2$_{0.42}$	2.04	26	0.094
M-sPFCB3	1.75	33	0.052
Nafion212	0.92	56	0.134

Figure 3.13 shows the proton conductivity results of the sPFCB polymer membranes at 80 °C under different relative humidity conditions (e.g., 20-100% RH). As seen in Figure 3.13, the conductivity of sPFCB samples is more dependent on relative humidity than Nafion®. This may be because the acidity of sPFCB samples is weaker than Nafion®. In general, the proton conductivity increases with increasing relative humidity and with sulfonation degree at a given relative humidity.

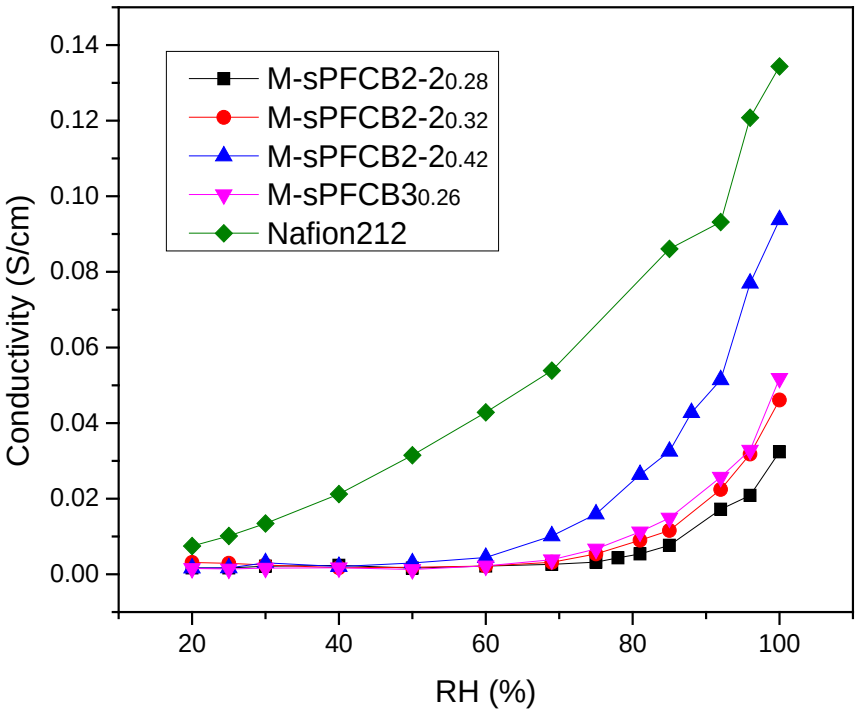

Figure 3.13 Conductivity of sPFCB copolymer membranes **(**M-sPFCB2-2$_{0.28}$, M-sPFCB2-2$_{0.32}$, M-sPFCB2-2$_{0.42}$, and M-sPFCB3$_{0.26}$) and Nafion212 as a function of RH (%).

Water Uptake and Swelling Ratio of sPFCB membranes

The water uptake and swelling ratio of sPFCB membranes were measured at 25 °C and 80 °C. First, the water uptake of membranes was determined by the weight difference between dry and wet samples. The weight (W_{dry}) of vacuum dried membrane was measured and then soaked in deionized water at room temperature for 24 h. The wet membrane was blotted dry to remove surface water and immediately weighted again to determine the wet mass (W_{wet}) of the film. Water uptake was calculated by the following equation:

$$\text{Water uptake (wt\%)} = [(W_{wet} - W_{dry}) / W_{dry}] \times 100$$

Dimensional change of the hydrated membrane was also investigated after soaking membranes at 25 °C and 80 °C for 24 h in deionized water. The change of membrane length was measured and characterized as swelling ratio using the following equation:

$$\text{Swelling (\%)} = [(L_{wet} - L_{dry}) / L_{dry}] \times 100$$

where L_{wet} and L_{dry} are the length of hydrated and dry membrane, respectively. The results are listed in Table 3.8.

Table 3.8 Water uptake and swelling ratio of membranes.

Membrane	IEC (meq/g)	Water Uptake [a] (%)		Swelling Ratio [b] (%)	
		25 (°C)	80 (°C)	25 (°C)	80 (°C)
M-sPFCB2-2$_{0.28}$	1.73	20	40	7	15
M-sPFCB2-2$_{0.32}$	1.88	25	80	15	30
M-sPFCB2-2$_{0.42}$	2.04	100	320	50	100
M-sPFCB3$_{0.26}$	1.75	2	26	10	20

[a ,b]Average values, [a]Calculated by *Water Uptake (%) = [(W_{wet} – W_{dry}) / W_{dry}] × 100*, [b] *Swelling Ratio (%) = [(L_{wet} – L_{dry}) / L_{dry}] × 100* where W_{wet}, W_{dry} , L_{wet} and L_{dry} are the weight and length of hydrated and dry membrane, respectively.

sPFCB membranes presented generally similar characteristics in water uptake and swelling; that is, higher IEC membranes absorbed more water and exhibited greater swelling. The M-sPFCB3$_{0.26}$ sample showed lower water uptake than M-sPFCB2-2$_{0.28}$ although they have the similar sulfonation degrees of 0.26 and 0.28, respectively. This result seems reasonable because the M-sPFCB3$_{0.26}$ sample contains a compositionally higher content of the 6F unit than that present in the M-sPFCB2-2$_{0.28}$ sample.

Conclusion

The sulfonated PFCB segmented copolymers were successfully prepared via thermal initiated step growth [2 + 2] cyclopolymerization, followed by selective post-sulfonation. The segmented copolymer showed outstanding sulfonation selectivity. Because of isofluoropropyl electron withdrawing groups in the 6F segment, the 6F segment is electronically deactivated toward electrophilic aromatic substitution reactions. Hydrophilic and hydrophobic phase separation was confirmed by DMA. The sPFCB segmented copolymer samples exhibited two glass transitions (T_{g1} and T_{g2}, respectively). The appearance of the second glass transition at T_{g2} of ~200 °C suggests that hydrophilic and hydrophobic domains have been well separated in the membranes. The behavior of sulfonated segmented copolymers in DMA indicate that the change in morphology takes place with microstructure of pristine polymers and post-functionalization. This approach allows for preparation of thermally stable PFCB-based proton-exchange membrane, and control over hydrophilic channel morphology, water uptake, and swelling. The sPFCB copolymers consisting of long-chain segments exhibited relatively well-controlled phase separation, compared with the short-chain segmented copolymers in AFM. In general, all of the results indicate that the sPFCB segmented copolymers are suitable in use as a proton-exchange membrane.

Experimental Details

Materials

Chlorosulfonic acid (CSA) and sodium hydroxide (0.01 N) were purchased from Alfa Aesar and Fisher Scientific. Commercially available monomers, 4,4'-bis(4-trifluorovinyloxy)biphenyl (BP) and 2,2'-bis(4-trifluorovinyloxy) biphenyl-1,1,1,3,3,3-hexafluoropropane (6F) and their oligomers (BPo and 6Fo) were donated by Tetramer Technologies, L.L.C. 6F monomer was purified by column with hexane before use. All other chemicals and solvents were obtained from Aldrich and used as received unless stated otherwise.

Instrumentations

^{1}H and ^{19}F NMR spectra were recorded on a JEOL Eclipse + 300. Gel permeation chromatography (GPC) data were collected in $CHCl_3$ from a Waters 2690 Alliance System with photodiode array detection. Molecular weights were obtained using polystyrene as a standard. Elemental microanalysis data for carbon, hydrogen, and fluorine were obtained from Atlantic Microlab, Inc. (Norcross, GA). Thermal gravimetric analysis (TGA) was performed on a Mettler-Toledo 851 instrument in nitrogen and air at a heating rate of 10 °C/min up to 800 °C. Differential scanning calorimetry (DSC) analysis was performed on a TA Q1000 instrument in nitrogen at a heating rate of 10 °C/min up to 200 °C. Dynamic mechanical analysis (DMA) was conducted with DMA Q800 at an oscillation frequency of 10 Hz. Temperature scanning from 25 °C to 250 °C was performed with a heating rate of 5°C/min.

Preparation of Polymers

Synthesis of PFCB2-2 (Copolymerization of BPo with 6Fm.) Synthesis of copolymer PFCB2-2 was conducted as follows: 10g of BP oligoemr (BPo, Mn= 8,000 g/mol), 5g of 6F monomer (6Fm), 10 mL of diphenylether were added to three-neck 250 mL flask, equipped with a condenser, argon inlet, and a mechanical stirrer. The reaction mixture was slightly heated at 60 °C and the melted system was sparged with argon gas for 30 min. The thermal step-growth cyclopolymerization was conducted at 140 °C for 24 h, 160 °C for 72 h, 180 °C for 24 h, and 210 °C for 14 h under argon blanket. The resulting viscous crude polymer was cool down and dissolved in tetrahydrofuran (THF). The solution was precipitated in a large excess of methanol. The resulting fibrous copolymer was purified in a soxhlet extractor with methanol for 24 h to remove diphenylether and unreacted monomers. The copolymer was dried at 60 °C in vacuum for 24 h. Yield: 80-85%, ^{1}H NMR (300 MHz, $CDCl_3$) δ 7.47 (d, J = 9 Hz, $H_{f'}$), 7.40–7.30 (m, $H_{g'}$), 7.30–7.20 (m, overlapped by $H_{e'}$ and $CDCl_3$), 7.07 (d, J = 6 Hz, $H_{h'}$); ^{19}F NMR (283 MHz, $CDCl_3$) δ –64 (s, $F_{d'}$), –126 – (–133) (m, the overlap of cyclobutyl–F_6 on BP and 6F segments). Elemental Analysis: Found: C, 52.86; H, 2.02; F, 36.91.

Sulfonation of PFCB Aryl Ether Copolymers

Five grams of PFCB aryl ether copolymer was dissolved in 100 mL of dichloromethane (DCM). The chlorosulfonic acid (CSA) was added at 36 °C internal temperature and then the mixture was stirred vigorously for 1 h at the same temperature. The various degree of sulfonation was obtained by controlling the equivalent of

chlorosulfonic acid (Sample No: weight ratio CSA (g)/polymers(g), sPFCB2-(1): 1.5/1, sPFCB2-(2): 2.0/1, sPFCB2-(1): 2.5/1, sPFCB2-$2_{0.28}$: 1.0/1, sPFCB2-$2_{0.32}$: 1.5/1, sPFCB2-$2_{0.36}$: 2.0/1, sPFCB2-$2_{0.42}$: 2.5/1, sPFCB$3_{0.26}$: 2.5/1). The precipitate, being sPFCB, was recovered by decanting DCM into a crushed ice and then washed in cold and boiling deionized water several times to remove excess acids. The supernatant has been removed and the final precipitate was recovered by filtration and dried in a vacuum oven for 24 h at 60 °C. Yield: 90-97%, ^{1}H NMR (300 MHz, DMSO-d_6) δ 8.05 (s, br, H_e), 7.70 (s, br, H_b), 7.50 (s, br, H_d), 7.35 (s, br, H_a), 7.20 (s, br, H_c); **^{19}F** NMR (283 MHz, DMSO-d_6) δ –63 (s, -CF_3, 6F), –94–(–140) (m, br, the overlap of cyclobutyl-F_6 on BP and 6F). Elemental Analysis: **sPFCB2-(1)** - Found: C, 39.38; H, 2.38; F, 27.11; S, 6.25; **sPFCB2-(2)**- Found: C, 38.51; H, 2.34; F, 26.30; S, 6.75; **sPFCB2-(3)** - Found: C, 37.81; H, 1.93; F, 28.06; S, 6.84; **sPFCB2-$2_{0.28}$** - Found: C, 41.55; H, 2.09; F, 28.41; S, 5.54; **sPFCB2-$2_{0.32}$** - Found: C, 41.01; H, 2.15; F, 27.82; S, 6.00; **sPFCB2-$2_{0.36}$** - Found: C, 40.69; H, 2.26; F, 27.39; S, 6.47; **sPFCB2-$2_{0.42}$** - Found: C, 38.73; H, 2.38; F, 26.28; S, 6.54; **sPFCB$3_{0.26}$** - Found: C, 40.76; H, 1.69; F, 32.85; S, 5.60

Membrane Preparation

Sulfonated polymer was dissolved in N,N-dimethylacetamide (DMAc) to 20 wt% concentration. The solutions were filtered through a 0.45 μm syringe filter and cast on a glass plate. The solvent was evaporated on the casting table for 15 min at 70 °C and completely dried in a vacuum oven for 24 h at 100 °C. The polymer membranes were carefully peeled off by grief immersion in water and acidified by soaking in 1M HCl for

24 h at room temperature for the pure acid form membranes. Membranes were washed several times with deionized water to remove any residual HCl and dried under vacuum for 24 h at 60 °C.

References

1. Zhang, H.; Shen, P. K. Recent Development of Polymer Electrolyte Membranes for Fuel Cells. *Chem. Rev.* **2012,** *112*, 2780-2832.

2. Steele, B. C. H.; Heinzel, A. Materials for Fuel-cell Technologies. *Nature* **2001,** *414*, 345-352.

3. Epping Martin, K.; Kopasz, J. P. The U.S. DOEs High Temperature Membrane Effort. *Fuel Cells* **2009,** *9*, 356-362.

4. Laberty-Robert, C.; Valle, K.; Pereira, F.; Sanchez, C. Design and Properties of Functional Hybrid Organic-inorganic Membranes for Fuel Cells. *Chem. Soc. Rev.* **2011,** *40*, 961-1005.

5. Peighambardoust, S. J.; Rowshanzamir, S.; Amjadi, M. Review of the Proton Exchange Membranes for Fuel Cell Applications. *Int. J. Hydrogen Energy* **2010,** *35*, 9349-9384.

6. Schoeman, H.; Krieg, H. M.; Kruger, A. J.; Chromik, A.; Krajinovic, K.; Kerres, J. H_2SO_4 Stability of PBI-blend Membranes for SO_2 Electrolysis. *Int. J. Hydrogen Energy* **2012,** *37*, 603-614.

7. O'Brien, J. A.; Hinkley, J. T.; Donne, S. W.; Lindquist, S. E. The Electrochemical Oxidation of Aqueous Sulfur Dioxide: A Critical Review of Work with respect to the Hybrid Sulfur Cycle. *Electrochim. Acta* **2010,** *55*, 573-591.

8. Staser, J. A.; Norman, K.; Fujimoto, C. H.; Hickner, M. A.; Weidner, J. W. Transport Properties and Performance of Polymer Electrolyte Membranes for the Hybrid Sulfur Electrolyzer. *J. Electrochem. Soc.* **2009,** *156*, B842-B847.

9. Elvington, M. C.; Colón-Mercado, H.; McCatty, S.; Stone, S. G.; Hobbs, D. T. Evaluation of Proton-conducting Membranes for use in a Sulfur Dioxide Depolarized Electrolyzer. *J. Power Sources* **2010,** *195*, 2823-2829.

10. Sivasubramanian, P.; Ramasamy, R. P.; Freire, F. J.; Holland, C. E.; Weidner, J. W. Electrochemical hydrogen production from thermochemical cycles using a proton exchange membrane electrolyzer. *Int. J. Hydrogen Energy* **2007,** *32*, 463-468.

11. Karo, J.; Aabloo, A.; Thomas, J. O.; Brandell, D. Molecular Dynamics Modeling of Proton Transport in Nafion and Hyflon Nanostructures. *J. Phys. Chem. B* **2010,** *114*, 6056-6064.

12. Oh, J. M. Electrolyte Incorporation into Composite Electrodes for Proton-Exchange Membrane Fuel Cells and Lithium-Ion Batteries. Ph.D Thesis, Clemson University, 2011.

13. Banerjee, S.; Curtin, D. E. Nafion® Perfluorinated Membranes in Fuel Cells. *J. Fluorine Chem.* **2004,** *125*, 1211-1216.

14. Mauritz, K. A.; Moore, R. B. State of Understanding of Nafion. *Chem. Rev.* **2004,** *104*, 4535-4586.

15. Kim, Y. S.; Dong, L.; Hickner, M. A.; Glass, T. E.; Webb, V.; McGrath, J. E. State of Water in Disulfonated Poly(arylene ether sulfone) Copolymers and a

Perfluorosulfonic Acid Copolymer (Nafion) and Its Effect on Physical and Electrochemical Properties. *Macromolecules* **2003,** *36*, 6281-6285.

16. Hickner, M. A.; Ghassemi, H.; Kim, Y. S.; Einsla, B. R.; E., M. J. Alternative Polymer Systems for Proton Exchange Membranes (PEMs). *Chem. Rev.* **2004,** *104*, 4587-4612.

17. Einsla, M. L.; Kim, Y. S.; Hawley, M.; Lee, H.-S.; McGrath, J. E.; Liu, B.; Guiver, M. D.; Pivovar, B. S. Toward Improved Conductivity of Sulfonated Aromatic Proton Exchange Membranes at Low Relative Humidity. *Chem. Mater.* **2008,** *20*, 5636-5642.

18. Rusanov, A. L.; Likhatchev, D.; Kostoglodov, P. V.; Müllen, K.; Klapper, M.; Schmidt, M. Proton-Exchanging Electrolyte Membranes Based on Aromatic Condensation Polymers. *Adv. Polym. Sci.* **2005,** *179*, 25-69.

19. Iojoiu, C.; Maréchal, M.; Chabert, F.; Sanchez, J. Y. Mastering Sulfonation of Aromatic Polysulfones: Crucial for Membranes for Fuel Cell Application. *Fuel Cells* **2005,** *5*, 344-354.

20. Bishop, M. T.; Karasz, F. E.; Russo, P. S.; Langley, K. H. Solubility and Properties of a Poly(aryl ether ketone) in Strong Acids. *Macromolecules* **1985,** *18*, 86-93.

21. Shibuya, N.; Porter, R. S. Kinetics of PEEK Sulfonation in Concentrated Sulfuric Acid. *Macromolecules* **1992,** *25*, 6495-6499.

22. Ding, J.; Chuy, C.; Holdcroft, S. A Self-organized Network of Nanochannels Enhances Ion Conductivity through Polymer Films. *Chem. Mater.* **2001,** *13*, 2231-2233.

23. Nolte, R.; Ledjeff, K.; Bauer, M.; Mülhaupt, R. Partially Sulfonated Poly(arylene ether sulfone) - A Versatile Proton Conducting Membrane Material for Modern Energy Conversion Technologies. *J. Membr. Sci.* **1993,** *83*, 211-220.

24. Roziere, J.; Jones, D. J. Non-fluorinated Polymer Materials for Proton Exchange Membrane Fuel Cells. *Annu. Rev. Mater. Res.* **2003,** *33*, 503-555.

25. Hubner, G.; Roduner, E. EPR Investigation of HO/ Radical Initiated Degradation Reactions of Sulfonated Aromatics as Model Compounds for Fuel Cell Proton Conducting Membranes. *J. Mater. Chem.* **1999,** *9*, 409-418.

26. Kreuer, K. D. On the Development of Proton Conducting Polymer Membranes for Hydrogen and Methanol Fuel Cells. *J. Membr. Sci.* **2001,** *185*, 29-39.

27. Dockheer, S. M.; Gubler, L.; Bounds, P. L.; Domazou, A. S.; Scherer, G. G.; Wokaun, A.; Koppenol, W. H. Damage to Fuel Cell Membranes. Reaction of $HO^{\cdot}$ with an Oligomer of Poly(sodium styrene sulfonate) and Subsequent Reaction with O_2. *Phys. Chem. Chem. Phys.* **2010,** *12*, 11609-11616.

28. Pinteala, M.; Schlick, S. Direct ESR Detection and Spin Trapping of Radicals Generated by Reaction of Oxygen Radicals with Sulfonated Poly(ether ether ketone) (SPEEK) Membranes. *Polym. Degrad. Stab.* **2009,** *94*, 1779-1787.

29. Perrot, C.; Gonon, L.; Bardet, M.; Marestin, C.; Pierre-Bayle, A.; Gebel, G. Degradation of a Sulfonated Aryl Ether Ketone Model Compound in Oxidative Media (sPAEK). *Polymer* **2009,** *50*, 1671-1681.

30. Fujimoto, C. H.; Hickner, M. A.; Cornelius, C. J.; Loy, D. A. Ionomeric Poly(phenylene) Prepared by Diels-Alder Polymerization: Synthesis and Physical Properties of a Novel Polyelectrolyte. *Macromolecules* **2005,** *38*, 5010-5016.

31. Asano, N.; Aoki, M.; Suzuki, S.; Miyatake, K.; Uchida, H.; Watanabe, M. Aliphatic/Aromatic Polyimide Ionomers as a Proton Conductive Membrane for Fuel Cell Applications. *J. Am. Chem. Soc.* **2006,** *128*, 1762-1769.

32. Zhang, F.; Cui, Z.; Li, N.; Dai, L.; Zhang, S. Synthesis of Sulfonated Poly(arylene-co-naphthalimide)s as Novel Polymers for Proton Exchange Membranes. *Polymer* **2008,** *49*, 3272-3278.

33. Marestin, C.; Gebel, G.; Diat, O.; Mercier, R. Sulfonated Polyimides. *Adv. Polym. Sci.* **2008,** *216*, 185-258.

34. Tan, N.; Xiao, G.; Yan, D. Sulfonated Polybenzothiazoles: A Novel Candidate for Proton Exchange Membranes†. *Chem. Mater.* **2010,** *22*, 1022-1031.

35. PU, H.; WANG, L.; PAN, H.; WAN, D. Synthesis and Characterization of Fluorine-Containing Polybenzimidazole for Proton Conducting Membranes in Fuel Cells. *J Polym Sci, Part A: Polym Chem* **2010,** *48*, 2115–2122.

36. Souzy, R.; Ameduri, B. Functional Fluoropolymers for Fuel Cell Membranes. *Prog. Polym. Sci.* **2005,** *30*, 644-687.

37. Souzy, R.; Ameduri, B.; Boutevin, B.; Gebel, G.; Capron, P. Functional Fluoropolymers for Fuel Cell Membranes. *Solid State Ionics* **2005,** *176*, 2839-2848.

38. Miyatake, K.; Oyaizu, K.; Tsuchida, E.; Hay, A. S. Synthesis and Properties of Novel Sulfonated Arylene Ether/Fluorinated Alkane Copolymers. *Macromolecules* **2001,** *34*, 2065-2071.

39. Yu, X.; Roy, A.; Dunn, S.; Badami, A. S.; Yang, J.; Good, A. S.; McGrath, J. E. Synthesis and Characterization of Sulfonated-fluorinated, Hydrophilic-hydrophobic Multiblock Copolymers for Proton Exchange Membranes. *J Polym Sci, Part A: Polym Chem* **2009,** *47*, 1038-1051.

40. Nakabayashi, K.; Higashihara, T.; Ueda, M. Highly Sulfonated Multiblock Copoly(ether sulfone)s for Fuel Cell Membranes. *J Polym Sci, Part A: Polym Chem* **2010,** *48*, 2757-2764.

41. Qian, G.; Smith, D. W., Jr.; Benicewicz, B. C. Synthesis and Characterization of High Molecular Weight Perfluorocyclobutylcontaining Polybenzimidazoles (PFCB–PBI) for High Temperature Polymer Electrolyte Membrane Fuel Cells. *Polymer* **2009,** *50*, 3911–3916.

42. Kim, D.-J.; Chang, B.-J.; Kim, J.-H.; Lee, S.-B.; Joo, H.-J. Sulfonated Poly(fluorenyl ether) Membranes containing Perfluorocyclobutane Groups for Fuel Cell Applications. *J. Membr. Sci.* **2008,** *325*, 217-222.

43. Iacono, S. T.; Budy, S. M.; Jin, J. Y.; Smith, D. W., Jr. Science and Technology of Perfluorocyclobutyl Aryl Ether Polymers. *J Polym Sci, Part A: Polym Chem* **2007,** *45*, 5705-5721.

44. Yang, Y.; Holdcroft, S. Synthetic Strategies for Controlling the Morphology of Proton Conducting Polymer Membranes. *Fuel Cells* **2005,** *5*, 171-186.

45. Miyatake, K.; Chikashige, Y.; Higuchi, E.; Watanabe, M. Tuned Polymer Electrolyte Membranes Based on Aromatic Polyethers for Fuel Cell Applications. *J. Am. Chem. Soc.* **2007,** *129*, 3879-3887.

46. Bae, B.; Miyatake, K.; Watanabe, M. Sulfonated Poly(arylene ether sulfone ketone) Multiblock Copolymers with Highly Sulfonated Block. Synthesis and Properties. *Macromolecules* **2010,** *43*, 2684-2691.

47. James, P. J.; Antognozzi, M.; Tamayo, J.; McMaster, T. J.; Newton, J. M.; Miles, M. J. Interpretation of Contrast in Tapping Mode AFM and Shear Force Microscopy. A Study of Nafion. *Langmuir* **2000,** *17*, 349-360.

CHAPTER FOUR

PFCB BASED PROTON EXCHANGE MEMBRANES FOR HYDROGEN PRODUCTION

Introduction

Thermochemical water splitting cycles, using the heat of nuclear power plants, offer an alternate highly efficient route for the large scale hydrogen production. Especially, the sulfur-based cycle, hybrid sulfur (HyS) process, leads the competition in overall energy efficiency among the many possible thermochemical cycles (e.g., zinc zinc-oxide cycle, and copper-chlorine cycle). This hydrogen production cycle is the simplest process involving a thermochemical step using nuclear power and an electrochemical step using a sulfur dioxide depolarized electrolyzer (SDE).[1-3] The two-steps are illustrated in Scheme 4.1.

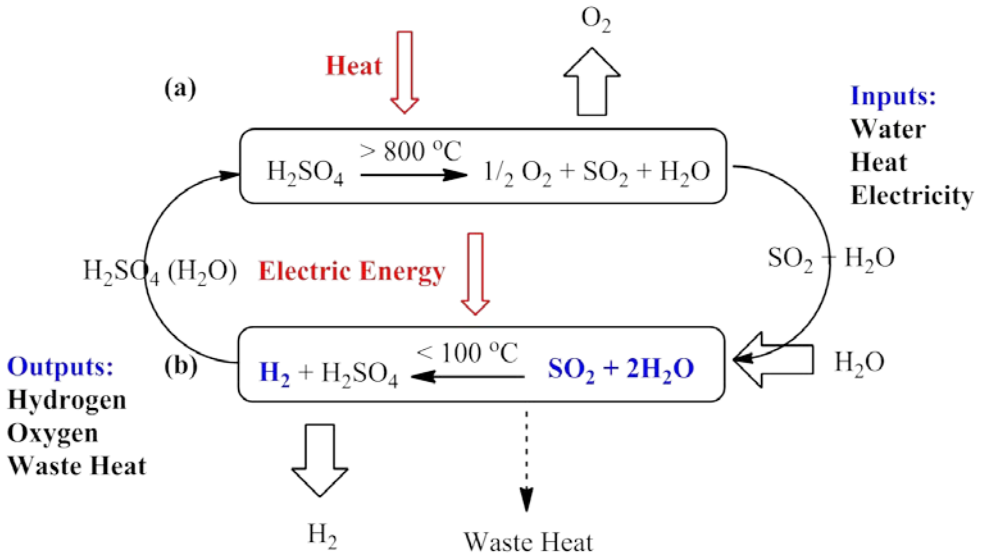

Scheme 4. 1 Illustration of HyS Process: (a) Thermal step and (b) Electrochemical step.[2]

As comparison with direct thermal decomposition (> 2500 ºC) from water to hydrogen, the thermochemical cycles can produce pure hydrogen at significantly lower temperatures around 800–1000 ºC.[4] As shown in Scheme 4.1, sulfuric acid is first thermally decomposed to sulfur dioxide, water, and oxygen at high temperature (>800 ◦C). After the removal of O_2, SO_2 is fed into a sulfur dioxide depolarized electrolyzer (SDE) with water and electrochemically reacts at the anode catalyst layer. The electrochemical step in SDE is described in Scheme 4.2. The overall electrochemical cell reaction consists of the production of H_2SO_4 and H_2. At the anode, SO_2 dissolved in water is oxidized to sulfuric acid and protons. The regenerated sulfuric acid is cycled back to the thermal decomposition step the protons migrate through the membranes to the cathode and reduced to H_2.

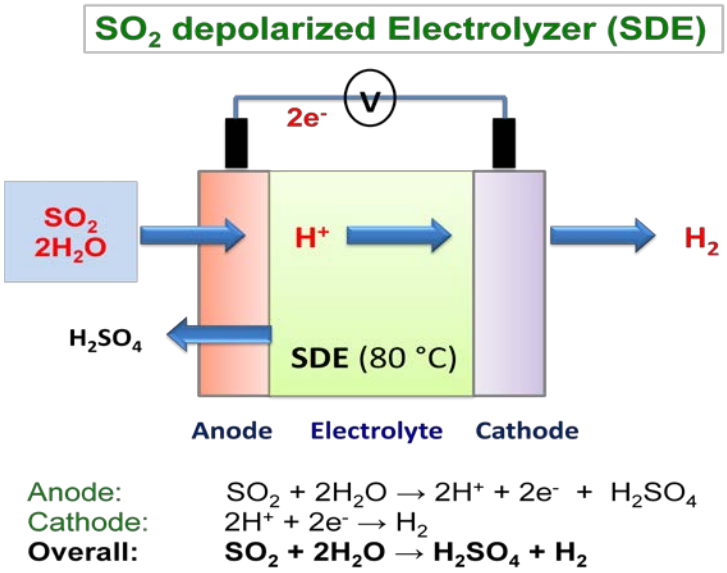

Scheme 4. 2 PEM concept for SO_2 depolarized electrolyzer (SDE).[2]

The Savannah River National Laboratory (SRNL), which is leading the electrolyzer component development effort for the Hybrid Sulfur Process, selected the fuel cell MEA design concept for the SDE in the HyS process since the MEA concept provides a much smaller cell footprint than conventional parallel plate technology. This smaller footprint is a major benefit in scaling the electrolyzer to the size that will be required for commercial production. Key attributes of the SDE are high energy efficiency and long operating lifetime. To achieve high energy efficiency, the electrolyzer must exhibit rapid reaction kinetics at each electrode, little crossover of reagents and products across the membrane, and excellent chemical stability of each of the components to concentrated sulfuric acid solutions. Therefore, the ion-conducting proton exchange membrane is a key component of the electrolyzer.

However, commercially available membranes, such as the Nafion® family of perfluorinated sulfonic acid membranes have shown excessive transport of sulfur dioxide across the membrane resulting in reduced electrical efficiency and the production of undesirable sulfur-containing byproducts while commercial hydrocarbon type membranes (e.g., sulfonated polyetherketones (SPEKs)), showed good conductivity in water, but quickly degraded when exposed to high sulfuric acid concentrations. Thus, there is a significant need to provide the membrane materials that exhibit reduced sulfur dioxide transport characteristics without sacrificing other important properties such as high ionic conductivity and excellent chemical stability in highly concentrated sulfuric acid solutions saturated with sulfur dioxide.

As an alternative membrane, sulfonated Perfluorocyclobutyl aromatic ether polymer (sPFCB) were expected to posses low SO_2 permeability due to their stiff backbones as well as high proton conductivity and improved mechanical properties. These sPFCB electrolytes have been developed for automotive PEMFCs by Smith and co-workers at Clemson and Tetramer Technologies, L.L.C. which has provided starting materials for this project.[5-10] The major accomplishments of this project were the synthesis, characterization, and optimization of suitable electrolyzers for good SDE performance and higher chemical stability against sulfuric acid. SDE performance results of developed sPFCB polyelectrolytes have shown that these membranes exhibit good chemical stability against H_2SO_4. The properties of the membranes for their potential application in large scale hydrogen production will be discussed in this chapter.

SO_2 Crossover of Nafion membrane

Morphology and distribution of different elements was studied and compared for fresh and tested membranes by scanning electron microscope (SEM) analysis and energy dispersive X-ray spectroscopy (EDXS) (Figure 4.1 and 4.2). In cross-section SEM micrograph, morphology of Nafion117 membranes revealed sulfur deposition at the membrane-cathode interface after electrolysis. EDXS mapping data also supports the deposition of sulfur after testing while uniform distribution of fluorine (F) and sulfur (S) was observed in fresh membranes.

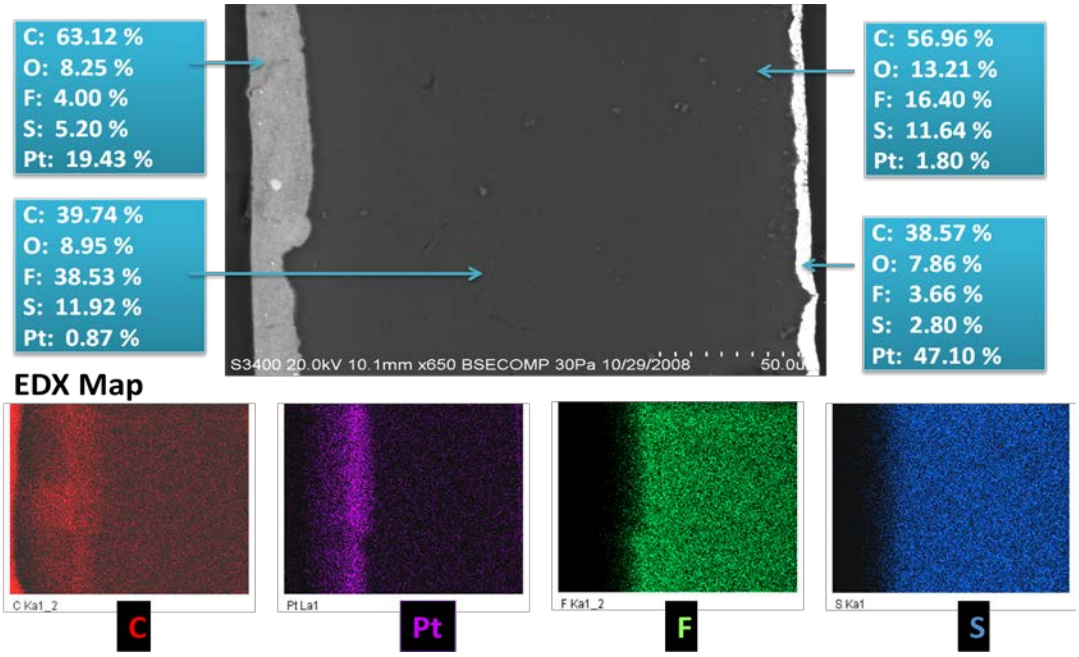

Figure 4.1 Cross-section SEM micrograph and EDXS of a fresh membrane electrode assembly (MEA).

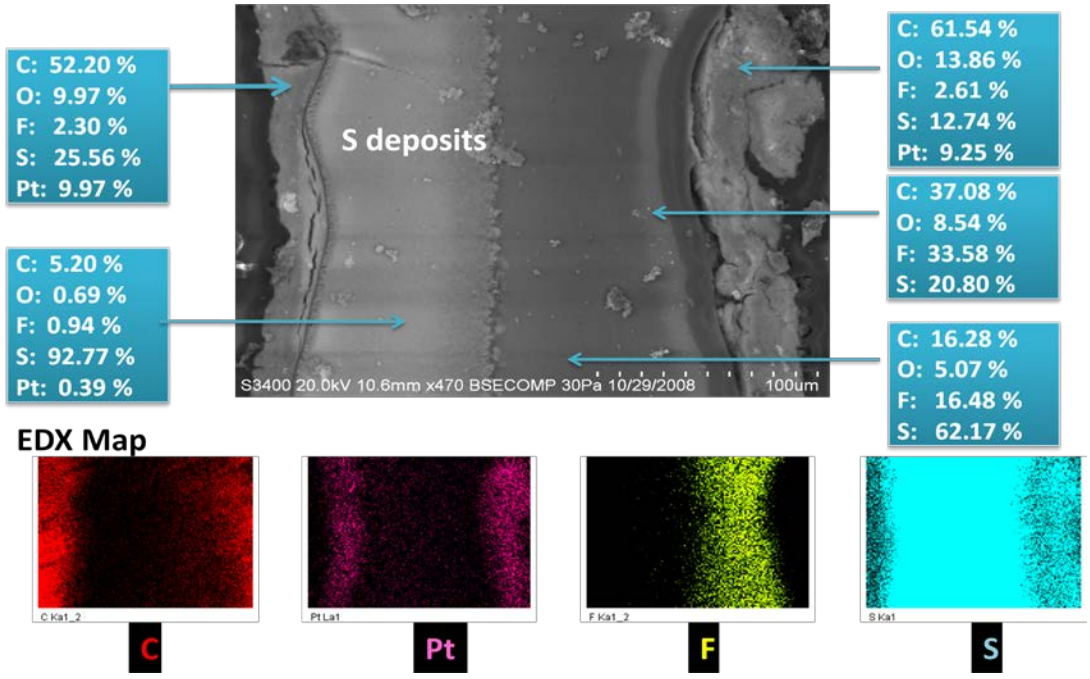

Figure 4.2 Cross-section SEM micrograph and EDXS of a SO_2 cross-over tested MEA.

Characterization of Tetramer PFCB PEMs for HyS Process

To evaluate the potential utility of PFCB based membranes for large scale hydrogen production, chemical stability and proton conductivity of Tetramer PFCB PEMs were evaluated. The molecular weight of unsulfonated PFCB polymers and ion exchange capacity ($IEC_{titration}$) of developed membrane are summarized in Table 4.1. We note that the lower molecular weight homopolymer membrane was a little bit brittle, but suitable for the test.

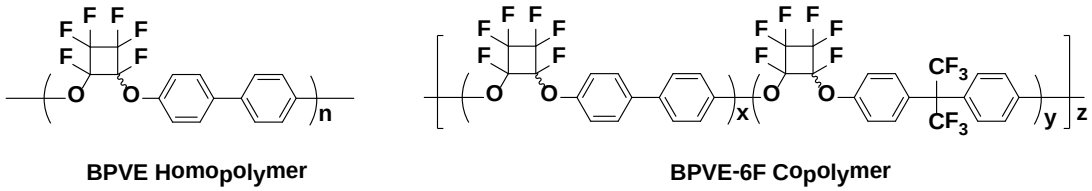

Scheme 4.3 Tetramer PFCB (a) homopolymer and (b) block copolymer.

Table 4.1 Properties of Tetramer PFCB homopolymer and block copolymer membranes.

Sample Code	Mn[a] (g mol^{-1})	IEC[b] (meq/g)	Thickness (µm)
BPVE	80,000	1.7	18
B1F1	30,000	0.8	16
B2F1	70,000	2.0	19

[a] GPC data in $CHCl_3$ using polystyrene standard in Waters 2690 Alliance. [b] Ion Exchange Capacity (IEC) by titration method.

As sulfuric acid is produced in overall electrochemical cell reaction of Hybrid-Sulfur (HyS) process, the chemical stability of these membranes were examined in 60 wt (%) of H_2SO_4 at 80 ºC for 0-24 h. Copolymer membranes were found to be more stable than homopolymer during chemical stability test. ATR-IR analysis indicated no degradation of perfluorocyclobutyl aryl ether polymer backbones for block copolymer, while BPVE homopolymer membranes gave increased intensity at 1030 cm^{-1} corresponding to sulfonic acid group that indicates sulfonation occurred during the chemical stability test (Figure 4.3).

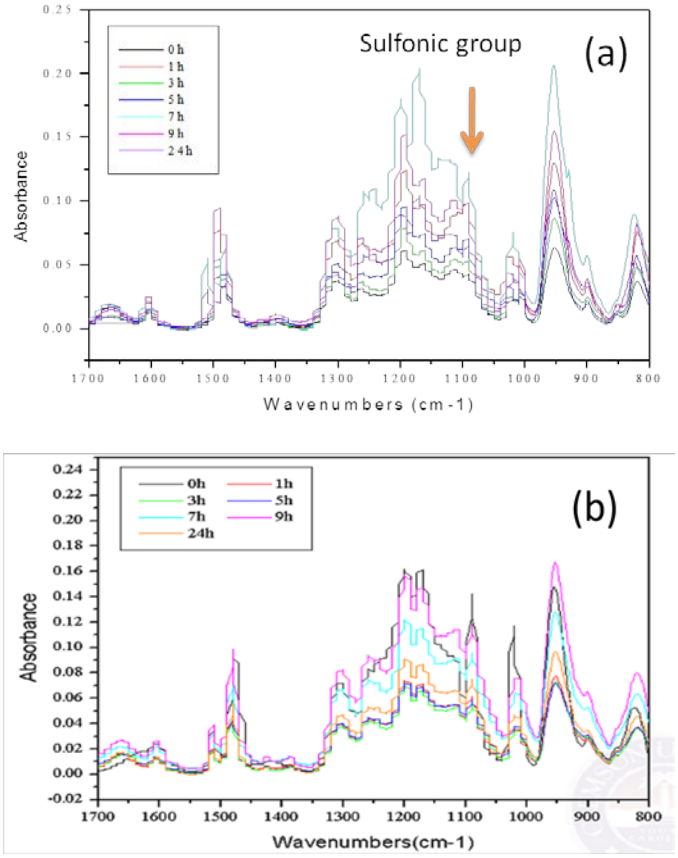

Figure 4.3 ATR- IR of Homopolymer (a) and Block copolymer (b) after acid test under 60 wt% H_2SO_4 at 80 ºC.

Electrochemical impedance measurements of the BPVE-6F (2:1) polymer membranes showed high proton conductivity (0.1069 S cm $^{-1}$) at 80 ºC and relative humidity (RH) of 100% (Figure 4.4). Higher ionic conductivity (0.2368 S cm $^{-1}$) was observed for these membranes after refluxing, as shown in Figure 4.4, which may imply that sulfonation on the copolymer backbone took place during stability test too.

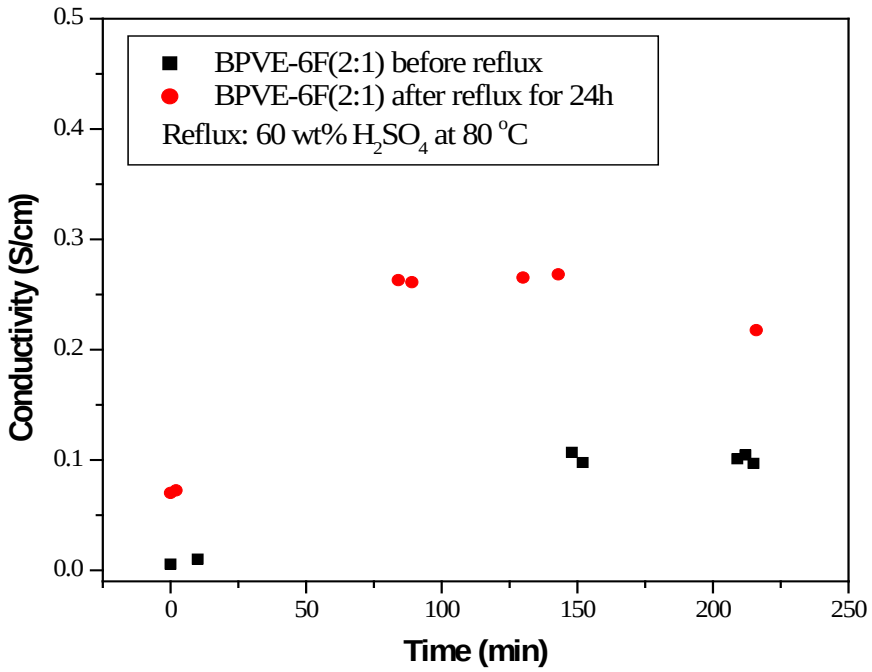

Figure 4.4 Ion conductivity of the BPVE-6F membrane as a function of time at 80 ºC and 100 RH%.

Morphology of Membranes

Morphology, connectivity and phase separation between hydrophilic and hydrophobic domains was studied by Atomic Force Microscopes (AFM) as shown in Figure 4.5.[11-13] Domain size and connectivity are both different between the sulfonated BPVE homopolymer and BPVE-6F block copolymer. The block copolymer shows more uniform distribution of channels and co-continuous morphology than homopolymer. This morphology can be responsible for higher proton conductivity and current density as shown in Table 4.2.

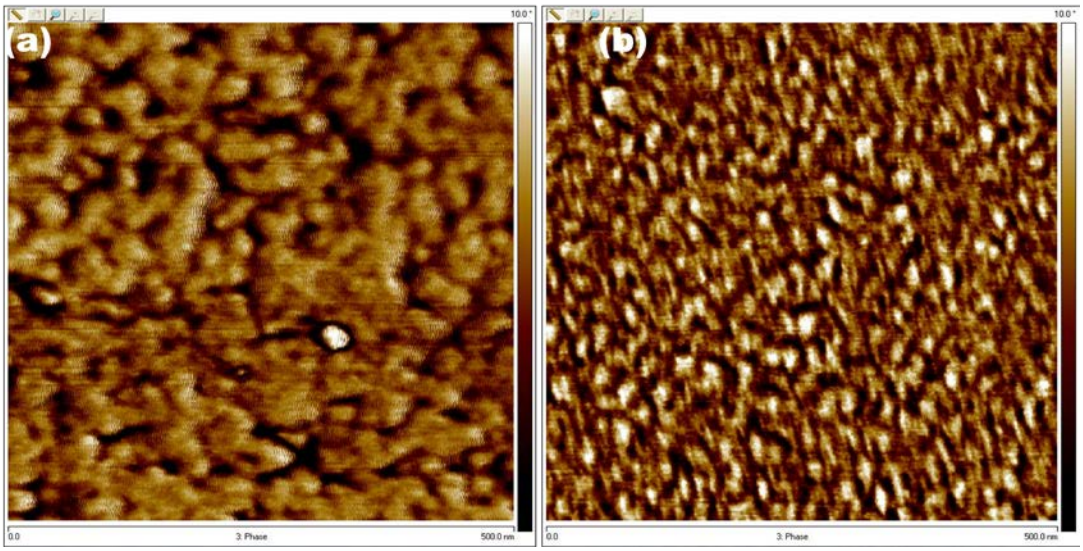

BPVE Homopolymer	BPVE-6F(2:1) Block Copolymer
Less Channel	More Channel
Irregular Channel	Uniform distribution of Channel
Close to Co-Continuous morphology	Co-Continuous morphology

Figure 4.5 AFM phase images of (a) BPVE homopolymer (M1) and (b) BPVE-2F (2:1) block copolymer membranes (M3).

SDE Performance of Tetramer PFCB Membranes in HyS Process

For conductivity and current density test, membrane electrode assemblies (MEAs) were prepared with Pt loading on the anode: 1.8 mg, Pt loading on the cathode: 0.9 mg, Nafion loading: ~25 wt%, and Catalyst for both sides: 45 wt% Pt/C in SRNL.

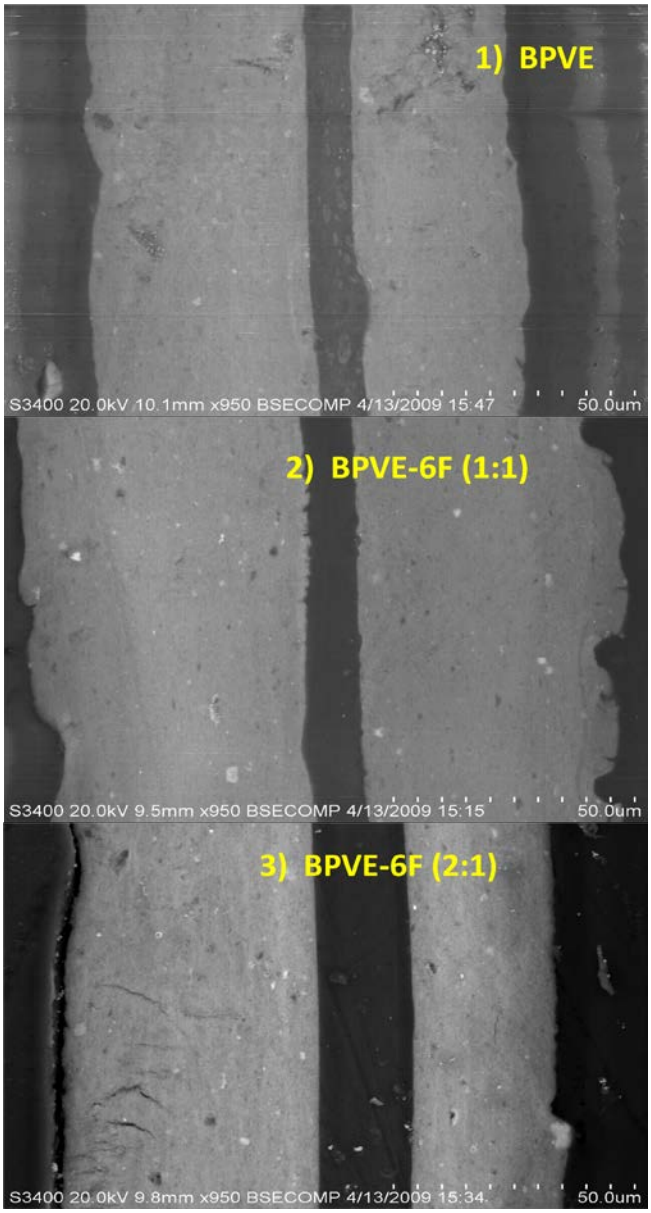

Figure 4.6 SEM image of Homo and Block Copolymer MEA for SDE performance test.

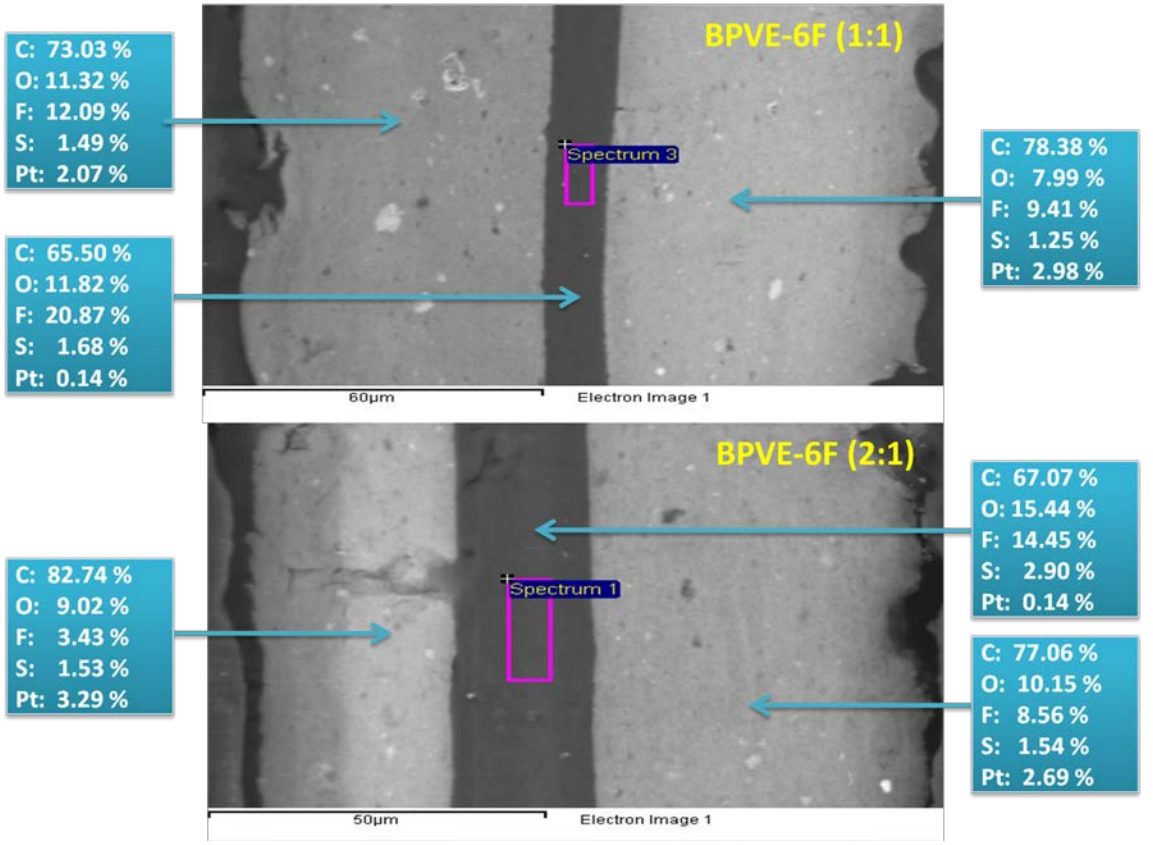

EDX Map of BPVE-6F(2:1) MEA

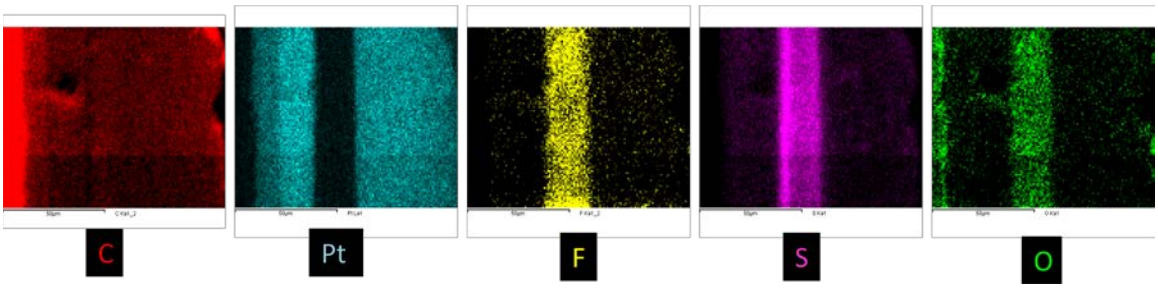

Figure 4.7 SEM of BPVE-6F (1:1) and BPVE-6F (2:1) and EDX Map of BPVE-6F (2:1).

Figure 4.6 and 4.7 show the SEM/EDXS images of prepared MEA for SDE performance test. The conductivity and performance (current density) measurements in HyS process were performed at 1 V, with 30 wt% H_2SO_4 saturated with SO_2 on the anode side, and H_2O on the cathode side using SO_2 transport characterization cell (Figure 4.8). In this process, the hybrid-sulfur electrolyzer consumes sulfur dioxide and water to produce sulfuric acid at the anode and hydrogen at the cathode.

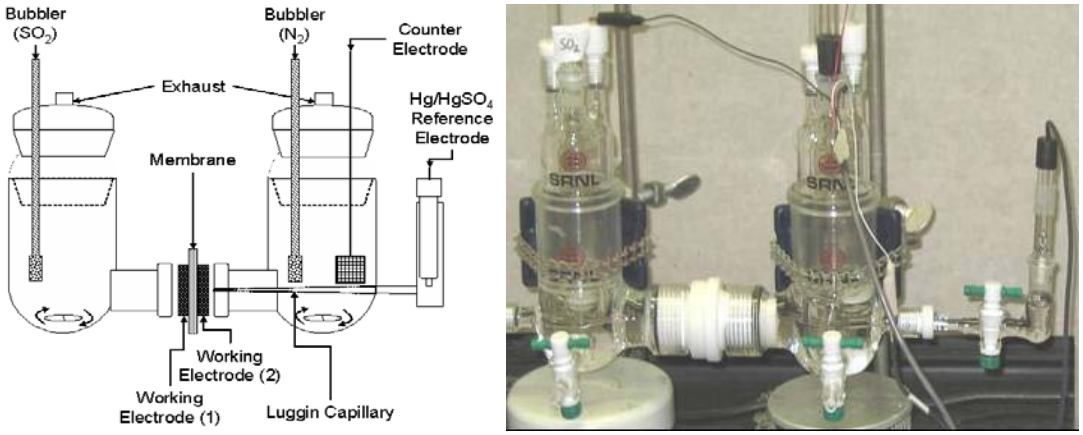

Figure 4.8 Simplified schematic (Working electrode (1) : used during the ionic conductivity measurements, Working electrode (2) : used during the SO_2 transport measurements) and image of the SO_2 transport characterization cell (SRNL).[2]

As shown in Figure 4.9 and listed in Table 4.2, all the membranes of homopolymer (M1, 3.50×10^{-8} cm^2 s^{-1}) and block copolymers (M3, 3.07×10^{-8} cm^2 s^{-1}) showed less SO_2 transport than Nafion 115 (6.10×10^{-8} cm^2 s^{-1}) and Nafion 211 (5.09×10^{-8} cm^2 s^{-1}). For high performance SDE material, higher current density is required. Although, all of our membranes showed lower conductivities than Nafion, the membranes gave better current densities than Nafion 115. Current density of our membranes ranged from 320 to 337 mA cm^{-2}, which is better than Nafion 115.

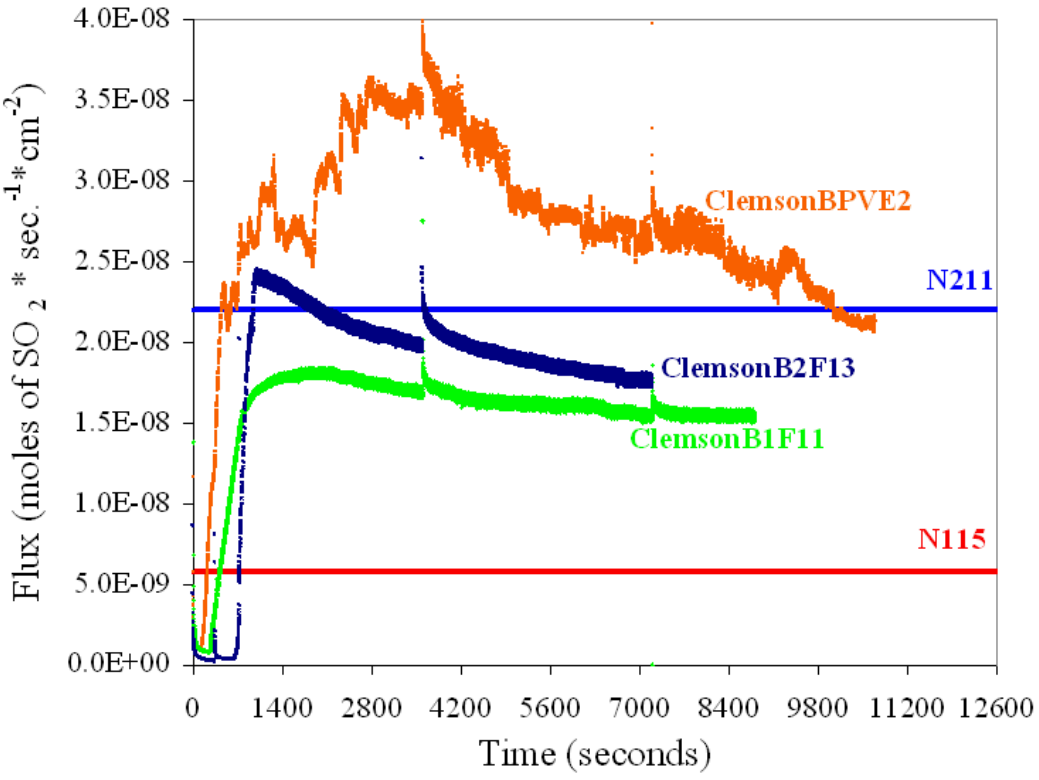

Figure 4.9 Comparison of SO_2 cross-over of Nafion with BPVE homopolymer membrane (M1) and BPVE-6F Block copolymer membranes (M1 and M2).

Table 4.2 SO_2 transport ($cm^2\ s^{-1}$), conductivity (Scm^{-1}), and current density ($mA\ cm^{-2}$) along with membrane thickness for PFCB membranes and Nafion.

Sample	Membrane Type	Thickness (μm)	SO_2 transport ($cm^2 s^{-1}$)	Conductivity ($S\ cm^{-1}$)	Current Density ($mA\ cm^{-2}$)
BPVE (M1)	PFCB	18	3.50E-08	0.0048	320
B1F1 (M2)	PFCB	16	2.37E-08	0.0063	337
B2F1 (M3)	PFCB	19	3.07E-08	0.0109	335
Nafion 115	PFSA	127	6.10E-08	0.0241	270
Nafion 211	PFSA	25.4	5.09E-08	0.0159	393

Preparation of Cross-linked PFCB Aryl Ether Polyelectrolyte Membranes

In general, all of results indicate that the sPFCB block copolymers are suitable for use as a proton-exchange membrane rather than homopolymer. Therefore, sPFCB block copolymer membranes were applied in sulfur dioxide depolarized electrolyzer (SDE) for hydrogen production. The results in Chapter 3 showed that our sulfonated PFCB membranes possess desired thermal and conductivity properties for use as a polyelectrolyte membrane in PEM fuel cell systems. However, highly sulfonated/conductive membranes exhibited high water uptake and volume swelling in an aqueous solution. The large volume swelling can cause the delamination of membrane and it become unavailable in application. Cross-linking has been used as an efficient tool

to limit gas crossover in PEM fuel cells and also to enhance mechanical properties of the highly sulfonated polymers. Recently, many cross-linking pathways through hydrogen bonds, ionic or covalent bonds formation have been reported for aromatic based proton exchange membranes.[11, 14, 15] For example, Friedel–Crafts alkylation and acylation reactions have been reported as an effective way to couple carbon–carbon bonds in aromatic compounds.[16-19]

Therefore, cross-linked hydrophilic-hydrophobic block copolymers were prepared via Friedel–Crafts acylation to overcome the trade-off between proton conductivity and mechanical strength of hydrated membranes and to investigate the effect on the sulfur dioxide crossover. Herein, we discuss the preparation of cross-linked highly sulfonated PFCB aryl ether copolymer membranes and their properties. In our attempt to achieve such proton-exchange membranes, cross-linked PFCB-based block copolymer membranes consisting of a hydrophobic segment and a hydrophilic segment was prepared via Friedel-Crafts acylation using crosslinking agents such as 4,4'-oxybis(benzoic acid), 4,4′-(hexafluoroiso-propylidene)bis(benzoic acid), and 4,4'-((1,2,3,3,4,4-hexafluoro cyclo-butane-1,2-diyl)bis(oxy))dibenzoic acid (Scheme 4.4). The cross-linking reaction of sPFCB copolymers expected to be based on the Friedel-Craft acylation reaction between the unsulfonated phenyl moiety on the BP segment of a copolymer and the activated carbonyl group of a crosslinker as shown in Scheme 4.4. In this study, OBBA (4,4'-oxybis(benzoic acid)) was selected as a cross-linking reagent for detail membrane characterization.

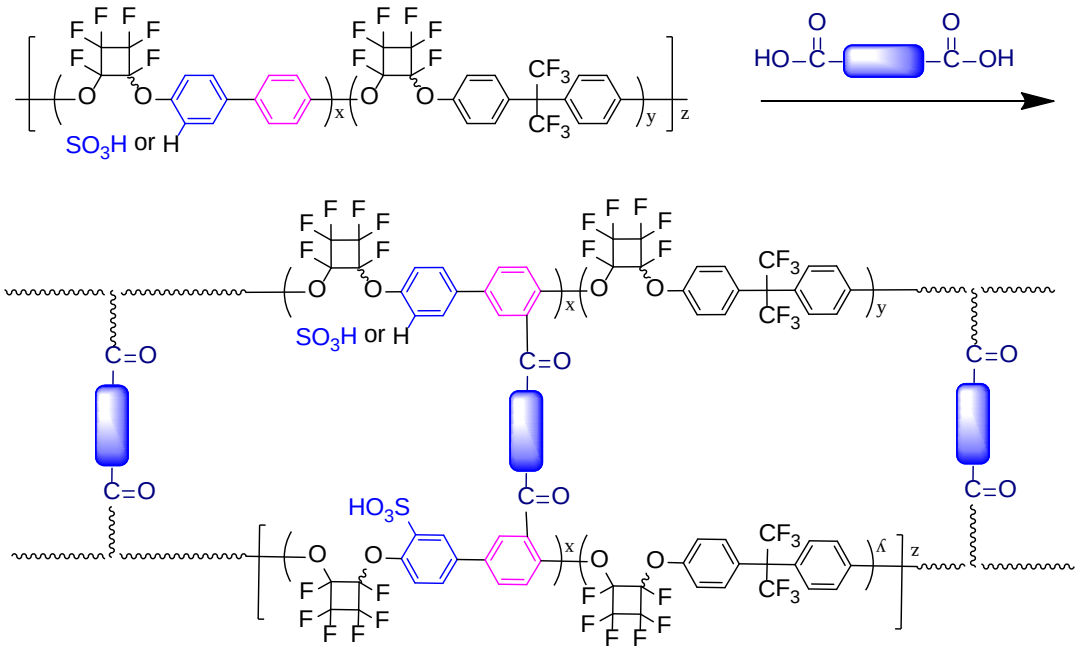

Scheme 4.4 Cross-linking of sPFCB polymers with difunctional carboxylic acid cross-linkers.

The preparation of cross-linked sPFCB membranes was performed in a simple way. The sulfonated PFCB copolymer solution in dimethylacetamide (DMAc) containing 5 wt% or 10 wt% cross-linker were cast into films and thermally treated at 160 °C in vacuum oven for 10 h. In general, the sulfonated PFCB copolymer commonly afford a transparent and flexible membrane because of their amorphous characteristic with stereo-radom PFCB aryl ether copolymer backbone. All of the membranes containing cross-linker were transparent after solution casting and during thermal treatment around 100 °C. On the other hand, all of resulting cross-linked membranes were opaque as shown in Figure 4.10.

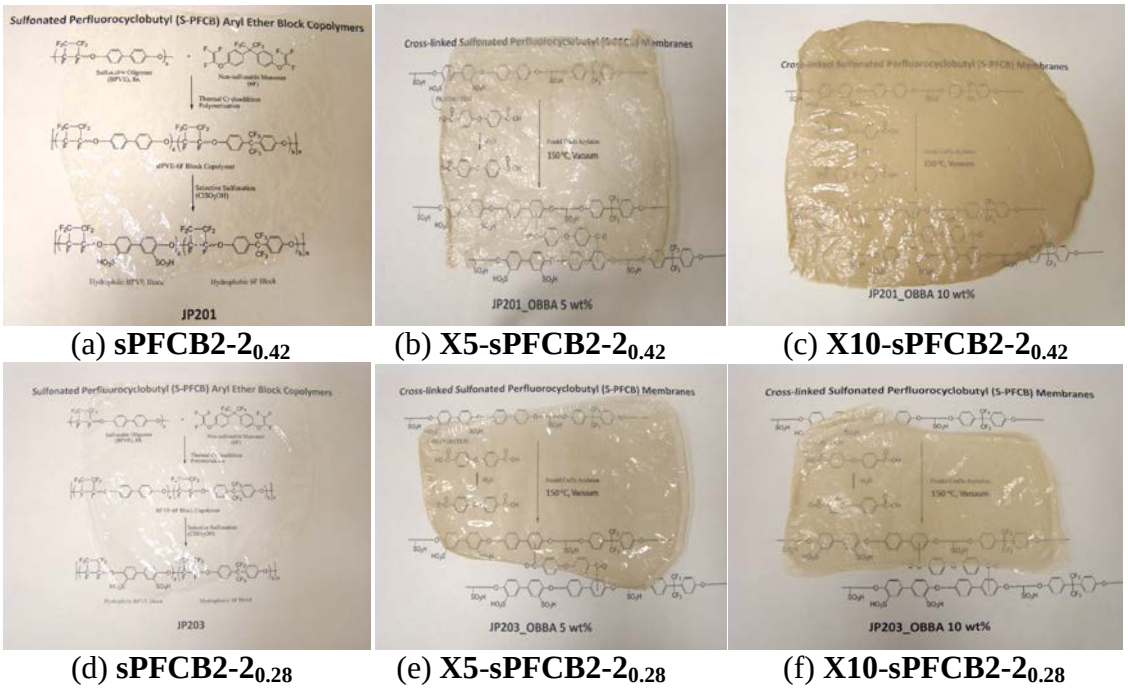

(a) **sPFCB2-2$_{0.42}$** (b) **X5-sPFCB2-2$_{0.42}$** (c) **X10-sPFCB2-2$_{0.42}$**

(d) **sPFCB2-2$_{0.28}$** (e) **X5-sPFCB2-2$_{0.28}$** (f) **X10-sPFCB2-2$_{0.28}$**

Figure 4.10 Photos of membranes (approx. 6 inch^2) before and after cross-linking treatment (a) sPFCB2-2$_{0.42}$, (b) cross-linked with 5wt% OBBA (X5-sPFCB2-2$_{0.42}$), (c) cross-linked with 10wt% OBBA (X10-sPFCB2-2$_{0.42}$), (d) sPFCB2-2$_{0.28}$, (e) cross-linked with 5wt% OBBA (X5-sPFCB2-2$_{0.28}$), and (f) cross-linked with 10wt% OBBA (X10-sPFCB2-2$_{0.28}$).

During the drying process at around 100-160 °C, the cross-linking of sPFCB polymer membranes changed the degree of transparency which indicates the change of polymer characteristic from amorphous to semi-crystalline and/or crystalline. In addition, the cross-linking of sulfonated PFCB copolymers made membranes more brittle but the mechanical strength was still excellent. This result shows that the cross-linking treatment affects the membrane flexibility and morphology. During the drying and cross-linking processes, the pre-dried membranes still contain DMAc solvent. As a result, the solvent residues serve as a plasticizer that can reorients the molecular chains along with

the cross-linking reaction at high temperature above 100 °C. All of films prepared from polymers offered good uniformity and the thickness of the membranes was in the range of 20–40 μm. The presence of more unsulfonated phenyl groups in sPFCB2-$2_{0.28}$ polymer led to better quality films in appearance and toughness than polymer sPFCB2-$2_{0.42}$.

The cross-linked sPFCB membranes prepared via Friedel-Crafts acylation using 4,4'-oxybis(benzoic acid) (O-BBA) were confirmed by solubility test (Figure 4.11). The uncrosslinked membrane was soluble in DMAc, while crosslinked membranes were not soluble in the same solvent. The insolubility of the membrane indicated that the sPFCB block copolymer was successfully cross-linked.

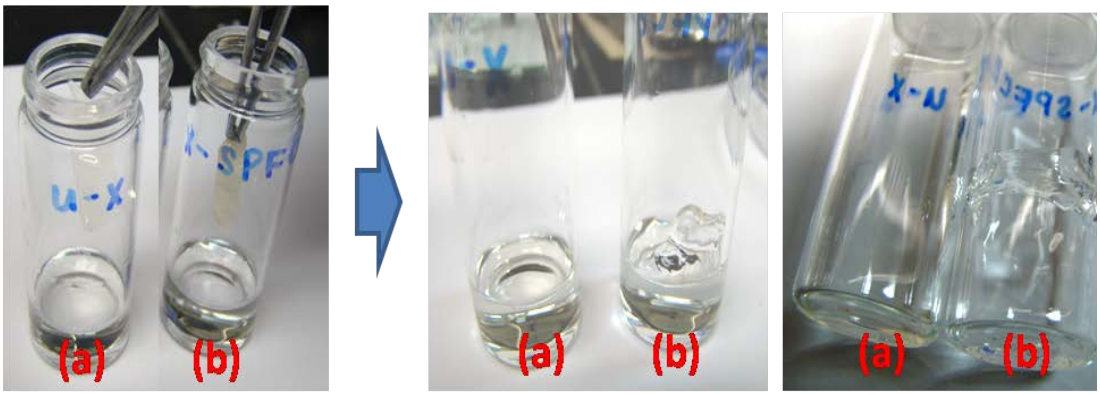

Figure 4.11 Solubility test of (a) uncross-linked sPFCB membrane (sPFCB2-$2_{0.42}$) and (b) cross-linked S-PFCB membrane (X10-sPFCB2-$2_{0.42}$).

Table 4.3 Solubility of membranes in DMAc before and after cross-linking treatment.

Sulfonated Polymer	Membrane Code	Cross-linking Treatment	Solubility in DMAc
sPFCB2-$2_{0.42}$ [a]	sPFCB2-$2_{0.42}$	No	Soluble
	X5-sPFCB2-$2_{0.42}$	5 wt%	+– [c]
	X10-sPFCB2-$2_{0.42}$	10 wt%	++ [d]
sPFCB2-$2_{0.28}$ [b]	sPFCB2-$2_{0.28}$	No	Soluble
	X5-sPFCB2-$2_{0.28}$	5 wt%	+– [c]
	X10-sPFCB2-$2_{0.28}$	10 wt%	++ [d]

[a,b] Sulfonated PFCB aryl ether copolymer (Experimental compositional ratio of BP and 6F unit determined by ^{19}F NMR = 76:24, Sulfonation level = 42% and 28% respectively), [c] Partially soluble, [d] Swollen.

In a simple mechanistic view of cross-linking, the acidic sulfonic acid groups serve as acid sources for the Friedel-Craft reaction with the aid of vacuum for dehydration. As illustrated in Figure 4.12, the proton can transport from the sulfonic acid groups to the benzoic acid group of cross-linker because of their higher acidity. The pKa of sulfonic acid and carboxylic acid is about -2.6 and 4~6, respectively. The second step consists of dehydration of carboxylic acid to form an acyl cation. This is followed by nucleophilic attack of the arene toward the acyl group.

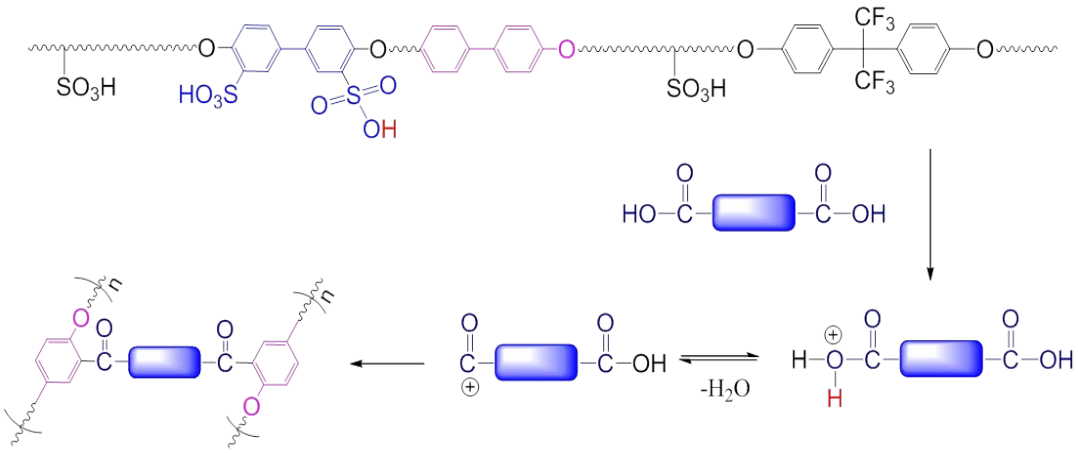

Figure 4.12 Proposed mechanism of Friedel-Crafts acylation of copolymer with bisbenzoic acid crosslinker.

The cross-linking reaction was verified by comparing the ATR-IR spectra of the sulfonated polymers before and after thermal cross-linking treatment. Figure 4.13 shows the ATR-IR spectra of neat sPFCB copolymer membranes and cross-linked membrane. The decrease of the absorption peak at 1174 cm^{-1} corresponding to the Ar-C-F stretching were observed after the crosslinking process, while other characteristic peaks of sulfonated PFCB copolymers remained identical. For example, no change was observed at 1020 cm^{-1} which is correspond to the stretch vibration of the sulfonic acid group. This indicate that the sulfonic acid groups were not consumed during the reaction and the bis-benzoic acid cross-linker was effectively reacted with phenyl ring in the polymer chain to form the crosslinked polymers.

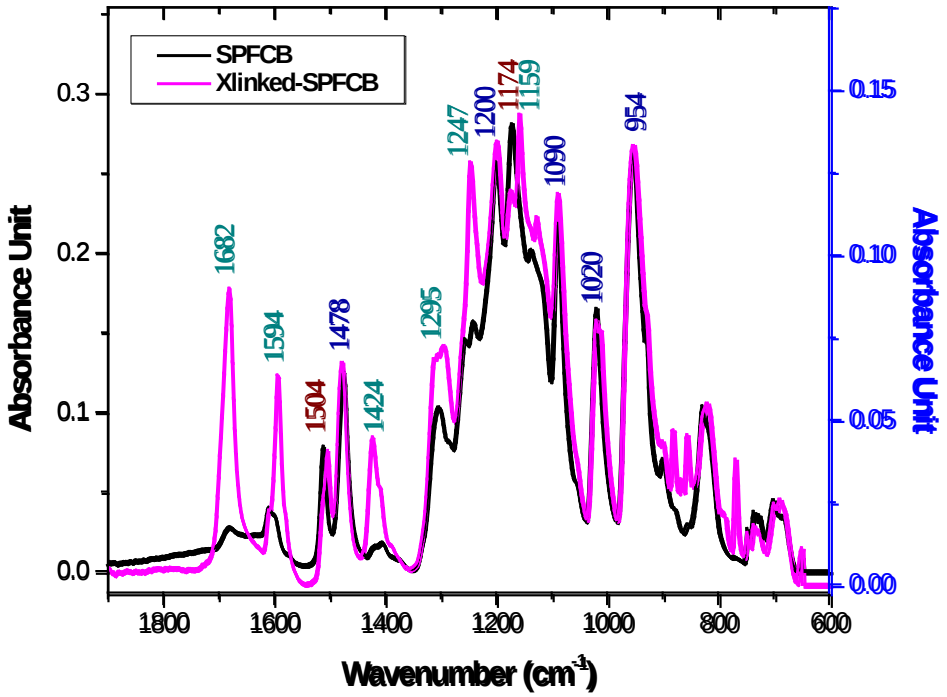

Figure 4.13 ATR-IR of uncross-linked sPFCB membrane and crosslinked S-PFCB membrane.

Properties of Cross-linked PFCB Aryl Ether Polyelectrolyte Membranes

Thermal Properties of Cross-linked Membranes

The thermal stabilities of the uncross-linked and cross-linked membranes were evaluated by TGA (See Figure 4.14 and 4.15). The membranes showed obvious several stage thermal decomposition with dehydration in the first step. The membranes were thermally stable up to 200 ºC which is similar to the degradation of unsulfonated membranes. The second stage at around 220 ºC is associated with the loss of cross-

linked OBBA and sulfonic acid groups, and the third one at around 400 ºC is caused by the decomposition of the PFCB aryl ether polymer backbone. It was clear that the second-stage weight loss at 220 ºC ~ 400 ºC increased with the incorporation of cross-linker. The glass transitional temperature of cross-linked membranes was estimated using a DSC. Although, a glass transition temperature (T_g) was not resolved clearly, a higher T_g for the membrane is expected because of the cross-linking that commonly restrict the molecular motion of PFCB aryl ether polymer backbone.

Table 4.4. TGA datas of uncross-linked (sPFCB2-$2_{0.42}$, sPFCB2-$2_{0.28}$) and cross-linked (X5-sPFCB2-$2_{0.42}$, X10-sPFCB2-$2_{0.42}$, X5-sPFCB2-$2_{0.28}$, and X10-sPFCB2-$2_{0.28}$) membranes.

Membranes	2^{nd} stage (Sulfonic group + OBBA)		3^{rd} stage (Polymer backbone)
	$T_{d\ (5\%)}$ (°C)	Weight Loss (%)	Weight Loss (%)
sPFCB2-20.42	301	18.43	42.48
X5-sPFCB2-$2_{0.42}$	268	24.75	37.82
X10-sPFCB2-$2_{0.42}$	271	27.26	35.69
sPFCB2-$2_{0.28}$	255	15.56	44.02
X5-sPFCB2-$2_{0.28}$	289	20.55	41.05
X10-sPFCB2-$2_{0.28}$	270	24.62	38.74

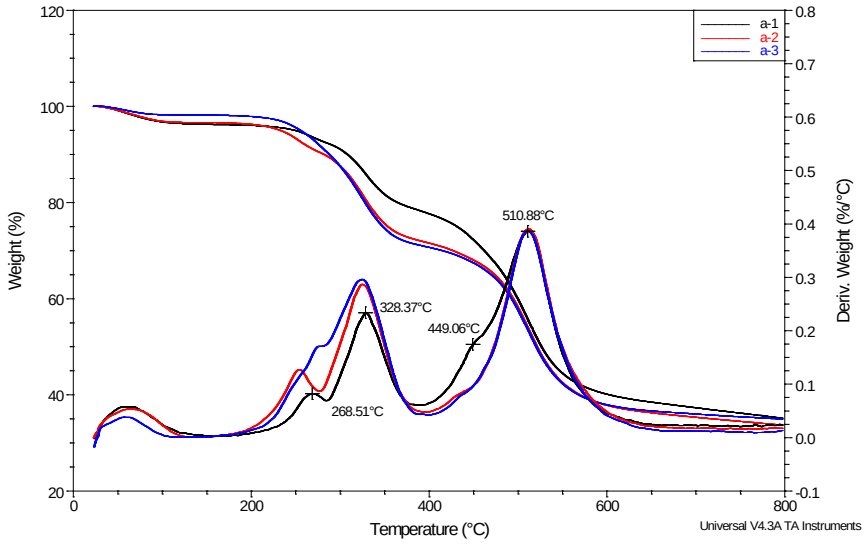

Figure 4.14 TGA curves of uncross-linked membrane (a-1) sPFCB2-$2_{0.42}$ and cross-linked S-PFCB membranes (a-2) X5-sPFCB2-$2_{0.42}$, and (a-3) X10-sPFCB2-$2_{0.42}$.

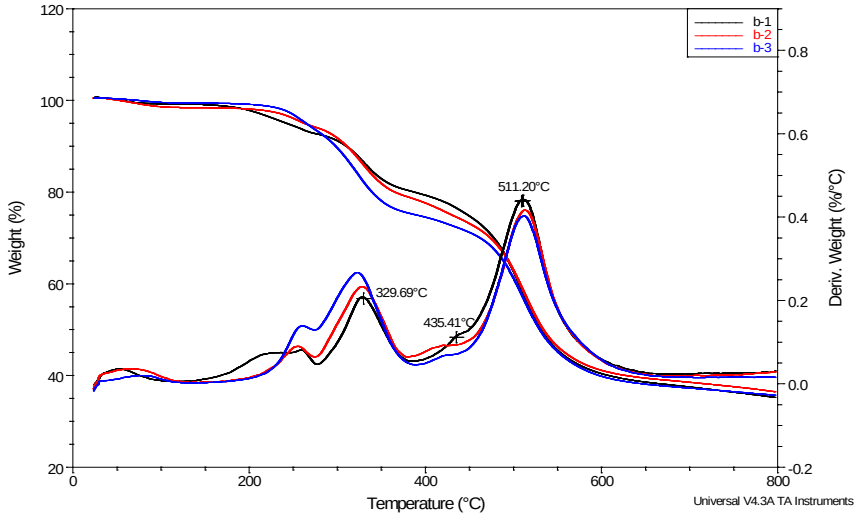

Figure 4.15 TGA curves of uncross-linked membrane (b-1) sPFCB2-$2_{0.28}$ and cross-linked S-PFCB membranes (b-2) X5-sPFCB2-$2_{0.28}$, and (b-3) X10-sPFCB2-$2_{0.28}$.

Water Uptake, Swelling Ratio, and Proton Conductivity of Cross-linked PFCB Membranes

The water in the membrane is closely related to proton conductivity because it is a carrier for the proton. Therefore, the incorporation of high degree of sulfonic acid groups in the membrane enhances water uptake and thereby leads high proton conductivity. However, highly sulfonated membranes is accompanied by excessive volume swelling of the membranes as discussed in Chapter 3 and shown in Figure 4.16.

Table 4.5 shows that highly sulfonated PFCB aryl ether polymer membrane, sPFCB2-$2_{0.42}$, possessed extremely high water uptakes (100%) and swelling ratio (50%) even at room temperature. After cross-linking, the water uptake and swelling ratio for the cross-linked membrane, X10-sPFCB2-$2_{0.42}$, were significantly reduced than the uncross-linked membrane, for example 100% to 55% water uptake and 50% to 5% volume swelling (See Figure 4.15) at room temperature. In addition, at higher temperature (80 ^{o}C), the cross-linked membrane showed acceptable volume swelling having a value of 20%.

On the other hand, the water uptake was not remarkably reduced as comparison with volume swelling at 80 ^{o}C. Water uptake is strongly related to the morphology as well as the content of acid groups. In addition, it is known that cross-linking can make larger free volume in the membrane as compared with uncross-linked one. Our results indicated that the increase in free volume of cross-linked membrane helps to maintain water absorption while improve a dimensional stability.

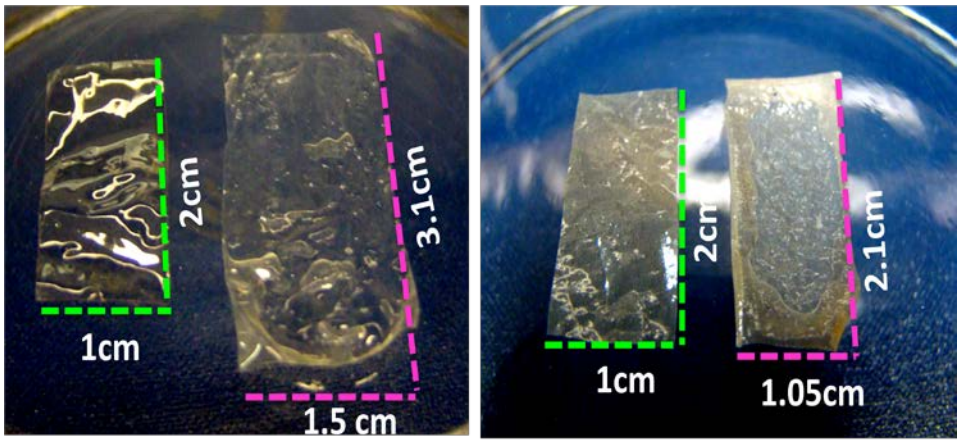

sPFCB2-$2_{0.42}$ **X10-sPFCB2-$2_{0.42}$**

Figure 4.16. Before (green) and after (pink) water uptake at room temperature of uncross-linked sPFCB-3 (Left) and cross-linked sPFCB-3 (X-sPFCB) membrane (Right).

Table 4.5 Thickness, water uptake, swelling ratio, and proton conductivity of sPFCB membranes.

Membranes	Thickness (μm)	Water Uptake (%)[a]		Swelling Ratio (%)[b]		Conductivity (S/cm)[c]	
		25 (°C)	80 (°C)	25 (°C)	80 (°C)	25 (°C)	80 (°C)
sPFCB2-$2_{0.42}$	28	100	320	50	100	0.12	0.22
X10-sPFCB2-$2_{0.42}$	24	55	155	5	20	0.11	0.18
sPFCB2-$2_{0.28}$	20	23	43	60	82	0.09	0.17
X10-sPFCB2-$2_{0.28}$	24	24	34	15	35	0.06	0.13
Nafion212	25.4	5	50	10	15	0.15	0.28

[a]Water Uptake (wt%) = $[(W_{wet} - W_{dry}) / W_{dry}] \times 100$, [b] Swelling Ratio (%) = $[(L_{wet} - L_{dry}) / L_{dry}] \times 100$, [c] Estimated using a Solartron 1280B potentiostat/frequency analyzer.

Proton conductivity is also strongly related to the sulfonation level in the polymers. In general, our sulfonated PFCB polymer membrane exhibit lower relative proton conductivity compared with Nafion membranes (Table 4.6) because of their lower degree of dissociation without electron withdrawing on the carbon in which sulfonic acid groups attached. The proton conductivity of highly sulfonated PFCB membrane (sPFCB2-$2_{0.42}$) and Nafion 212 were 0.12 and 0.15 S cm^{-1} at room temperature, respectively. The proton conductivity value of sPFCB2-$2_{0.42}$ is closed to Nafion, but it appears not suitable for applications because of its high swelling ratio in water. After cross-linking, the membrane (X10-sPFCB2-$2_{0.42}$) exhibited similar proton conductivity (0.18 S cm^{-1} at 80 ºC) with uncross-linked membrane (0.22 S cm^{-1} at 80 ºC).

In addition, the PFCB aryl ether copolymer membranes exhibited great properties less sulfur dioxide cross-over than Nafion 211 as shown in Figure 4.17. Especially, it turned out that the dense network formed by cross-linking can reduce the transport of sulfur dioxide, which is reflected in the measured SO_2 transport (1.54×10^{-8} cm2 s^{-1}), which are significantly lower than the Nafion membrane. This combination of high proton conductivity and less SO_2 transport makes the cross-linked PFCB membranes a promising further study on SDE performance for hydrogen production.

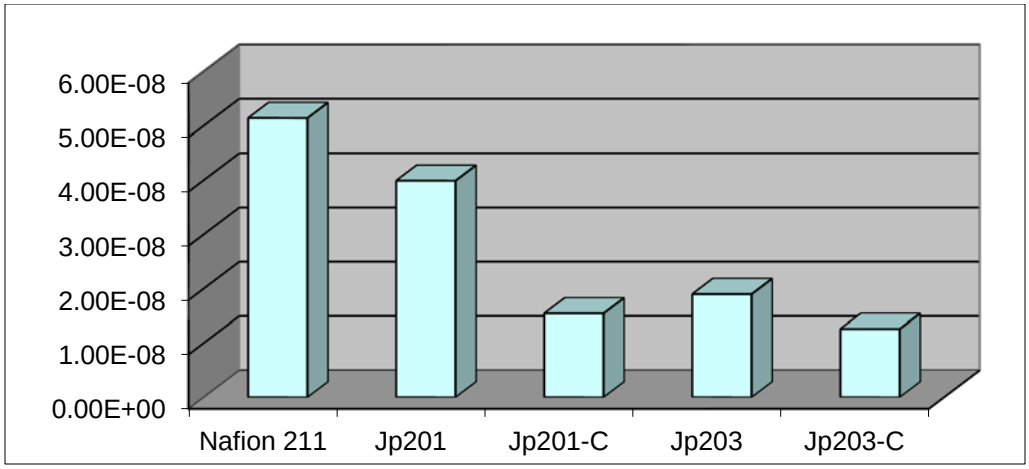

Figure 4.17 SO_2 Cross-over of (a) uncross-linked JP201 (sPFCB2-$2_{0.42}$) and JP203 (sPFCB2-$2_{0.28}$) and (b) their cross-linked membranes (X10-sPFCB2-$2_{0.42}$ and X10-sPFCB2-$2_{0.28}$) and Nafion 211.

Table 4.6 SO_2 Cross-over of (a) uncross-linked JP201 (sPFCB2-$2_{0.42}$) and JP203 (sPFCB2-$2_{0.28}$), (b) their cross-linked membranes (X10-sPFCB2-$2_{0.42}$ and X10-sPFCB2-$2_{0.28}$) and Nafion 211.

Sample	Membrane Code	Thickness (μm)	SO_2 transport ($cm^2\ s^{-1}$)
Jp201	sPFCB2-$2_{0.42}$	27	**3.99E-08**
Jp201-C	X10-sPFCB2-$2_{0.42}$	25	**1.54E-08**
Jp203	sPFCB2-$2_{0.28}$	19	**1.90E-08**
Jp203-C	X10-sPFCB2-$2_{0.28}$	30	**1.26E-08**
Nafion 211	Nafion 211	25.4	**5.14E-08**

Conclusions

With help of base materials from collaborator, Tetramer Technologies, LLC., block copolymer membranes were characterized as comparison with homopolymer membrane. Phase separation of membranes was confirmed by AFM. The sPFCB block copolymers exhibited relatively well-controlled phase separation, compared with homopolymer. The conductivity and acid stability of these block copolymers were better than homopolymer. The less SO_2 cross-over and higher current density were observed in our membranes as compared to Nafion 115 and Nafion 211 which are essential requirements of HyS process. In the HyS process, although all PFCB membranes showed lower conductivities than Nafion, two more essential requirement of HyS process of less SO_2 crossover and higher current density (SDE performance) was shown by PFCB membranes as compared to Nafion 115. These results indicated that the proton exchange membranes have strong potential for high-temperature hydrogen production in the next-generation of nuclear power plants. Cross-linked membranes were prepared through the Friedel-Craft reaction and an initial investigation of membranes was conducted for SDE. During the cross-linking process, the sulfonic acid groups in the polymer backbone served as not only proton transport facilitators but also as acid sources. The conductivity and water uptake study was used to characterize these membranes. These membranes exhibited reduced volume swelling and less sulfur dioxide cross-over, compared with those of the uncross-linked counterparts, while maintaining their high proton conductivity (e.g., 0.2828 S/cm at 80 ºC and 100% RH.)

Experimental Details

Materials

4,4'-oxybis(benzoic acid) and 4,4′-(hexafluoroiso-propylidene)bis(benzoic acid), were purchased from Aldrich. 4,4'-((1,2,3,3,4,4-hexafluorocyclobutane-1,2-diyl)bis(oxy))dibenzoic acid was donated by Tetramer Technologies, L.L.C. All other chemicals and solvents were obtained from Aldrich and used as received unless stated otherwise.

Instrumentations

Scanning electron microscopy (SEM) micrographs and energy-dispersive X-ray spectroscopy (EDX) data was obtained from a Hitachi S-3400N SEM at the CU electron microscope facility. The proton conductivities of membranes were estimated from electrochemical impedance spectroscopy (EIS) using Solartron 1280B potentiostat/frequency analyzer. SO2 Cross-over was measured as reported in the literature at SRNL.[2] ^{1}H NMR spectra was recorded on a JEOL Eclipse + 300.

Thermal gravimetric analysis (TGA) was performed on a Mettler-Toledo 851 instrument in nitrogen and air at a heating rate of 10 °C/min up to 800 °C. Differential scanning calorimetry (DSC) analysis was performed on a TA Q1000 instrument in nitrogen at a heating rate of 10 °C/min up to 200 °C. The glass transition temperature (T_g) of PFCB copolymers was obtained from a second heating cycle using TA Universal Analysis 2000 software suite.

Membrane Preparation

Sulfonated polymer was dissolved in N,N-dimethylacetamide (DMAc) to 20 wt% concentration. 5wt% or 10 wt% of cross-linking agent was added into the solution and the solutions were cast on a glass plate. The solvent was evaporated on the casting table for 15 min at 70 °C and dried in a vacuum oven for 24 h at 160 °C. The polymer membranes were carefully peeled off by grief immersion in water and acidified by soaking in 1M HCl for 24 h at room temperature for the pure acid form membranes. Membranes were washed several times with deionized water to remove any residual HCl and dried under vacuum for 24 h at 60 °C.

References

1. Sivasubramanian, P.; Ramasamy, R. P.; Freire, F. J.; Holland, C. E.; Weidner, J. W. Electrochemical Hydrogen Production from Thermochemical Cycles using a Proton Exchange Membrane Electrolyzer. *Int. J. Hydrogen Energy* **2007,** *32*, 463-468.

2. Elvington, M. C.; Colón-Mercado, H.; McCatty, S.; Stone, S. G.; Hobbs, D. T. Evaluation of Proton-conducting Membranes for use in a Sulfur Dioxide Depolarized Electrolyzer. *J. Power Sources* **2010,** *195*, 2823-2829.

3. O'Brien, J. A.; Hinkley, J. T.; Donne, S. W.; Lindquist, S. E. The Electrochemical oOidation of Aqueous Sulfur Dioxide: A Critical Review of Work with Respect to the Hybrid Sulfur Cycle. *Electrochim. Acta* **2010,** *55*, 573-591.

4. Rosen, M. A. Energy and Exergy Analyses of Electrolytic Hydrogen Production. *Int. J. Hydrogen Energy* **1995,** *20*, 547-553.

5. Iacono, S. T.; Budy, S. M.; Jin, J. Y.; Smith, D. W., Jr. Science and Technology of Perfluorocyclobutyl Aryl Ether Polymers. *J Polym Sci, Part A: Polym Chem* **2007,** *45*, 5705-5721.

6. Iacono, S. T.; Ewald, D.; Sankhe, A.; Rettenbacher, A.; Smith, D. W., Jr. Sulfonated Fluorovinylene Aromatic Ether Polymers for Proton Exchange Membranes. *High Perform. Polym.* **2007,** *19*, 581–591.

7. Wagener, E.; Smith Jr, D. W.; Topping, C.; Jayasinghe, R.; Jin, J.; Singh, A.; Mackinnon;, S. M.; Timothy J, F.; Craig S, G., In *Workshop on Advances in Polymer Electrolyte Membrane Fuel Cell Systems, Am. Chem. Soc., Div. Polym. Chem.*: Pacific Grove CA, 2009.

8. Fuller, T. J.; MacKinnon, S. M.; Schoeneweiss, M. R., Polyelectrolyte Membranes derived from Soluble Perfluorocyclobutane Polymers with Sulfonyl Chloride Groups, U.S. Patent 7,989,512 Aug 02, 2011.

9. Fuller, T. J.; MacKinnon, S. M.; SchoeneWeiss, M. R., Polyelectrolyte Membranes made of Poly(Perfluorocyclobutanes) with Pendant Perfluorosulfonic Acid Groups and Blends with Poly(Vinylidene Fluoride) U.S. Patent 8,053,530, Nov 08, 2011.

10. Mackinnon, S. M.; Fuller, T. J.; Coms, F., Sulfonated Perfluorocyclobutane Block Copolymers and Proton Conductive Polymer Membranes. U.S. Patent 7,897,692, Mar 1, 2011.

11. Hou, H.; Di Vona, M. L.; Knauth, P. Building Bridges: Crosslinking of Sulfonated Aromatic Polymers—A Review. *J. Membr. Sci.* **2012,** *423–424*, 113-127.

12. James, P. J.; Antognozzi, M.; Tamayo, J.; McMaster, T. J.; Newton, J. M.; Miles, M. J. Interpretation of Contrast in Tapping Mode AFM and Shear Force Microscopy. A Study of Nafion. *Langmuir* **2001,** *17*, 349-360.

13. Brown, D.; Park, J.; Verma, R.; Tomar, N.; Jayasinghe, R.; Colon-Mercado, H.; Elvington, M.; Hobbs, D.; Sharif, I.; DesMarteau, D.; Creager, S.; Smith Jr, D. W. Phase Separation of TFVE Base Block Copolymers and their Applicatiobs. *Polym. Prepr. (Am. Chem. Soc., Div. Polym. Chem.)* **2010,** *51*, 626.

14. Park, K. T.; Chun, J. H.; Kim, S. G.; Chun, B.-H.; Kim, S. H. Synthesis and Characterization of Crosslinked Sulfonated Poly(arylene ether sulfone) Membranes for High Temperature PEMFC Applications. *Int. J. Hydrogen Energy* **2011,** *36*, 1813-1819.

15. Zhong, S.; Liu, C.; Na, H. Preparation and Properties of UV Irradiation-induced Crosslinked Sulfonated Poly(ether ether ketone) Proton Exchange Membranes. *J. Membr. Sci.* **2009,** *326*, 400-407.

16. Rhoden, S. L. N. H.; Linkous, C. A.; Mohajeri, N.; Díaz, D. J.; Brooker, P.; Slattery, D. K.; Fenton, J. M. Low Equivalent Weight Friedel-Crafts Cross-linked Sulfonated Poly(ether ether ketone). *J. Membr. Sci.* **2011,** *376*, 290-301.

17. Zhang, Y.; Wan, Y.; Zhang, G.; Shao, K.; Zhao, C.; Li, H.; Na, H. Preparation and Properties of Novel Cross-linked Sulfonated Poly(arylene ether ketone) for Direct Methanol Fuel Cell Application. *J. Membr. Sci.* **2010,** *348*, 353-359.

18. Phu, D. S.; Lee, C. H.; Park, C. H.; Lee, S. Y.; Lee, Y. M. Synthesis of Crosslinked Sulfonated Poly(phenylene sulfide sulfone nitrile) for Direct Methanol Fuel Cell Applications. *Macromol. Rapid Commun.* **2009,** *30*, 64-68.

19. Han, M.; Zhang, G.; Shao, K.; Li, H.; Zhang, Y.; Li, M.; Wang, S.; Na, H. Carboxyl-terminated Benzimidazole-assisted Cross-linked Sulfonated Poly(ether ether ketone)s for Highly Conductive PEM with Low Water Uptake and Methanol Permeability. *J. Mater. Chem.* **2010,** *20*, 3246-3252.

CHAPTER FIVE

TELECHELIC PERFLUOROCYCLOBUTYL ARYL ETHER POLYELECTROLYTES

Introduction

Fluorinated ionomers are widely used in electrochemical devices including fuel cells, batteries and capacitors. The most widely used materials are the perfluorosulfonic acid ionomers (PFSIs) such as Nafion™,[1, 2] however other fully and partially fluorinated ionomers have also been described. In most cases the materials are high-molecular-weight polymers for which the end groups are unknown and / or difficult to control. End groups provide sites for degradation and can also offer a means of controlling ionomer morphology, for example via intentional crosslinking or grafting onto solid surfaces. A need exists for new fluorinated ionomer oligomers which have relatively low molecular weights, so that end groups are a significant fraction of the polymer structure, and for which the chemical nature of the end groups may be controlled so as to allow for rational design of materials via chemical reactions at the end groups. For example, surface grafting of such an ionomer onto an electronically conductive porous support could create a material having high electronic and also high ionic conductivity. Such a material could be useful in a wide range of electrochemical devices.

Recently, Wang and co-workers reported poly(vinylidene fluoride)-based ferroelectric polymers terminated with phosphonic acid end groups for direct coupling with zirconia (ZrO_2) fillers.[4] A marked improvement of nanoparticle dispersion was

observed in the nanocomposite prepared using end-group functionalized polymers relative to polymers without phosphonate end groups. To the best of our knowledge, fluorinated ionomers bearing ionic groups on/in the polymer chain and binding sites at the end group sites have not been investigated. We herein describe such a material.

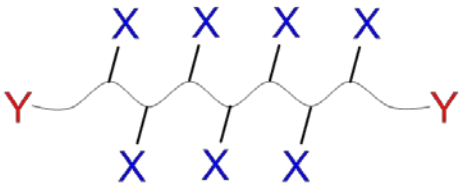

X = SO_3H (water-soluble group)
Y = PO_3H_2 (binding site)

Scheme 5.1 Telechelic fluorinated ionomers.

Scheme 5.1 illustrates a polymer architecture consisting of a sulfonate-functionalized main chain with phosphonate-functionalized end groups. Our version of such a polymer is prepared via radical-mediated [2 + 2] step-growth thermal cycloaddition reactions of aryl bis-(trifluorovinyl ether) (TFVE) monomers as shown in Scheme 5.2*(i)*.[5, 6] The resulting polymers, which are referred to as perfluorocyclobutyl (PFCB) polymers, are highly processible and have high chemical and thermal stability.[7, 8] The polymers are telechelic in nature with intact TFVE end groups which are good candidates for further transformation.[9-11] For example, aryloxylation of substituted phenols with aryl TFVEs provides a facile tailorable methodology for incorporating functionalizable moieties on the polymer chain ends (Scheme 5.2 *(ii)*).[12]

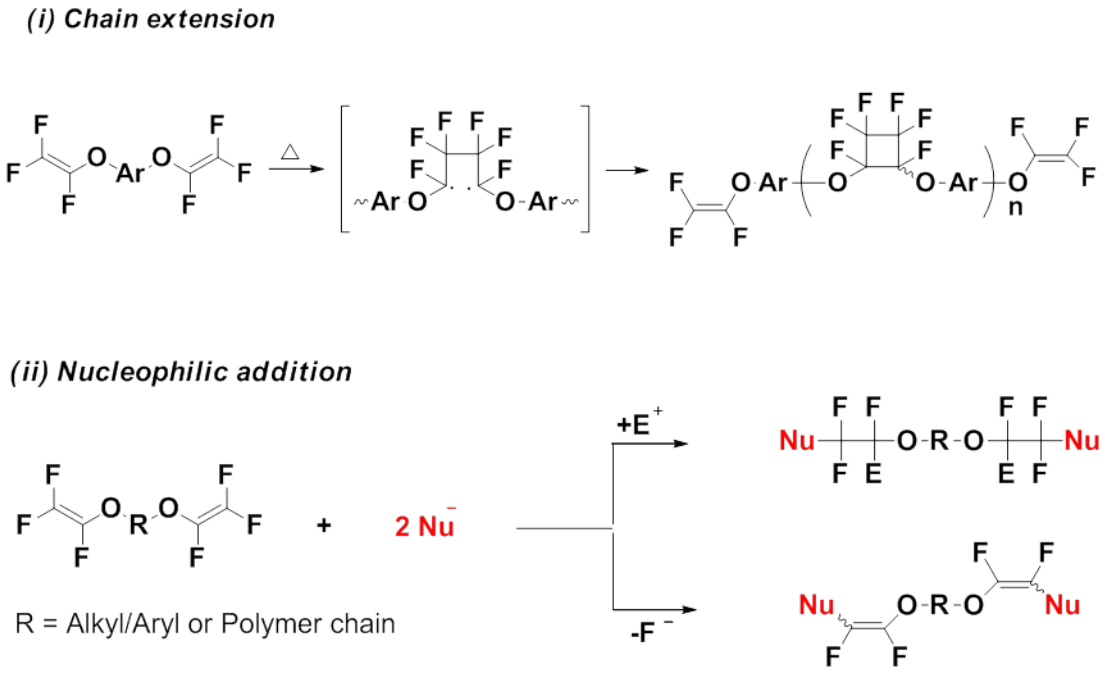

Scheme 5.2 *(i)* [2 + 2] Thermal polymerization of aryl TFVE and *(ii)* Nucleophilic addition to terminal fluorinated alkenes affording addition or vinyl substitution product.

Water-soluble perfluorocyclobutyl (PFCB) aryl ether ionomers bearing sulfonic acid groups in the main chain and phosphonic acid end groups were prepared through three steps: (1) aryloxylation of substituted phenols with aryl TFVEs, (2) post-sulfonation and (3) acid-catalyzed hydrolysis. This telechelic ionomer was used to modify the surfaces of mesoporous carbon materials containing dispersed zirconia nanoparticles.

Synthesis of Telechelic PFCB Aryl Ether Polyelectrolytes

To investigate the potential utility of chain-end-functionalized ionomers for surface grafting, water-soluble telechelic PFCB materials were prepared in three steps consisting of nucleophilic addition of aryl phosphonic diethyl esters onto the TFVE end groups, followed by aryl group sulfonation throughout the polymer, followed by hydrolysis of the phosphonate esters as shown in Scheme 5.3. This synthetic route is straightforward with technical simplicity and reactions can be performed on a large-scale with good yield.

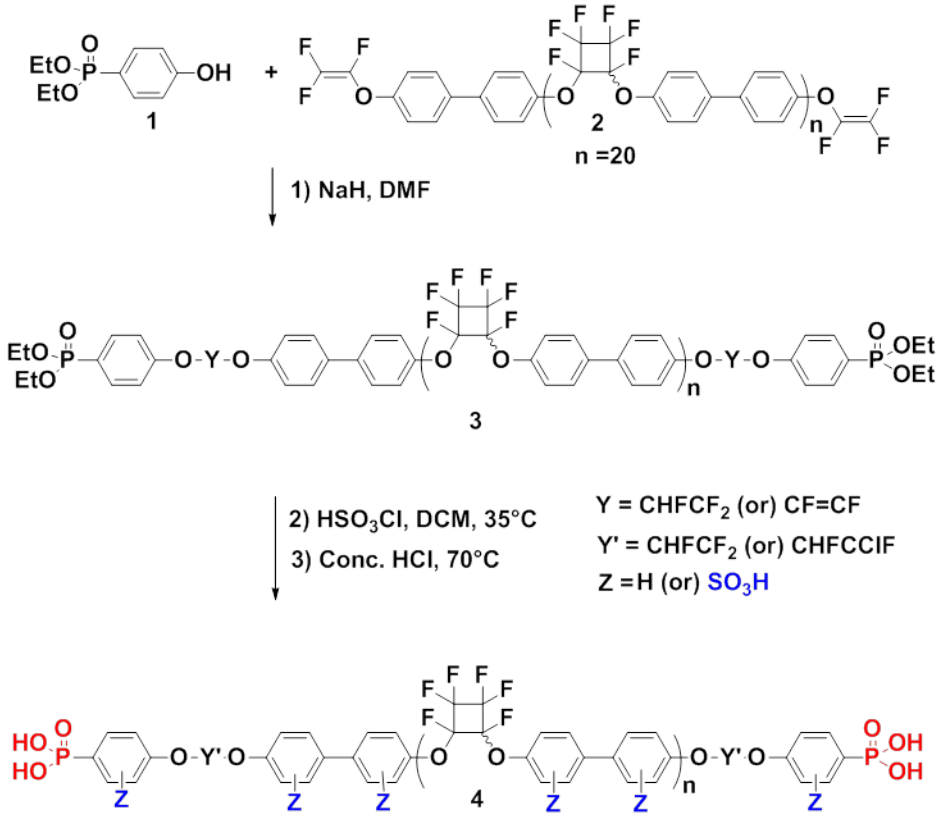

Scheme 5.3 Synthetic route for the polymer 4; (1) nucleophilic addition, (2) post-sulfonation via electrophilic aromatic substitution reaction, and (3) acid-catalyzed hydrolysis.

First, PFCB aryl ether polymer 2 was synthesized via a [2 +2] step-growth cyclopolymerization of TFVE bisphenol monomers at 160 °C. The conversion of trifluorovinyl ether end groups to the PFCB aryl ether rings and molecular structure of polymers were confirmed from ^{1}H and ^{19}F NMR spectroscopy. As shown in ^{19}F NMR spectroscopic data (Figure 5.1), peaks range from -128.7 to -131.2 ppm that corresponds to PFCB moieties appeared along with decreasing the characteristic AMX pattern at -119.2, -126.1 and -133.8 ppm of fluorovinyl end groups. The number-average molecular weight of the resulting polymer was estimated by ^{19}F-NMR end-group analysis as 7,300.

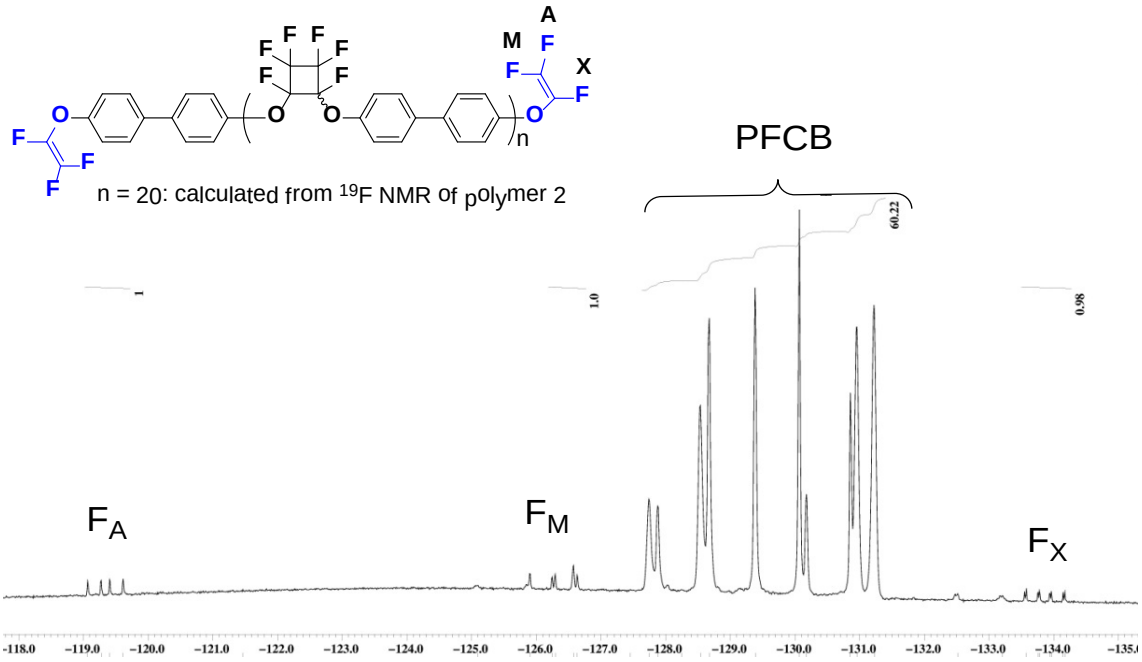

Figure 5.1 ^{19}F NMR (in Acetone-d_6) spectrum of PFCB aryl ether polymer 2.

Then, the chain-end-functionalized polymer was prepared via nucleophilic addition of diethyl(4-hydroxyphenyl) phosphonate 1 onto the terminal TFVE groups of polymers 2 in the presence of NaH in 89% yield. The diethyl(4-hydroxyphenyl) phosphonate 1 was synthesized through nickel-catalyzed cross-coupling from triethylphosphite and 4-bromophenol using nickel(II) bromide.[13] The number-average molecular weight of the resulting polymer 3 was found to be 7,700 by NMR and 5,600 by size-exclusion chromatography. The polymer 3 was a mixture of hydrofluorinated addition product (approximately 50%) and fluoroolefin (approximately 50%) as 50:50 (cis : trans) isomers as confirmed by ^{1}H and ^{19}F NMR spectra (Figure 5.2 and Figure 5.15). In the ^{19}F NMR, the disappearance of the trifluorovinyl end groups' signals indicated the completeness of the phosphonate reaction. A doublet at -86.6 ppm and a doublet at -141.3 ppm in ^{19}F NMR supported the hydrofluoroethylene moiety. The trans-fluroolefin isomer peaks overlap with the perfluorocyclobutyl peaks over the range -127.3 - (-131.1) ppm and the cis-fluoroolefin isomer peaks are shown as two sets of doublets at -122.0 and -123.5 ppm.

In the ^{1}H NMR, the peaks at 1.23 ppm, and 4.04 ppm for the diethyl esters groups and peak at 6.5 ppm correspond to the hydrofluoroethylene moieties. The hydrofluoroethylene moiety is a result of the protonation of the anion generated during the sodium phenoxide addition to the trifluorovinyl aryl ether moiety. The proton source is possibly derived from adventitious water as well as free phenol of diethyl(4-hydroxyphenyl)phosphonate. Two small peaks at 7.45 (d) and 7.85 ppm (c) are associate

with the protons on the phenyl moieties, connected with phosphonate group. The ^{31}P NMR provided further confirmation by the appearance of a distinct signal at 17.09 ppm.

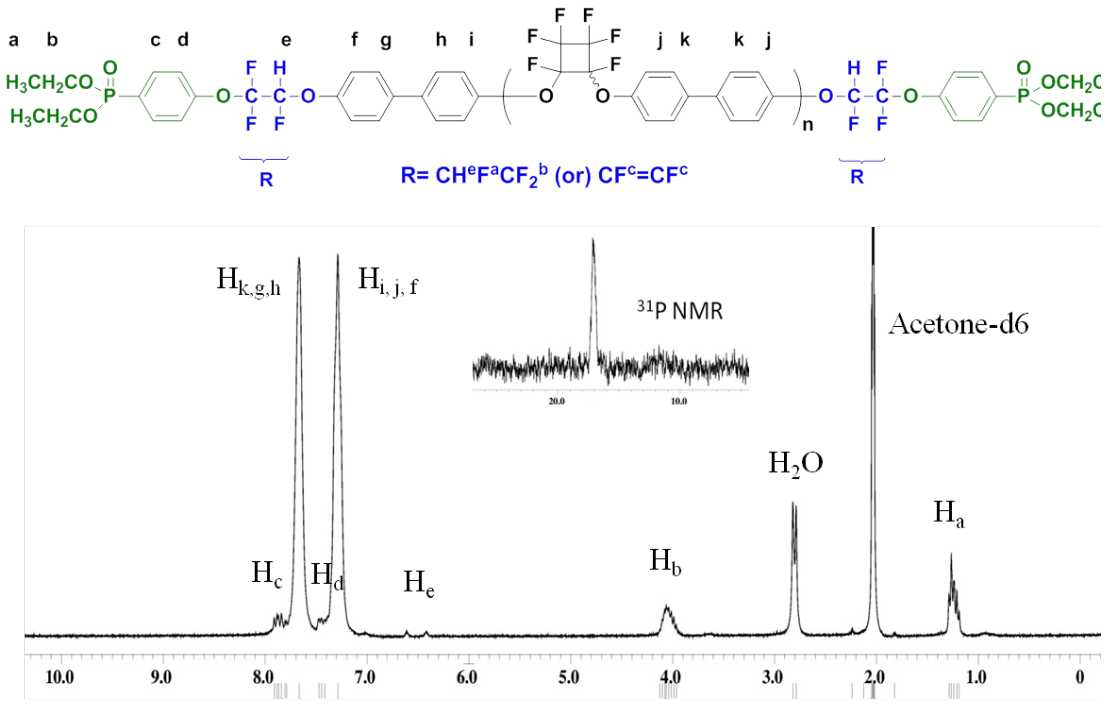

Figure 5.2 ^{1}H NMR and ^{31}P NMR (in Acetone-d_6*) spectra of polymer 3.

Next, sulfonation of polymer 3 was accomplished via electrophilic aromatic substitution using chlorosulfonic acid at 35 °C for 1 h. The sulfonation on the PFCB aryl ether polymer chain was confirmed by ^{1}H NMR. The protons adjacent to the sulfonic acid group appeared at the higher frequency than other aromatic protons due to deshielding from the strong electron withdrawing group. Although the benzene ring connected with phosphonate ester group is deactivated, the sulfonation was occurred in the deactivated aromatic rings as well as phenyl rings on the polymer backbone under

excess amount of CSA. The signal at the higher frequency (20.2 ppm) than original phosphonate diester (17.5 ppm) in the ^{31}P NMR confirmed the sulfonation on the deactivated terminal benzene rings. Due to the electron withdrawing sulfonic acid group in meta position, the phosphorous connected with sulfonated aromatic rings are more deshielded than those in P1 (Figure 5.3).

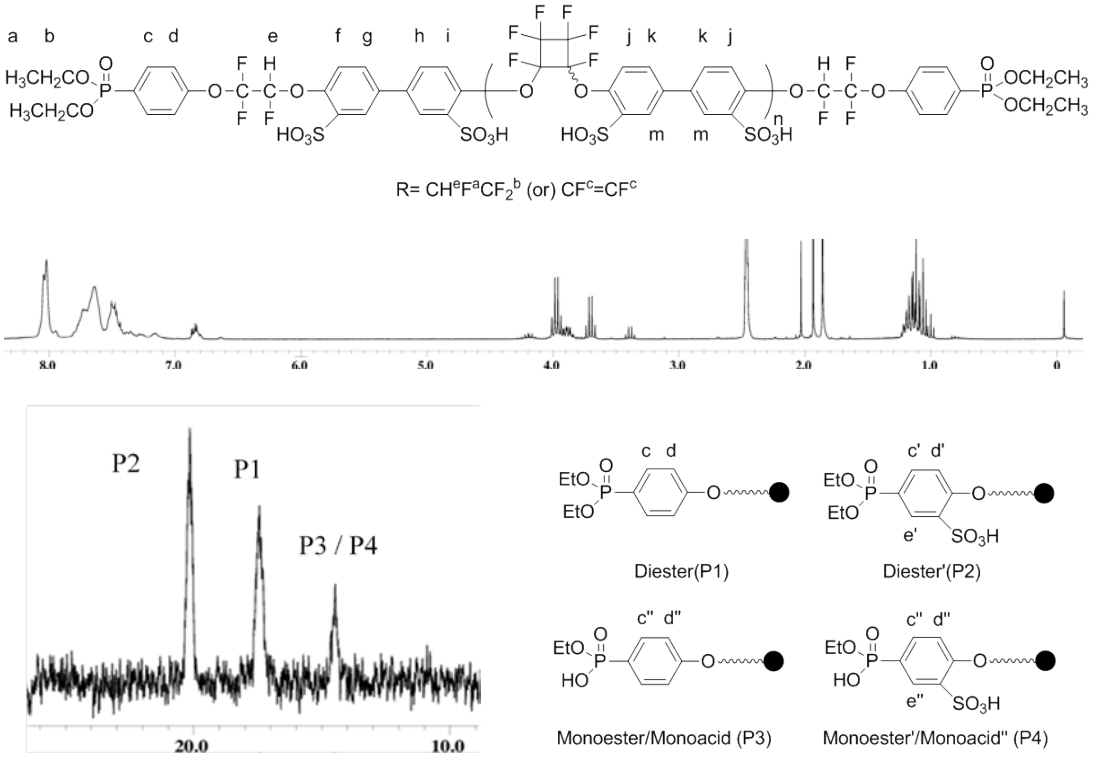

Figure 5.3 ^{1}H NMR and ^{31}P NMR (in DMSO) spectra of crude sulfonated PFCB polymer.

Partial hydrolysis of phosphonate diester groups and hydrochlorination of fluoroolefin moiety were also detected by ^{1}H, ^{19}F and ^{31}P NMR during sulfonation and is thought to have been caused by reaction with acid, HCl, derived from chlorosulfonic acid

(Figure 5.3). This partial hydrolysis reaction suggests a simple approach for further acid-catalyzed hydrolysis of the terminal phosphonate ester groups.

Finally, complete hydrolysis of the terminal phosphonate esters to phosphonic acids was achieved by refluxing of sulfonated polymer in concentrated HCl solution at 70 °C. Because the polymer 3 consist of hydrophilic and hydrophobic groups, the polymer can be aggregated as a micelle structure in the acidic aqueous solution and would lead to an increasing hydrolysis reaction time hiding phosphonate end groups inside of aggregated structure. As increasing reaction temperature, the hydrolysis was accelerated. However, the dealkylation of polymers was conducted at 70 °C because the solution formed soaps above 75 °C with stirring. The resulting telechelic phosphonic acid polymer 4 was obtained in quantitative yield after 10 days of refluxing in conc. HCl. A signal at 12.2 ppm in the ^{31}P NMR that corresponds to phosphonic acid moieties (P3) appeared along with decreasing phosphonic diester/monoester peaks at 17.5 and 14.5 ppm during the hydrolysis reaction (Figure 5.4). The faster disappearance of sP1 and sP2 peak indicates that diester groups attached into hydrophilic phenyl ring are easily hydrolyzed rather than the others. The phosphonate ester group connected with sulfonated benzene ring can be hydrolyzed faster than those connected with unsulfonated phenyl ring because possibly it can be easily exposured to the HCl aqueous solution.

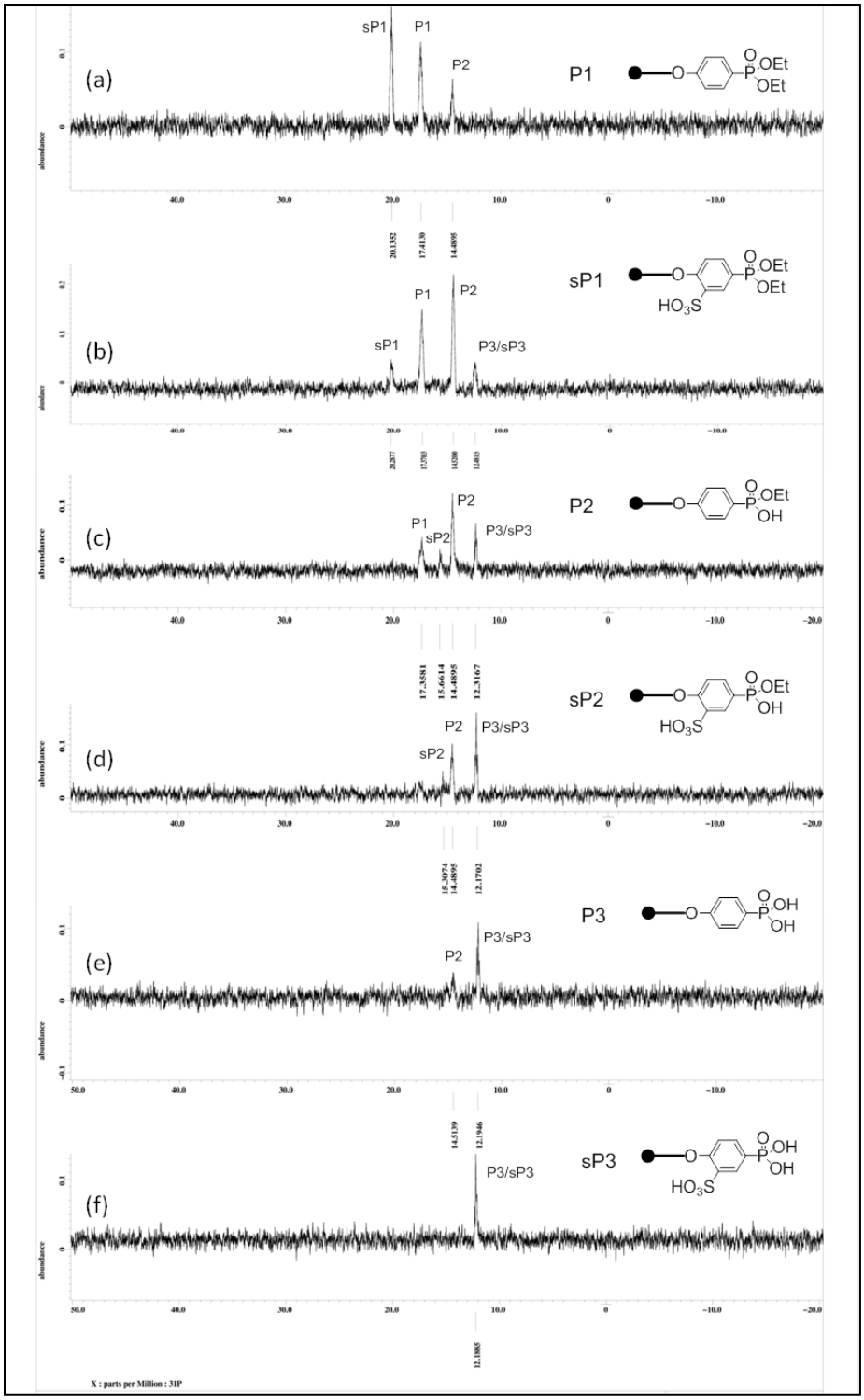

Figure 5.4 ^{31}P NMR (in DMSO-d_6) spectrum of (a) after sulfonation and (b-f) hydrolysis as a function of time.

Properties of Telechelic PFCB Aryl Ether Polyelectrolytes

Degree of sulfonation (DS) of the chain-end-functionalized ionomer 4 was assayed by ^{1}H NMR, elemental microanalysis, and neutralization titration (Table 5.1). The estimated DS value from ^{1}H NMR was 82% which corresponds to a ion-exchange capacity (IEC) of 3.44 meq/gram. The IEC values obtained from elemental microanalysis (3.11 meq/gram) and titration (3.30 meq/gram) were in good agreement with the result from NMR.

Table 5.1 Selected properties of polymers and composites.

	M_n		$T_{d5\%}$	Tg	IEC (mmol/g) [d]		
	NMR [a]	GPC	(°C) [b]	(°C) [c]	NMR	Tit	EA
3	7,700	5,600	413	113	–	–	–
4	10,500	–	276	>190	3.43	3.30	3.11

[a] Determined by ^{19}F and ^{1}H NMR, [b] TGA (10 °C/min) in nitrogen, [c] DSC (10 °C/min) in nitrogen determined by second heating, [d] IEC calculated from ^{1}H NMR, titration, and sulfur content determined by EA.

TGA and Differencital scanning calorimetry (DSC) analysis were performed to understand the thermal behaviors of the resulting polymer samples. In TGA curves, two step degradation was observed from all samples at around 270 and 405 °C (Figure 5.5). Next, glass transition temperatures (T_g) of these samples were estimated using DSC (Figure 5.6). T_gs of PFCB1, PFCB2, and PFCB3 were observed at 113 and 190 °C, respectively. In the PFCB1 sample, only T_g was observed, which implies their amorphous nature.

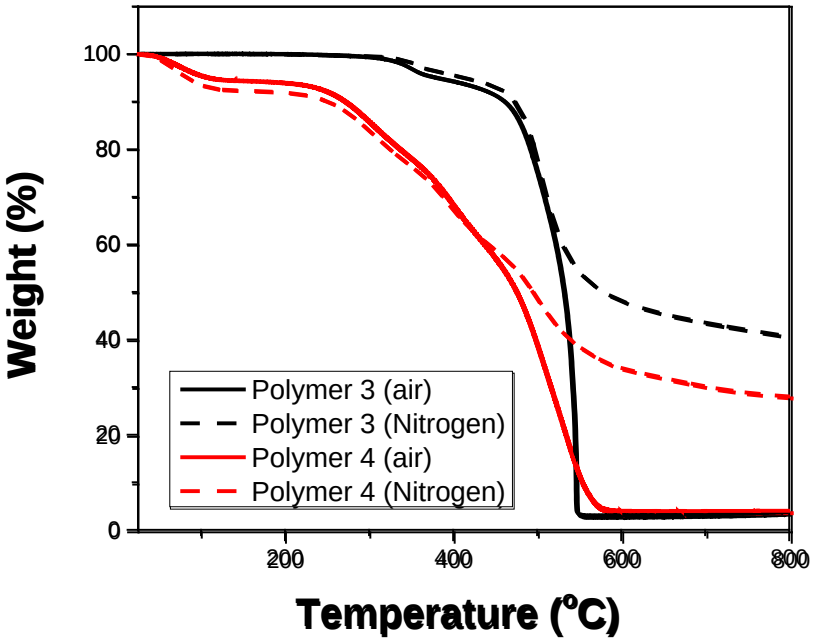

Figure 5.5 TGA curves of polymer 3 and 4.

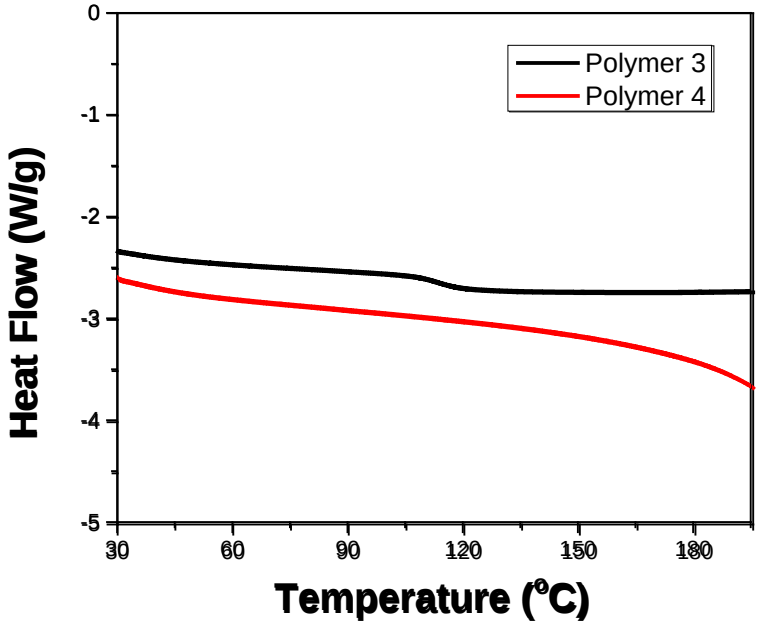

Figure 5.6 DSC of polymer 3 and 4.

We note that this highly sulfonated and thermally stable polymers are soluble in water as well as in common polar organic solvents. The solubility of polymers was determined in the common organic solvents at room temperature as shown in Table 5.2. The phosphonate diester polymer 3 was soluble in nonpolar organic solvents. On the other hand, the sulfonated polymers were found be soluble in water as well as in polar organic solvents.

Table 5.2 Solubility of the polymers in common organic solvents.

Polymer	DCM	THF	$CHCl_3$	MeOH	DMAc	DMSO	H_2O
3	++	++	++	–	–	–	–
4	–	+	+	++	++	++	++

++ soluble; + partially soluble; - insoluble

An important attribute of any soluble polymer, but particularly a soluble ionomer, is the hydrodynamic size of the polymer solutes. Size affects transport properties of solutes and particularly the ability of solutes to penetrate pores in porous media. The present ionomers in solution were examined using dynamic light scattering to assess the size of the dissolved polyelectrolytes. Figure 6.7 presents the results of this study as a set of bar graphs of ionomer corresponding to a particular size range in aqueous solutions (1 $mg \cdot mL^{-1}$) containing variable amounts of dissolved salt. Several key findings are evident in these data. First, the data with no added salt show clusters of material in two size regimes, one near 20-50 nm and the other near 100-400 nm. We assign the cluster near 20-50 nm to individual ionomer chain solutes and the cluster near 100-400 nm to

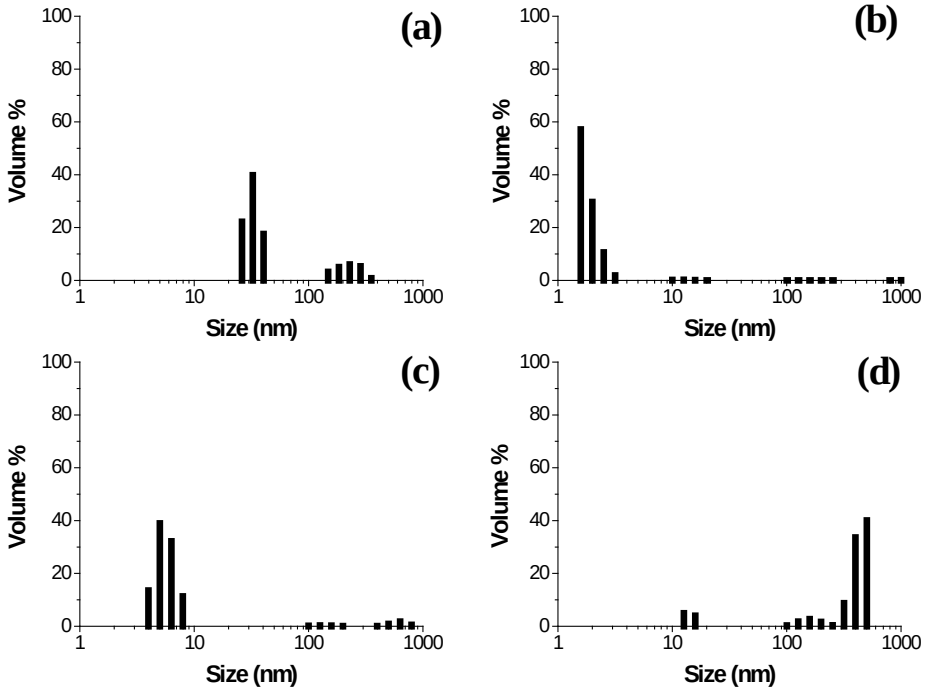

Figure 5.7 Relative particle size distributions by Dynamic Light Scattering of PFCB ionomer aqueous solutions (1 mg·mL^{-1}) with a different Na_2SO_4 concentration: (a) 0.00 M (b) 0.05 M, (c) 0.10 M, and (d) 1.00 M salt concentrations.[3]

aggregates of ionomer chains. It is common for polyelectroltyes to exhibit a degree of aggregation in solution, in fact Nafion^{TM} is known to exist in solution as a highly aggregated material that is more properly thought of as a dispersion.[14, 15] Interestingly, when a modest concentration of salt (0.05 M) is present in solution, the larger scatterers almost completely disappear and the size of the smaller scatterers decreases to a value below 10 nm. This finding is consistent with the idea that the added salt screens the charge on the individual polymer chains, thereby stabilizing them in solution and allowing them to adopt a less extended, more compacted conformation in solution[16] as illustrated Figure 6.8(b).

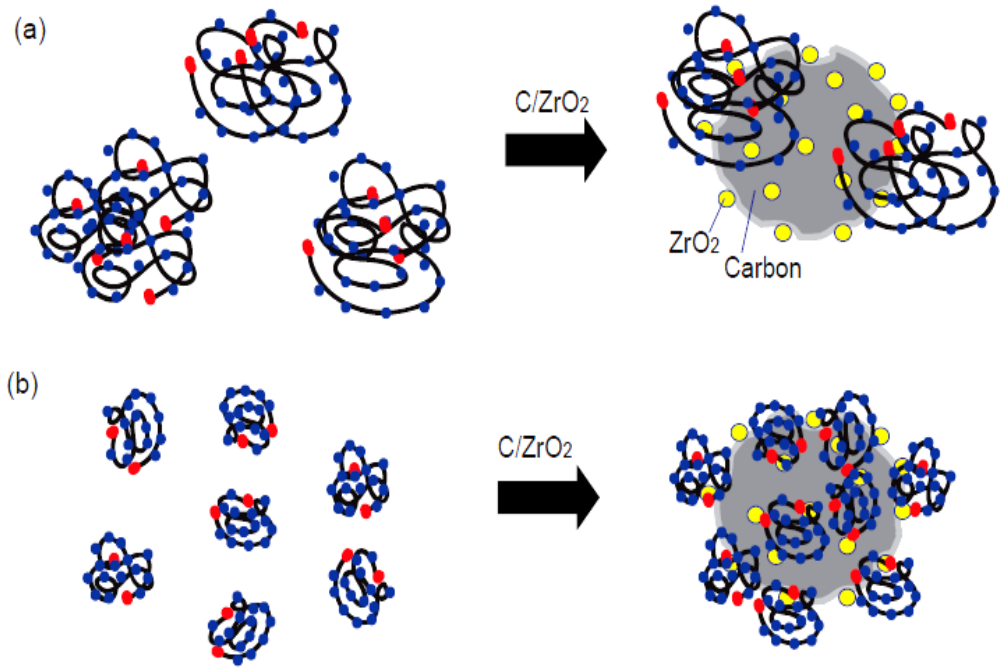

Figure 5.8 Schematic illustration of covalent bond formation between polymer and ZrO_2 under different salt concentration solution; (a) 0 M and (b) 0.05 M Na_2SO_4. Blue dots correspond to sulfonate groups, red dots to phosphonate groups, and black lines to polymer chains.

Increasing the salt concentration to 0.1 M results in an unexpected increase in scatterer size, and further increasing to 1.0 M shifts nearly all the scattering back to the larger scattering size regime. These findings are consistent with a salt-induced ionomer aggregation at higher salt concentration.[17] Indeed, over a time period of 1h, ionomer precipitation occurred in solutions containing 1.0 M salt.

Application of Telechelic PFCB Aryl Ether Polyelectrolytes

We recently described a group of templated mesoporous carbon / zirconia nanocomposites in which zirconia nanoparticles are homogeneously distributed throughout the carbon skeleton of the nanocomposite materials.[18] These materials are being developed as electrocatalyst supports for PEM-style hydrogen fuel cells. Water-soluble telechelic ionomers from the present work can interact with these mesoporous carbon / zirconia nanocomposites (C/ZrO_2) via covalent binding of the phosphonate end groups of the ionomer onto the exposed zirconia particles. This mode of binding is desirable because it provides materials in which the ionomer electrolyte stays bound even when exposed to liquid water. To maximize the amount of ionomer that is chemically attached onto the C/ZrO_2 nanocomposite pore surfaces, a compact ionomer is desired.

To investigate the effect of ionomer hydrodynamic size on the amount of ionomer that can be bound on / in the C/ZrO_2 nanocomposites, ionomer solutions containing different salt concentrations (0 M and 0.05 M) were used to accomplish ionomer grafting onto C/ZrO_2 surfaces and inside C/ZrO_2 pores. The amount of attached ionomer on the C/ZrO_2 nanocomposites was indirectly estimated from IEC values determined by titration, EA, TGA, and EDX (Table 5.3). As expected, larger amounts of ionomer were attached to the C/ZrO_2 nanocomposites when modification was accomplished from ionomer solutions containing 0.05 M Na_2SO_4 than from ionomer solutions containing no added salt. Since the phosphonic acid units could be located in the inner part of the aggregates in solutions formed without salt, covalent bond formation with ZrO_2 could be interrupted. On the other hand, as the ionomer aggregate size decreased, the opportunity

for binding between phosphonate end groups and ZrO_2 sites increased due to the phosphonic acid units being more exposing on the outside of the smaller micelle-like ionomers. Diminished steric crowding on the C/ZrO_2 surfaces when the ionomer molecules exist in a more compact conformation in solution could also contribute to the greater ionomer binding from ionomer solutions containing salt.

Table 5.3 Ion-exchange capacity (IEC) of C/ZrO_2 nanocomposites.

	$IEC_{Tit.}$[c]	IEC_{EA}[d]	IEC_{TGA}[e]	IEC_{EDX}[f]
0.05 M Na_2SO_4-C/ZrO_2	< 0.01	NA	NA	NA
[a] **SF-Ionomer-C/ZrO_2**	0.45	0.49	0.48	0.47
[b] **SA-Ionomer-C/ZrO_2**	0.55	0.59	0.62	0.61

[a] Salt free (0 M Na_2SO_4), [b] Salt added (0.05 M Na_2SO_4), [c, d, e, f] IEC (mmol/g) determined by titration, elemental analysis, TGA, and EDX, respectively.[3]

Conclusions

Water-soluble perfluorocyclobutyl (PFCB) aryl ether ionomers bearing sulfonic acid groups in the main chain and phosphonic acid end groups were prepared and used to modify the surfaces of mesoporous carbon materials containing dispersed zirconia nanoparticles. Ionomer surface grafting occurred via phosphonate bonding onto the zirconia particle surfaces. Water-soluble ionomer oligomers would normally not be considered useful in electrochemical devices such as PEM fuel cells because the ionomers could be easily swelled and/or washed out of the device by liquid water. The fact that these ionomers have controlled end group chemistries presents opportunities for ionomer stabilization that are not available for other low-EW ionomers.

Experimental Details

Materials

Chlorosulfonic acid (CSA) and 4-bromophenol were purchased from Alfa Aesar. Commercially available monomer 4,4'-bis(4-trifluorovinyloxy)biphenyl was generously donated by Tetramer Technologies, LLC and is also available through Oakwood Chemicals, Inc. Anhydrous sodium sulfate (Na_2SO_4, 99%) was purchased from Mallinckrodt. Sodium hydroxide (NaOH, 0.01N) and hydrochloric acid (HCl, 0.0lN) were obtained from Fisher Scientific. Dimethylformamide (DMF) (Sigma-Aldrich) was vacuum distilled prior to use. All other starting chemicals and solvents were purchased from Sigma-Aldrich and used as received.

General Methods

^{1}H, ^{19}F, and ^{31}P NMR spectra were recorded in $CDCl_3$, acetone- d_6 or DMSO-d_6 using a JEOL Eclipse + 300. Gel permeation chromatography (GPC) data were collected in $CHCl_3$ from a Waters 2690 Alliance System with photodiode array detection and molecular weights were obtained using polystyrene as a standard. Thermal gravimetric analysis (TGA) was carried out on a Mettler-Toledo 851 instrument in nitrogen and air at a heating rate of 10 °C/min up to 800 °C. Differential scanning calorimetry (DSC) analysis was performed on a TA Q1000 instrument in nitrogen at a heating rate of 10 °C/min up to 210 °C. The glass transition temperature (T_g) of polymers was obtained from a second heating cycle using TA Universal Analysis 2000 software suite. Energy-dispersive X-ray spectroscopy (EDX) was performed on a field emission scanning

electron microscope (FESEM-Hitachi S4800) equipped with an Oxford INCA energy 200 EDX system. Elemental microanalysis (EA) data for sulfur, carbon, hydrogen and fluorine were obtained from Atlantic Microlab, Inc. (Norcross, GA). Ion-exchange capacity (IEC) of ionomer samples was determined via a direct neutralization titration method using standard 0.01 N NaOH. The relative sizes of the ionomer solutes were investigated by dynamic light scattering (DLS) using a scattering angle of 90° at room temperature with a Coulter N4 Plus particle size analyzer equipped with a laser source of 10 mV helium-neon at 632.8 nm.

Preparation of Polymers

Synthesis of diethyl(4-hydroxyphenyl)phosphonate 1.[13] Diethyl (4-hydroxyphenyl) phosphonate was synthesized as described in literature.[13] A 4-bromophenol (1 g, 5.8 mmol), nickel(II) bromide (0.1 g, 0.46 mmol), and mesitylene (3 mL) were charged into a round-bottom flask equipped with a reflux condenser and stirred at 170 °C under nitrogen. Triethylphosphite (1.44 g, 8.7 mmol) was added drop wise to the mixture and stirred at 170 °C for 2 h under nitrogen. The mixture was then allowed to cool to room temperature and filtered through Celite. The crude mixture was dissolved in ether and extracted with a 10% sodium hydroxide solution. The aqueous phase was washed with ether, acidified by concentrated hydrochloric acid and extracted with diethyl ether several times. The collected organic phase was then dried using anhydrous magnesium sulfate and solvent was removed by rotary evaporation. Diethyl(4-hydroxyphenyl)phosphonate was obtained as a white solid. (0.96 g, 72% yield). ^{1}H NMR (300 MHz, $CDCl_3$): δ 1.30

(t, J = 7.1 Hz, CH_3–), 3.94–4.21 (m,–CH_2–), 6.99 (dd, J = 8.7, 3.7 Hz, Ar-H), 7.63 (dd, J = 13.0, 8.7 Hz, Ar-H), 9.47 (s, –OH); ^{13}C NMR (75 MHz, $CDCl_3$): δ 16.32 (d, J = 7.3 Hz, CH_3–), 62.44 (d, J = 5.8 Hz, –CH_2–), 116.12 (d, J = 15.9 Hz, C=C–OH), 116.54 (d, J = 197 Hz, C=C–P), 133.87 (d, J = 12.3Hz, C=C–P), 162.05 (s, C=C–OH); ^{31}P NMR (121 MHz, $CDCl_3$): δ 21.82 (s).

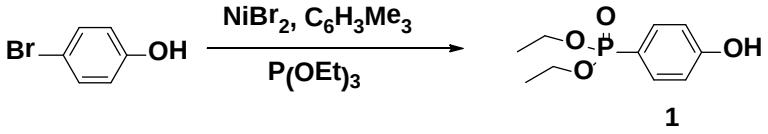

1

Scheme 5.4 Synthetic route for the diethyl(4-hydroxyphenyl) phosphonate 1.

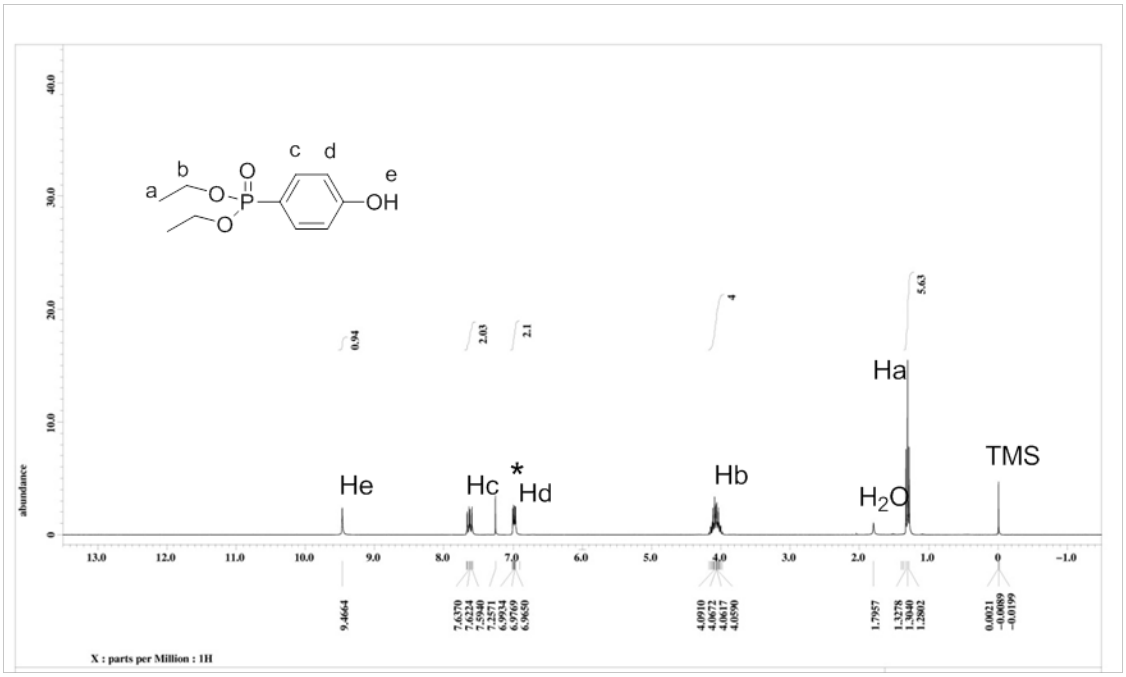

Figure 5.9 ^{1}H NMR (in $CDCl_3$*) spectrum of diethyl(4-hydroxyphenyl) phosphonate 1.

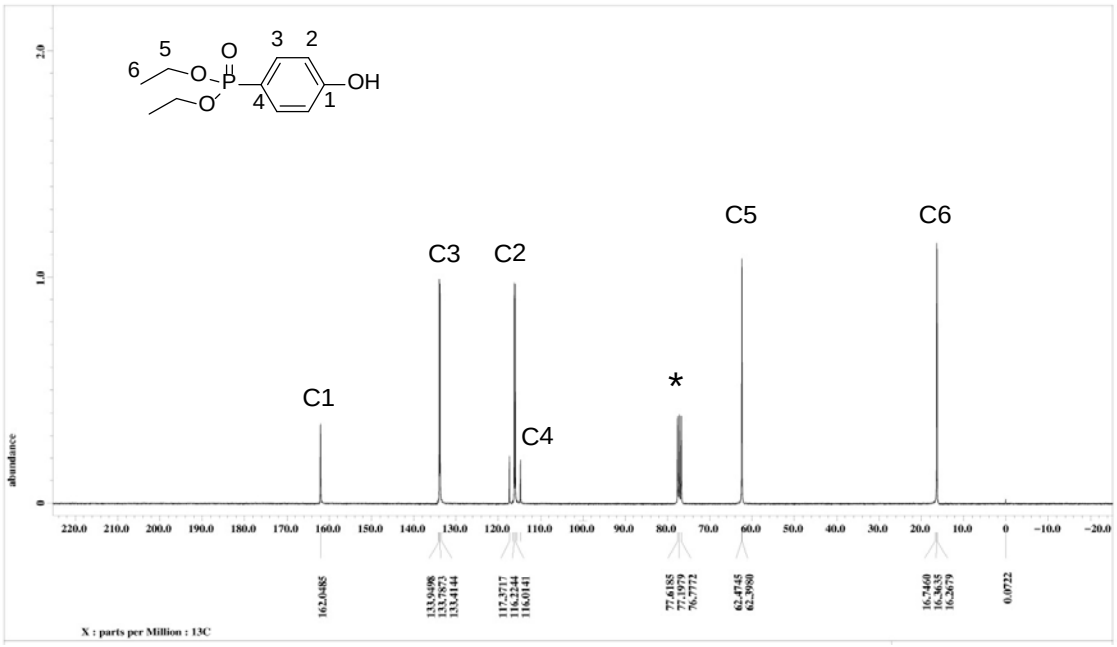

Figure 5.10 ^{13}C NMR (in $CDCl_3$*) spectrum of diethyl(4-hydroxyphenyl) phosphonate 1.

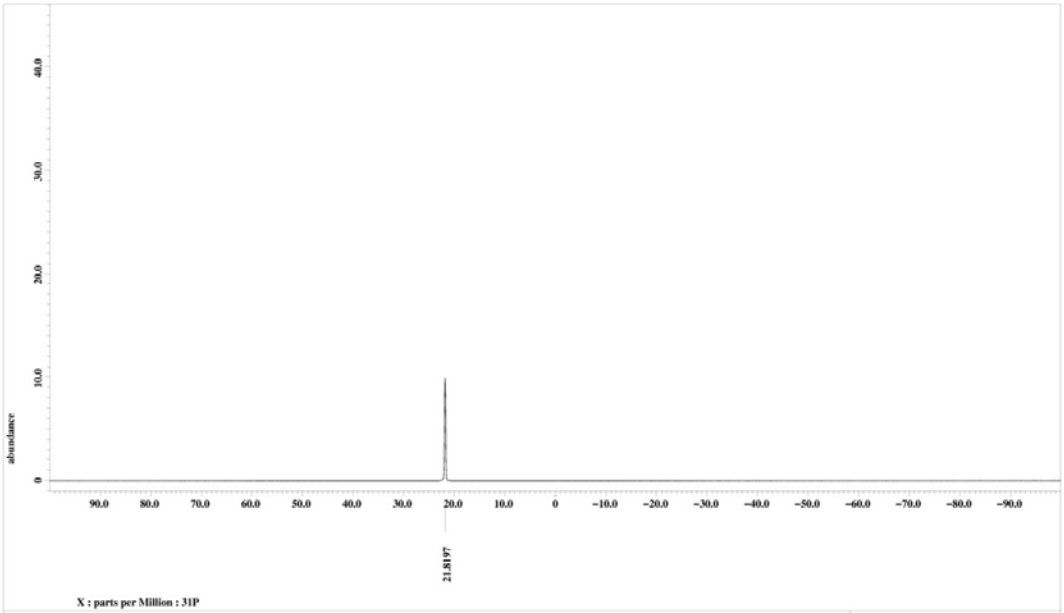

Figure 5.11 ^{31}P NMR (in $CDCl_3$*) spectrum of diethyl(4-hydroxyphenyl) phosphonate 1.

Synthesis of PFCB aryl ether polymer 2. 4,4'-bis(4-trifluorovinyloxy)biphenyl monomer (10 g, 28.88 mmol) was added into a three-neck round-bottom flask equipped with a mechanical stirrer, condenser, and argon gas inlet. The monomer was heated to 80 °C and the melted monomer system was sparged with argon gas for 30 min. Thermal step-growth cyclopolymerization was then conducted at 160 °C for 12 h under argon blanket. After cooling to room temperature, the viscous product was dissolved in tetrahydrofuran (THF) and precipitated in a large excess of methanol. The white precipitate was filtered, washed with methanol in a Soxhlet extractor for 24 h, and dried in a vacuum oven at 60 °C for 24 h. PFCB aryl ether polymer 2 was obtained as a white power (8.02 g, 80% yield). ^{1}H NMR (300 MHz Acetone-d_6): δ 7.28 (s, Ar-H), 7.66 (s, Ar-H); ^{19}F NMR (283 MHz, Acetone-d_6): δ –133.86 (dd, J = 110, 58.3 Hz, –CF=CF_2), –127.7-(–131.23) (m, cyclobutyl-F_6), –126.30 (dd, J = 110, 14.4 Hz, *trans*–CF=CF_2), –119.3 (dd, J = 96.4, 58.3 Hz, *cis*–CF=CF_2); M_n 7,300 (^{19}F NMR)

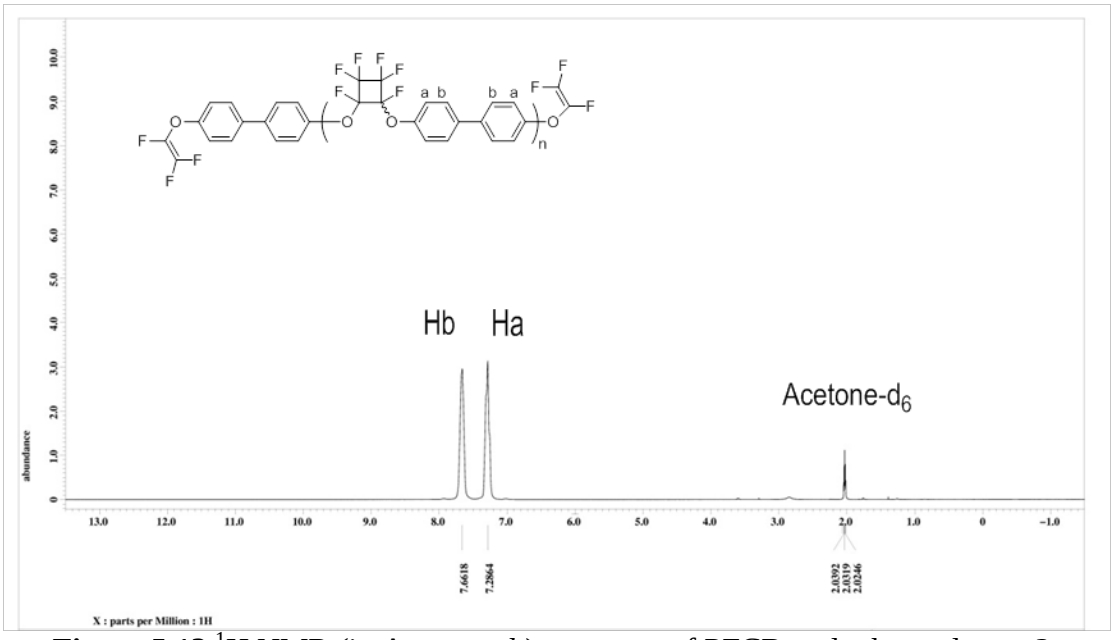

Figure 5.12 ^{1}H NMR (in Acetone-d_6) spectrum of PFCB aryl ether polymer 2.

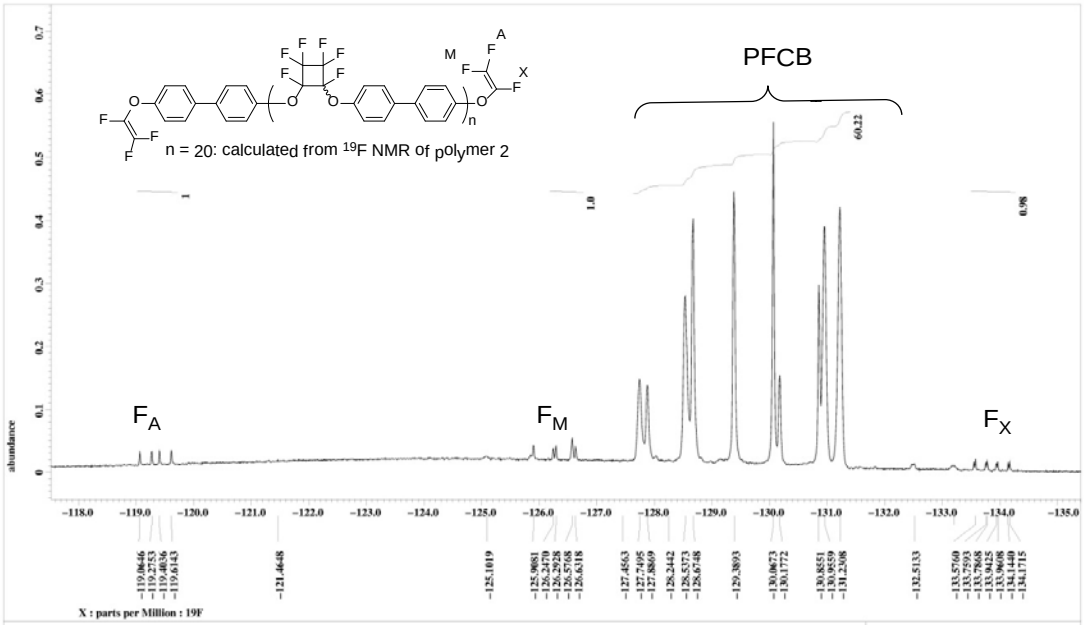

Figure 5.13 ^{19}F NMR (in Acetone-d_6) spectrum of PFCB aryl ether polymer 2.

Synthesis of polymer 3. Sodium hydride (28.80 mg, 1.20 mmol) and DMF (3 mL) were charged into a two-neck round-bottom flask equipped with a reflux condenser under nitrogen. Diethyl(4-hydroxyphenyl) phosphonate (0.23 g, 1 mmol) was added drop wise into a stirred suspension of NaH/DMF and polymer-2 (3.64 g, 0.50 mmol) dissolved in DMF (10 mL) was added into the solution at room temperature. The flask was then placed in a preheated oil bath at 80 °C and stirred for 5 h. The mixture was allowed to cool to room temperature and treated with DI H_2O. The white precipitate was filtered, washed with methanol and hexane, and dried under a vacuum at 60 °C. Polymer 3 was obtained as a white powder (3.43 g, 89% yield). ^{1}H-NMR (300 MHz, Acetone-*d6*): δ 1.19-1.29 (m, CH_3–), 3.96–4.10 (m, –CH_2–), 6.42-6.61 (d, J = 58.6 Hz, –C<u>H</u>F–), 7.29 (s,

Ar–H), 7.39–7.47 (m, Ar–H), 7.67 (s, Ar–H), 7.80–7.91 (m, Ar–H); ^{19}F-NMR (283 MHz, Acetone-*d6*): δ –141.36 (d, J = 59.4 Hz, –CHF–CF_2–), –127.7-(–131.23) (m, overlap of *trans*–CF=CF and cyclobutyl-F_6), –123.6 and –122.0 (d, J = 41.5, *cis*–CF=CF), –86.54 (dd, J = 2460, 144.2 Hz, –CHF–CF_2–); ^{31}P NMR (121 MHz, Acetone-*d6*): δ 17.04 (s); M_n 7,700 (^{19}F NMR); PDI = 2.08 (GPC, M_w/M_n = 11,603 /5,581)

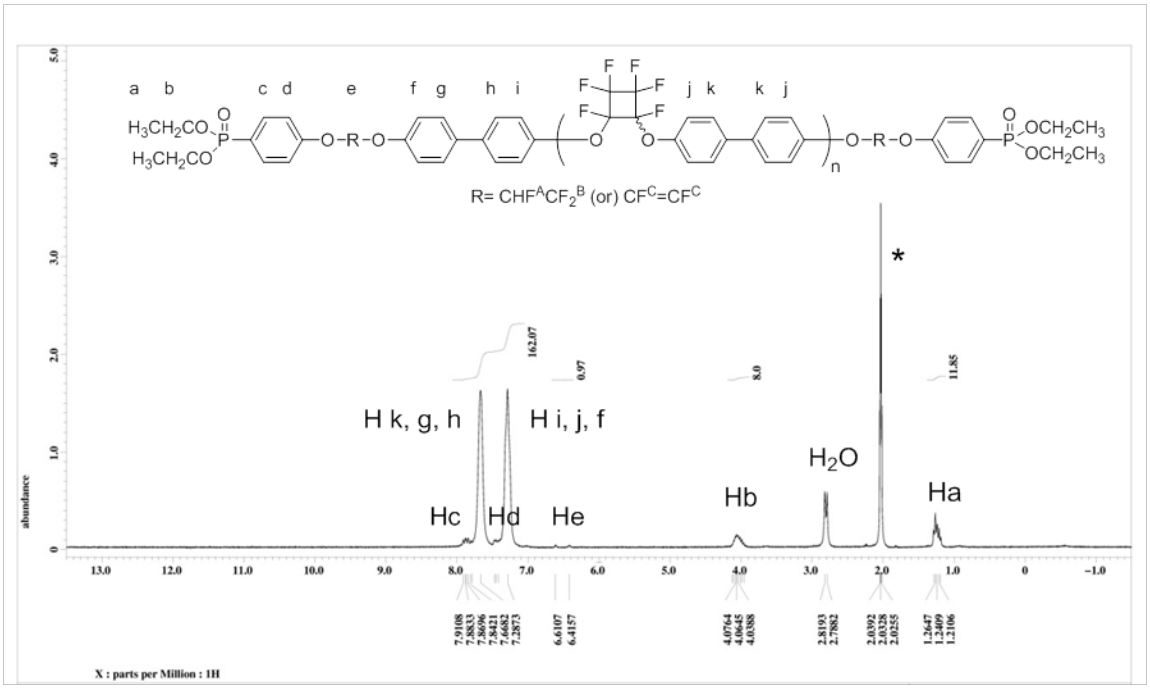

Figure 5.14 ^{1}H NMR (in Acetone-d_6*) spectrum of polymer 3.

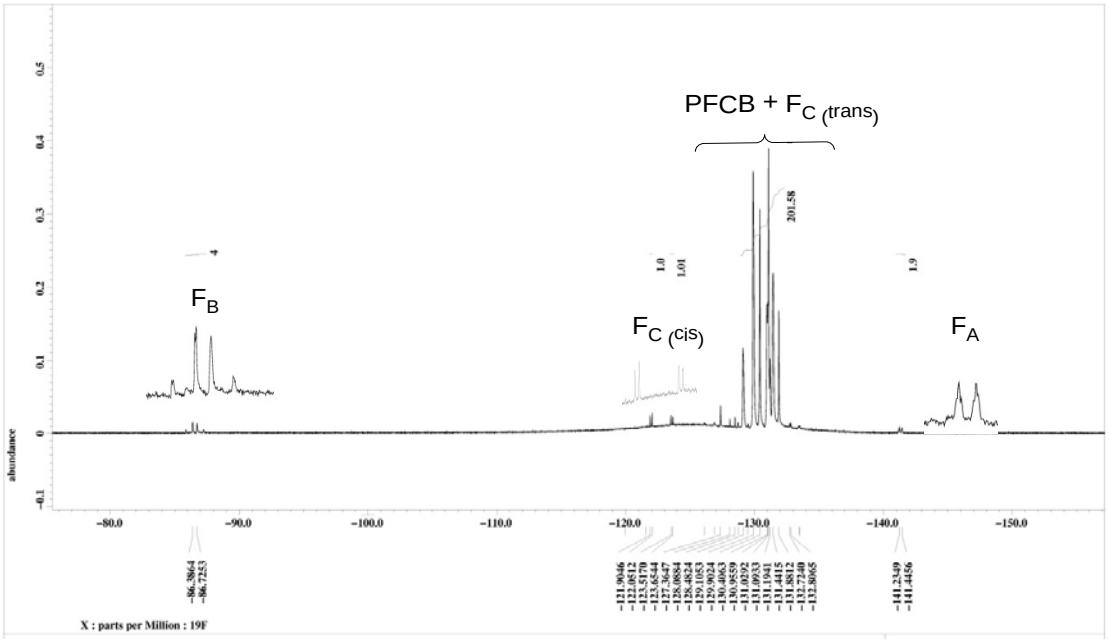

Figure 5.15 ^{19}F NMR (in Acetone-d_6) spectrum of polymer 3.

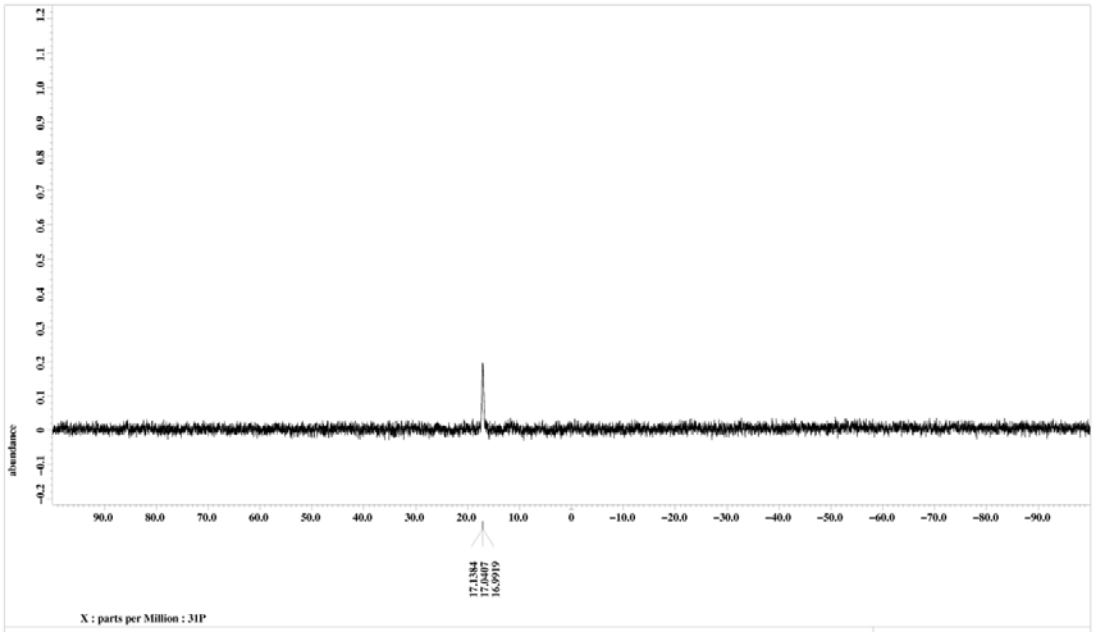

Figure 5.16 ^{31}P NMR (in Acetone-d_6) spectrum of polymer 3.

Synthesis of polymer 4. In a two-neck round-bottom flask equipped with a reflux condenser, polymer 3 (3 g, 0.321 mmol) was dissolved in dichloromethane (DCM, 25mL) and then chlorosulfonic acid (6.60 mL, 32.1 mmol) was added in a single portion at 36 °C internal temperature. After stirring vigorously for 1 h, gel-like precipitates were observed as a dark-brown color in the flask. After cooling to room temperature, distilled water (100 ml) was gradually added into the flask placed on the ice bath to quench excess chlorosulfonic acid. A small amount of ethyl acetate was added as a co-solvent and the solvents were removed slowly by rotary evaporation. The crude product, a pale brown powder, was washed with DCM, filtered under vacuum and dried at 60 °C under vacuum. The sulfonated polymer was then refluxed in concentrated hydrochloric acid (37%) at 70 °C for 10 days to de-protect the phosphonic acid groups. The resulting phosphonic acid polymer 4 was filtered under vacuum and washed with DCM several times. The final products were dried under vacuum at 60 °C for 24h. Polymer 4 was obtained as a pale brown powder (3.09 g, 92% yield). ^{1}H-NMR (300 MHz, Acetone-*d6*): δ 6.63-6.87 (m, –C<u>H</u>F–), 7.08–7.9 (m, Ar–<u>H</u>), 8.03 (s, Ar–<u>H</u> adjacent to -SO_3H); ^{19}F-NMR (283 MHz, DMSO-*d6*): δ –141.2 (d, J = 55.9 Hz, –CH<u>F</u>–CF_2–), –124.0-(–133.4) (m, cyclobutyl-F_6), (d) .5 (d, J_{ab} = 148.0 Hz, –CHF–C<u>F</u>$_2$–), –83.1 (d, J_{ab} = 148.0 Hz, –CHF–C<u>F</u>$_2$–), –79.54 (d, J = 112.4 Hz, –CHF–CCl<u>F</u>–); ^{31}P NMR (121 MHz, DMSO-d_6): δ12.19 (s); M_n 10,500 (^{1}H NMR); Elemental Analysis-Found: C, 36.15; H, 2.15; F, 20.59; S, 9.97.

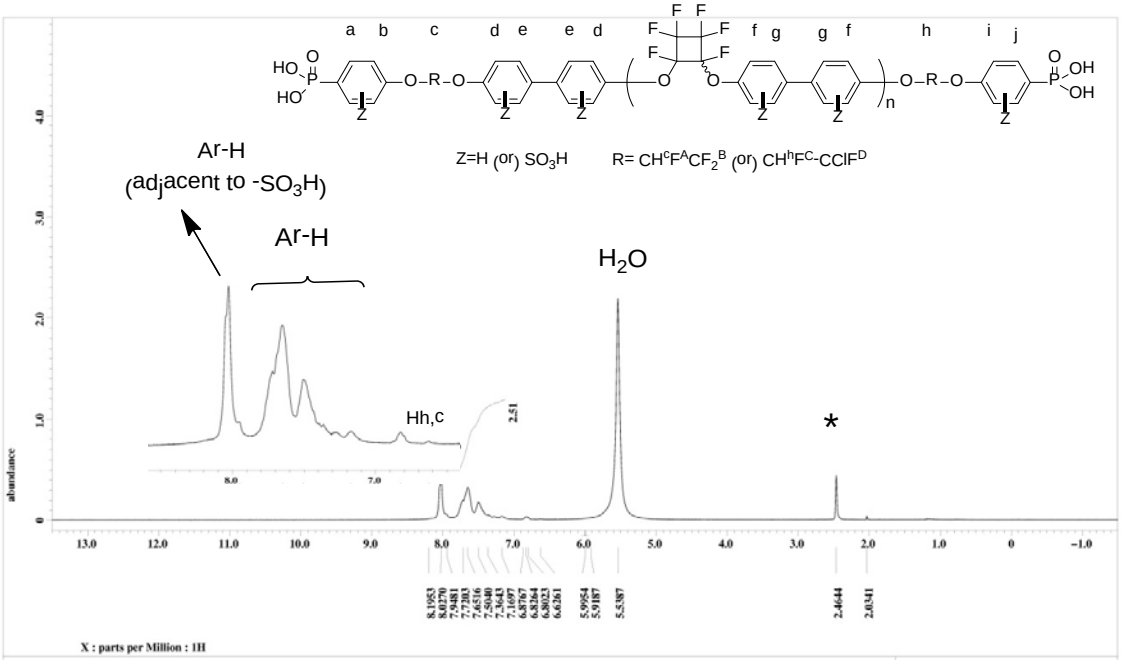

Figure 5.17 ^{1}H NMR (in DMSO-d_6*) spectrum of polymer 4.

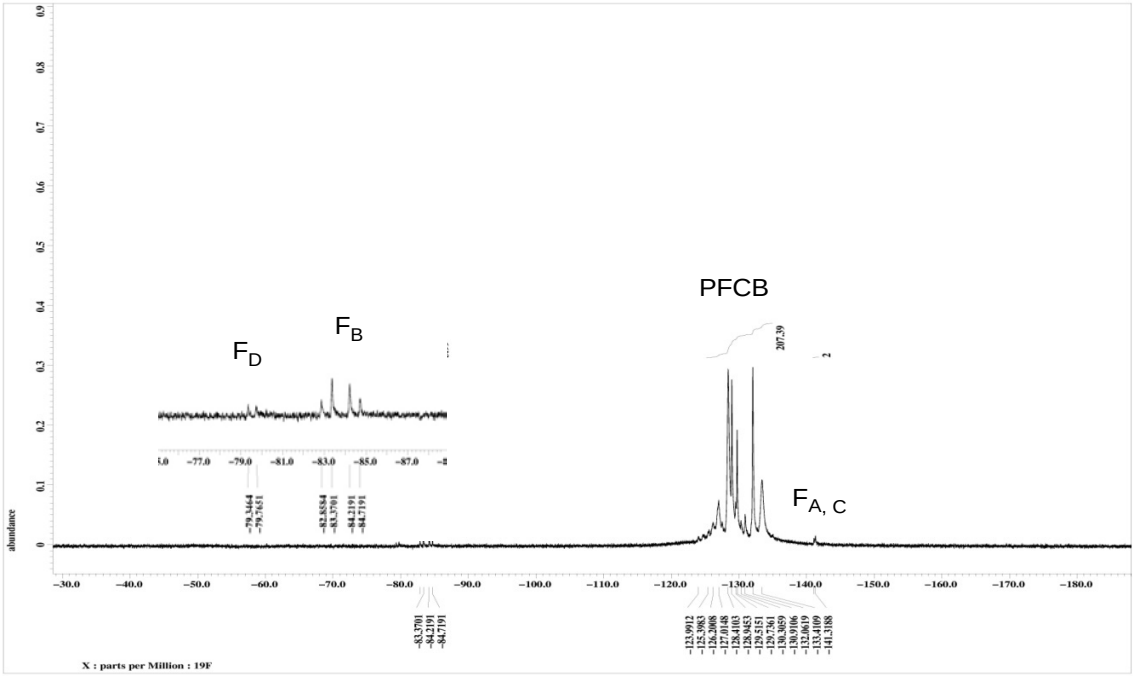

Figure 5.18 ^{19}F NMR (in DMSO-d_6) spectrum of polymer 4.

Preparation of aqueous ionomer solutions. Four salt-added ionomer aqueous solutions were prepared by adding a fixed amount (0.05 g) of ionomer into sodium sulfate (Na_2SO_4) aqueous solutions, which contained 0, 2.5, 5.0, and 50 mmol Na_2SO_4, respectively. The final solution volumes were then fixed at 50 mL.

Carbon/zirconia nanocomposite materials

Preparation of Mesoporous carbon/zirconia nanocomposites.[18] Mesoporous carbon/zirconia nanocomposites (ca. 16 wt.% ZrO_2) were prepared as described in literature.[18] The composite sample used in this work had a total BET surface area of 778 $m^2 \cdot g^{-1}$, a total pore volume of 2.22 $cm^3 \cdot g^{-1}$, and a porosity of 84.6 %. The pore size distribution calculated by the BJH method revealed that the specific pore volume of the composite was mostly composed of pores in the range of 10 to 30 nm with the most probable pore size at ~15 nm.

Preparation of SF-Ionomer-C/ZrO_2 and SA-Ionomer-C/ZrO_2 materials. Attachment of the ionomer onto C/ZrO_2 was performed by immersing 0.2 g of the C/ZrO_2 powder sample in the aqueous ionomer solution (50 mL) with salt (0.05 M Na_2SO_4) or without salt (0 M Na_2SO_4) at 100 °C for 5 h. To remove physically adsorbed ionomer, the treated samples were heated in DI water at 80 °C under continuous stirring for 2 h. The hot suspension was then centrifuged and the supernatant solution was removed by decantation. The C/ZrO_2 sample was then dispersed again in hot DI water (e.g., 80 °C). These successive washing steps were repeated seven times. The washed sample was

dried overnight at 80 °C under vacuum. The dried sample was then immersed in a 0.2 M HCl solution for 5 h under stirring to ensure that all acid groups are in the protonated form. Finally, the HCl-treated sample was centrifuged, rinsed with 10 mL DI water, and vacuum-dried at 120 °C for 24 h. The resulting samples prepared in the salt-free (SF) and salt-added (SA) ionomer solutions were designated as SF-Ionomer-C/ZrO_2 and SA-Ionomer-C/ZrO_2, respectively. As a control experiment, the identical treatment with a 0.05 M salt solution (no ionomer) was also applied to C/ZrO_2.

Ion exchange capacity of carbon/zirconia nanocomposite materials. A 0.1 g quantity of dried SF-Ionomer-C/ZrO_2 and SA-Ionomer-C/ZrO_2 was placed in 10 mL of a 2.0 M NaCl solution and mechanically stirred at room temperature for 72 h to allow for complete exchange of Na^+ ions with H^+ ions. Only the solution was retrieved by filtration. A 5 mL quantity of the retrieved solution was then mixed with 5 mL of a standard 0.01 N HCl solution so that a total 10 mL volume of titration solution was prepared. The resulting solution was titrated with a standard 0.01 N NaOH solution under a nitrogen blanket. The pH change was monitored to identify the endpoint using a pH meter (Accumet AB15, Fisher) with a double-junction pH electrode (Ag/AgCl reference, Accumet). EA (S, wt.%): SF-Ionomer- C/ZrO_2: 1.58, SA-Ionomer-C/ZrO_2: 1.89. EDX (S, wt%): SF-Ionomer- C/ZrO_2: 1.52, SF-Ionomer- C/ZrO_2: 1.95.

References

1. Mauritz, K. A.; Moore, R. B. State of Understanding of Nafion. *Chem. Rev.* **2004,** *104*, 4535-4586.

2. Ito, H.; Maeda, T.; Nakano, A.; Takenaka, H. Properties of Nafion Membranes under PEM Water Electrolysis Conditions. *Int. J. Hydrogen Energy* **2011,** *36*, 10527-10540.

3. Park, J.; Oh, J.-M.; Creager, S. E.; Smith Jr, D. W. Grafting of chain-end-functionalized perfluorocyclobutyl (PFCB) aryl ether ionomers onto mesoporous carbon supports. *Chem. Commun.* **2012,** *48*, 8225-8227.

4. Li, J.; Khanchaitit, P.; Han, K.; Wang, Q. New Route Toward High-Energy-Density Nanocomposites Based on Chain-End Functionalized Ferroelectric Polymers. *Chem. Mater.* **2010,** *22*, 5350-5357.

5. Spraul, B. K.; Suresh, S.; Jin, J.; Smith, D. W. Synthesis and Electronic Factors in Thermal Cyclodimerization of Functionalized Aromatic Trifluorovinyl Ethers. *J. Am. Chem. Soc.* **2006,** *128*, 7055-7064.

6. Mifsud, N.; Mellon, V.; Jin, J.; Topping, C. M.; Echegoyen, L.; Smith, D. W. First Identification of Biradicals during Thermal [2π + 2π] Cyclopolymerization of Trifluorovinyl Aromatic Ethers. *Polym. Int.* **2007,** *56*, 1142-1146.

7. Babb, D. A.; Ezzell, B. R.; Clement, K. S.; Richey, W. F.; Kennedy, A. P. Perfluorocyclobutane Aromatic Ether Polymers. *J. Polym. Sci., Part A: Polym. Chem.* **1993,** *31*, 3465-3477.

8. Iacono, S. T.; Budy, S. M.; Jin, J.; Smith, D. W. Science and Technology of Perfluorocyclobutyl Aryl Ether Polymers. *J. Polym. Sci., Part A: Polym. Chem.* **2007,** *45*, 5705-5721.

9. Iacono, S. T.; Budy, S. M.; Ewald, D.; Smith, J. D. W. Facile Preparation of Fluorovinylene Aryl Ether Telechelic Polymers with Dual Functionality for Thermal Chain Extension and Tandem Crosslinking. *Chem. Commun.* **2006**, 4844-4846.

10. Buquoi, J. Q.; Smith, D. W.; Iacono, S. T. Kinetic Study of Semifluorinated Arylene Vinylene Ether Polymers. *J. Polym. Sci., Part A: Polym. Chem.* **2011,** *49*, 4441-4447.

11. Keck, S.; Knoerzer, T. A.; Smith, D. W.; Iacono, S. T. Preparation of Partially Fluorinated Aryl/alkyl Vinylene Ether Polymers. *Polym. Int.* **2013,** *62*, 1485-1491.

12. Moody, J. D.; VanDerveer, D.; Smith Jr, D. W.; Iacono, S. T. Synthesis of Internal Fluorinated Alkenes via Facile Aryloxylation of Substituted Phenols with Aryl Trifluorovinyl Ethers. *Org. Biomol. Chem.* **2011,** *9*, 4842-4849.

13. Lejeune, N.; Dez, I.; Jaffrès, P.-A.; Lohier, J.-F.; Madec, P.-J.; Sopkova-de Oliveira Santos, J. Synthesis, Crystal Structure and Thermal Properties of Phosphorylated Cyclotriphosphazenes. *Eur. J. Inorg. Chem.* **2008,** *2008*, 138-143.

14. Cirkel, P. A.; Okada, T.; Kinugasa, S. Equilibrium Aggregation in Perfluorinated Ionomer Solutions. *Macromolecules* **1998,** *32*, 531-533.

15. Jiang, S.; Xia, K.-Q.; Xu, G. Effect of Additives on Self-Assembling Behavior of Nafion in Aqueous Media. *Macromolecules* **2001,** *34*, 7783-7788.

16. Wang, S.; Sun, G.; Wu, Z.; Xin, Q. Effect of Nafion® Ionomer Aggregation on the Structure of the Cathode Catalyst Layer of a DMFC. *J. Power Sources* **2007,** *165*, 128-133.

17. Zhu, A.; Dai, S.; Li, L.; Zhao, F. Salt Effects on Aggregation of O-carboxymethylchitosan in Aqueous Solution. *Colloids Surf. B* **2006,** *47*, 20-28.

18. Oh, J.-M.; Kumbhar, A. S.; Geiculescu, O.; Creager, S. E. Mesoporous Carbon/Zirconia Composites: A Potential Route to Chemically Functionalized Electrically-Conductive Mesoporous Materials. *Langmuir* **2012,** *28*, 3259-3270.

CHAPTER SIX

SUMMARY AND RECOMMENDATIONS FOR FUTURE WORK

Summary

Proton exchange membranes (PEMs) and ionomers are an essential electrolyte component used in PEM fuel cells.[1] PEMs have been also employed as electrolyte in the hybrid sulfur (HyS) cycle, which is a two-step water-splitting process composed of electrochemical and thermochemical steps to produce hydrogen in a large scale.[2] In both of the applications, a polymer electrolytes must possess high proton conductivity, thermal stability and mechanical stability. Perfluorocylobutyl (PFCB) aryl ether polymers are considered as one of the good candidates for use as PEMs because they fulfill the aforementioned requirements. In this regards, PFCB aryl ether polymer electrolytes were prepared for being used in membranes and catalyst layers.

Chapter 2, 3, and 4 discussed synthesis, characterization, properties of PFCB aryl ether segmented copolymer electrolytes, and their application as proton exchange membranes. Scheme 1 illustrates (a) segmented-copolymer formation *via* click-cyclopolymerization, (b) selective sulfonation through the segmented polymer backbone, and (c) cross-linking of hydrophilic-hydrophobic PFCB aryl ether segmented copolymers. The second portion of this dissertation, Chapter 5 (Reproduced by permission of The Royal Society of Chemistry)[3], described the synthesis of telechelic PFCB aryl ether ionomers bearing sulfonic acid groups in the main chain and phosphonic acid end groups.

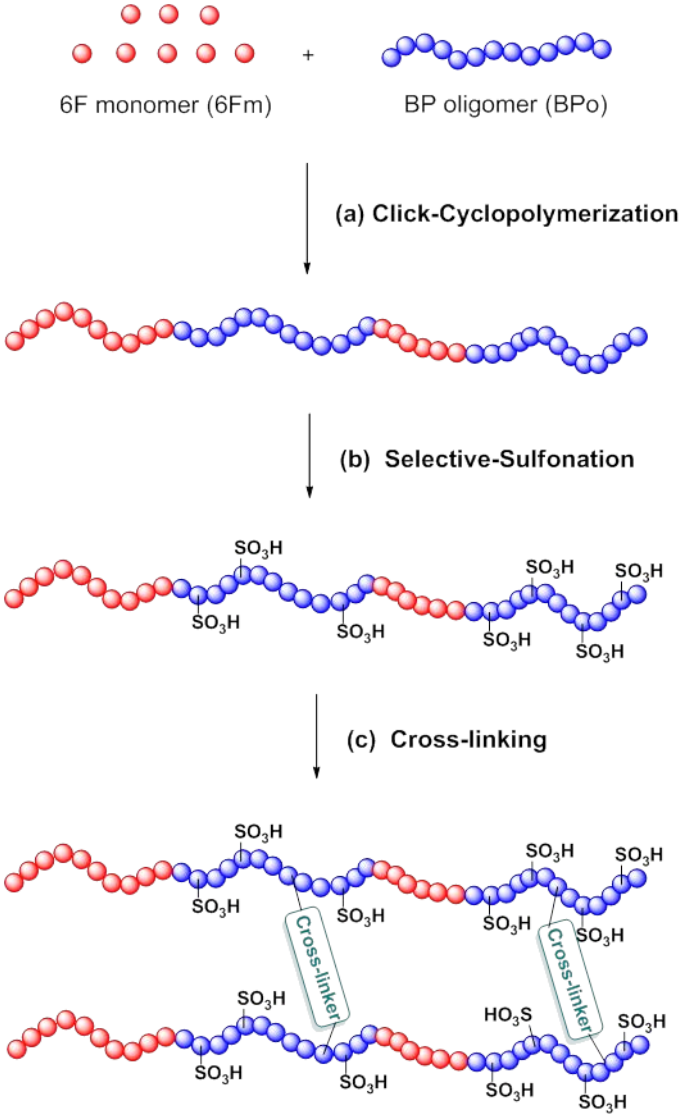

Scheme 6.1 Illustration of selective-copolymerization, sulfonation, and cross-linking.

High-molecular-weight PFCB aryl ether segmented copolymers were obtained in solvent/catalyst/initiator-free polymerization reactions (Chapter 2). The direct segmented-copolymer formation from oligomer/monomer or monomer/monomer couples

in an one-pot single copolymerization reactions was confirmed using ^{19}F NMR spectroscopy. Computational studies also confirmed that copolymerization of relatively electron-rich and electron-poor TFVE monomers results in segmented copolymers in a single polymerization. This is the first report to demonstrate a selective copolymerization of fluoro-olefins having different reactivity and to describe the monomer distributions in PFCB aryl ether copolymers. These findings extend the range of PFCB chemistry toward designing and/or developing novel PFCB copolymers having tuned microstructures by using reactivity differences of monomers and/or by controlling monomer feeding ratios.

Along with the selective copolymerization, the effect of copolymer microstructure on sulfonation selectivity and properties of polymer electrolytes as PEMs were discussed in Chapter 3 and 4. Selective sulfonation of high-molecular-weight segmented polymers afforded hydrophilic-hydrophobic polyelectrolytes with controllable ion content. All the polymers gave transparent membranes by solution casting and showed good properties as polyelectrolyte membrane materials. Effect of cross-linking on water uptake, volume swelling and mechanical strength of these highly sulfonated PFCB (sPFCB) aryl ether copolymer membranes was investigated. Cross-linked membranes showed good properties as a promising candidate for HyS process.

Water-soluble PFCB aryl ether ionomers bearing sulfonic acid groups in the main chain and phosphonic acid end groups were prepared in three steps consisting of (1) nucleophilic addition of aryl phosphonic diethyl esters onto the TFVE end groups, (2) sulfonation throughout the polymer backbone, and (3) acid catalyzed hydrolysis of the phosphonate esters (Chapter 5). Hydrodynamic size of the polymer solutes was

investigated by Dynamic Light Scattering and the telechelic ionomer was used to modify the surfaces of mesoporous carbon materials containing dispersed zirconia nanoparticles. Ionomer surface grafting occurred via phosphonate bonding onto the zirconia particle surfaces. These ionomers have controlled end group chemistries presents opportunities for ionomer stabilization that are not available for other low-EW ionomers.

Recommendations for Future Work

Metal oxide - embedded PFCB polymer membranes

PEM fuel cells are operated at a temperature around 80-100 ºC. During the operation, water in the proton-exchange membrane often evaporates. As a result, the proton transport through the membrane hardly occurs. To overcome this issue, the incorporation of metal oxide particles (e.g., TiO_2 and ZrO_2) into polymer membranes has been proposed as an effective method to enhance the water retention capability of the proton-conducting membranes.[4] However, metal oxide particles often aggregate randomly in the polymer matrix. Therefore, the existing challenges in preparation of such composite membranes are to obtain uniform particle dispersion and to introduce strong chemical bonding between the nanoparticles and the polymer matrix, which are necessary in order to take full advantages of the metal oxide-polymer composite system. However, it is assumed that the particle dispersion in the matrix and the bonding strength between the particles and the polymer matrix may be improved by introducing a proper functional group to the polymer structure and incorporating appropriate metal oxide particles reactive to that functional group. We have designed sulfonated PFCB-based

polymers having phosphonic acid end groups to which metal oxide particles such as zirconia particles can be specifically incorporated (Scheme 3.8). Chemical bonding and reactivity between a phosphonate and zirconia is well known. Preparation of a water-soluble sulfonated PFCB-based ionomer having phosphonic acid end groups has been accomplished via a following facile synthesis route: 1) step-growth polymerization of perfluorocyclobutyl (PFCB) aryl ether polymer from 4,4´-bis(4-trifluorovinyloxy)-biphenyl monomer; 2) phosphonation of PFCB polymers via a condensation reaction with diethyl(4-hydroxyphenyl)phosphonate; 3) sulfonation of the phosphonated PFCB using chlorosulfonic acid; and 4) hydrolysis of the phosphonate ester groups using concentrated HCl as discussed in Chapter 5. Based on this telechelic S-PFCB polymer having terminal phenyl-phosphonic acid groups, synthesis of zirconia-PFCB hybrid composite membranes will be possible. The structure of the proposed composite compound is illustrated in Scheme 3.8.

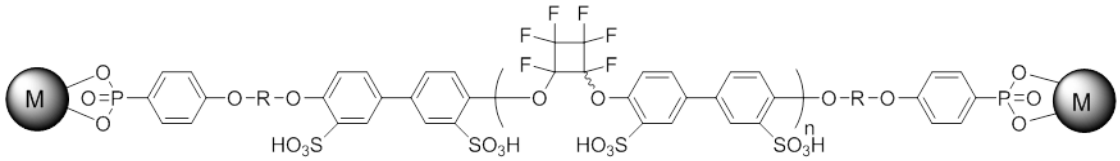

R= $CHFCF_2$ (or) CF=CF (50:50 *cis:trans*)

Scheme 6.2 Schematic illustration of a zirconia-incorporated PFCB polymer composite.

PFCB polymers containing sulfonated POSS as pendant sulfonic acid groups

Sulfonated aromatic polymers can be divided into two types (e.g., main-chain-type and side-chain-type), based on the attachment site of the sulfonic acid groups. Ionomers with sulfonic acid groups attached directly to their main chain often show intensive water uptake over a degree of sulfonation, resulting in unfavorably excessive water swelling of the membranes. Kreuer and co-workers reported that sulfonated aromatic polymers are unable to form well-defined and continuously interconnected hydrophilic domains because the rigid polyaromatic main chain hardly allows the formation of continuous ionic clustering.[5] One possible way to overcome this issue is to prepare for ionomers to form a phase-separated morphology of discrete hydrophilic and hydrophobic domains. The phase-separated morphology could be possible achieved by locating the sulfonic acid groups on side chains grafted onto the polymer main chain. In our approach, a polyoctahedral oligomeric silsesquioxane (POSS) cage possessing phenyl groups will be attached as a pedant unit to the main polymer chain. Then the phenyl groups present in the POSS units will be sulfonated. Some prior work with sulfonated POSS units can be found in literature. In their applications, sulfonated POSS cages were used as filling materials in membranes for the purpose of improving water retention and mechanical strength of membranes.[6] However, it has been reported that aggregation of POSS cages in membranes is problematic to control the phase morphology in the membranes. We have learned from our recent research results that this limitation can be overcome by covalently bonding POSS cages onto the polymer backbone.[7] These PFCB polymers containing sulfonated POSS cage pendant side chains (Scheme 3.9) will be a

good candidate to prepare and investigate their properties in terms of the phase morphology, water uptake, swelling, conductivity, and thermal / chemical / mechanical stability.

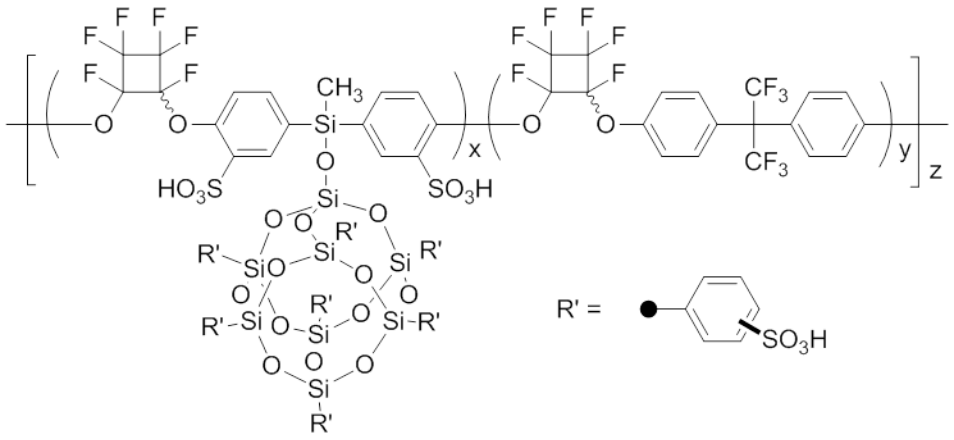

Scheme 6.3 PFCB polymers containing sulfonated POSS side chains.

References

1. Zhang, H.; Shen, P. K. Recent Development of Polymer Electrolyte Membranes for Fuel Cells. *Chem. Rev.* **2012,** *112*, 2780-2832.

2. Elvington, M. C.; Colón-Mercado, H.; McCatty, S.; Stone, S. G.; Hobbs, D. T. Evaluation of Proton-conducting Membranes for use in a Sulfur Dioxide Depolarized Electrolyzer. *J. Power Sources* **2010,** *195*, 2823-2829.

3. Park, J.; Oh, J.-M.; Creager, S. E.; Smith Jr, D. W. Grafting of Chain-end-functionalized Perfluorocyclobutyl (PFCB) Aryl Ether Ionomers onto Mesoporous Carbon Supports. *Chem. Commun.* **2012,** *48*, 8225-8227.

4. Navarra, M. A.; Croce, F.; Scrosati, B. New, High Temperature Superacid Zirconia-doped Nafion Composite membranes. *J. Mater. Chem.* **2007,** *17*, 3210-3215.

5. Kreuer, K. D. On the Development of Proton Conducting Polymer Membranes for Hydrogen and Methanol Fuel Cells. *J. Membr. Sci.* **2001,** *185*, 29-39.

6. Hartmann-Thompson, C.; Merrington, A.; Carver, P. I.; Keeley, D. L.; Rousseau, J. L.; Hucul, D.; Bruza, K. J.; Thomas, L. S.; Keinath, S. E.; Nowak, R. M.; Katona, D. M.; Santurri, P. R. Proton-conducting Polyhedral Oligosilsesquioxane Nanoadditives for Sulfonated Polyphenylsulfone Hydrogen Fuel Cell Proton Exchange Membranes. *J. Appl. Polym. Sci.* **2008,** *110*, 958-974.

7. Iacono, S. T.; Ewald, D.; Sankhe, A.; Rettenbacher, A.; Smith, D. W., Jr. Sulfonated Fluorovinylene Aromatic Ether Polymers for Proton Exchange Membranes. *High Perform. Polym.* **2007,** *19*, 581–591.